NCAR/TN-134+STR
NCAR TECHNICAL NOTE

March 1979

Case Studies on Convective Storms
Case Study 3

8 June 1976: First Echo Case

Daniel W. Breed

CONVECTIVE STORMS DIVISION

NATIONAL CENTER FOR ATMOSPHERIC RESEARCH
BOULDER, COLORADO

FOREWORD

This is one of a series of Technical Notes reporting data on aircraft penetrations in convective clouds, ranging from cumulus congestus to thunderstorms, in northeastern Colorado and adjacent portions of Wyoming and Nebraska. The June and July 1976 field season of the National Hail Research Experiment is the setting of the first six to ten of these Notes. The series may be extended later to the 1974, 1975 and 1978 seasons. All of the cases involve aircraft data, including vertical velocity, state parameters and cloud physical data, obtained in coordination with detailed S-band radar scans, normally taken with about two minute time resolution.

Some of these cases will be the subject matter of formal publications, in which case the Tech Note will supplement the publication by providing a more extensive presentation of data. Other cases will be presented as complete sets of data only in the Tech Notes, but usually some portions of the data will be included in publications on general properties of convective clouds over the high plains.

These Tech Notes will always have the following components: a brief synoptic setting, a representative sounding, a brief, general radar reflectivity history, a more detailed radar history of the cloud or storm investigated with the aircraft tracks superimposed, a presentation of the aircraft data, and a discussion. The presentation will not be truly complete either as regards radar data or cloud droplet or precipitation particle size spectra, because these data are too voluminous. However, the general data, such as particle concentrations and liquid water content, will be presented along with some examples of the more complete data and remarks on typical aspects.

The data quality is in some cases difficult to assess. There is no absolute standard for many in-cloud measurements, even of temperature. Trust in the listed values for liquid water content and droplet sizes and concentrations must always be qualified to some degree. These Technical Notes will include remarks on data quality that record the opinions of those closest to taking the data, and the reasons for the opinions. Work on the data reliability will be continuing, however, and because of this, some of these opinions may change. Any such changes will be recorded in the Tech Note series, along with reference to previous notes in which changes should be made.

The penetrating aircraft for the 1976 season were the NCAR/NOAA sailplane, the University of Wyoming Queen Air, and the South Dakota School of Mines and Technology armored T-28.

This series of Tech Notes is intended to provide a lasting record of cloud data in the high plains area that may be of use in unforeseeable ways in future atmospheric studies. The data were gathered as part of the National Hail Research Experiment, managed by the National Center for Atmospheric Research and sponsored by the Weather Modification Program, Research Applications Directorate, National Science Foundation.

Charles A. Knight
June 1978

ACKNOWLEDGMENTS

The help of G. Vali at the University of Wyoming and of D. Musil at the South Dakota School of Mines and Technology in providing some of the aircraft data and in reviewing the manuscript is greatly appreciated. The NCAR Research Aviation Facility made available the 304D aircraft data.

CONTENTS

LIST OF FIGURES

List of Figures (contd.)

ABSTRACT

Extensive coverage by three aircraft in the inflow region of a maturing storm highlighted the investigation of 8 June 1976. The synoptic conditions supported convection of moderate strength, with the activity initially forming and organizing northeast of Cheyenne. The resulting storm moved east, then southeast, maintaining a high reflectivity core on the southeast side in the direction of low-level inflow. Wyoming Queen Air 10UW and the South Dakota School of Mines and Technology armored T-28 made coordinated penetrations in turrets on the south and southeast flanks of the storm, while NCAR Queen Air 304D monitored subcloud conditions in the same region. The data from the aircraft investigations are presented in relation to the radar data. The data show the interactions of individual cells with each other and with the storm mass to be varied and complex.

I. METEOROLOGICAL SYNOPSIS

Figure 1 shows the surface synoptic conditions on 8 June 1976 at 1200 MDT, about the time of initial convection in the storm's genesis area. Strong, moist southerly flow across the Plains created a warm sector along the stationary front which extended across the north-central U.S. Although winds were light in the NHRE area (shaded region in Fig. 1), there was a rather strong east-west moisture gradient caused by this flow into the area. Data from the mesonetwork, located 10-85 km east of Grover, substantiated the gradient showing dew point temperatures to 15°C on the east side and 8.5°C on the west. South-southeasterlies prevailed across the network. There was some evidence of the typical dry air mass along the lee side of the Rockies, but the surface winds were too light to extend it very far onto the plains of Colorado.

The 500-mb analysis at 0600 MDT (Fig. 2) shows light winds over the NHRE area (shaded region) caused by a longwave ridge, with the jetstream located in the western U.S. Although cold air advection and a couple of short waves traveling around the ridge look like they may have affected the NHRE area during the day, neither feature was evident in the local soundings released during the day.

The sounding closest to the investigated storm in space and time was the 1531 ascent from Grover. The presentation of the sounding in Fig. 3 also shows temperature and dew point values along a straight-line descent from the storm to Grover in inflow conditions by NCAR Queen Air 304D (dotted line). Notable features are the negative buoyancy at cloud base, the thermal structure aloft, and the vertical wind structure. The nearly dry adiabatic lapse rate below 5 km was accompanied by light winds while a substantial change in lapse rate and wind velocity occurred at 6 km. The 0735 MDT sounding taken at Sterling showed light winds (< 15 m s^{-1}) throughout the troposphere, with the upper level winds increasing markedly through the afternoon. Note the fairly large wind shear across the tropopause (12 to 13 km) in Fig. 3. The synoptic conditions of the day showed adequate moisture and light winds in the boundary layer with moderate instability and fairly strong winds aloft. No large-scale events appeared to influence the convective activity.

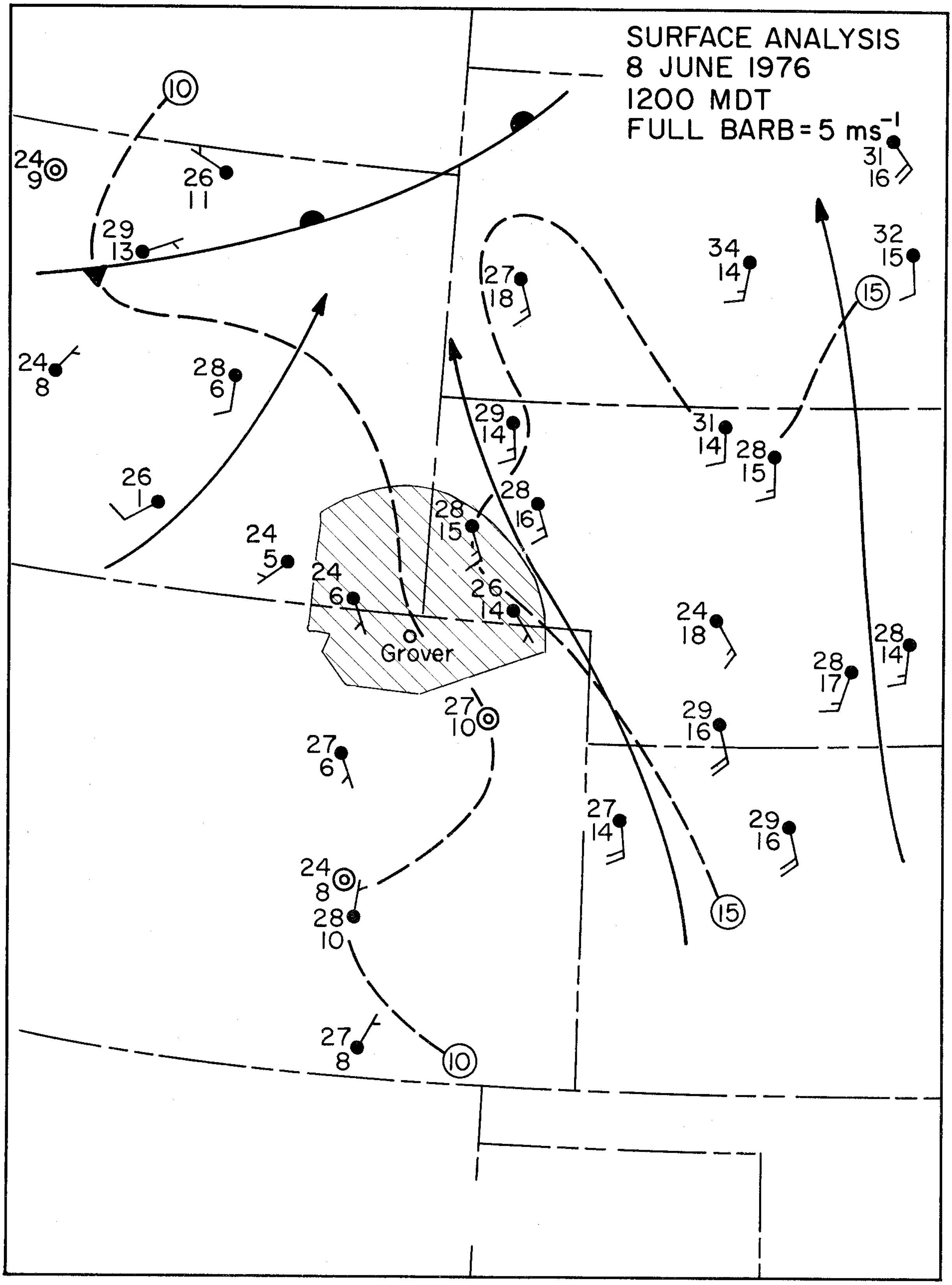

Fig. 1. Regional surface map for 1200 MDT on 8 June 1976 showing the synoptic scale conditions at about the time of initial convection in northeastern Colorado and southwestern Wyoming. Temperature, dew point, and winds are plotted at each station. Dashed lines are the 10°C and 15°C isodrosotherms, and the shaded area is the NHRE airspace.

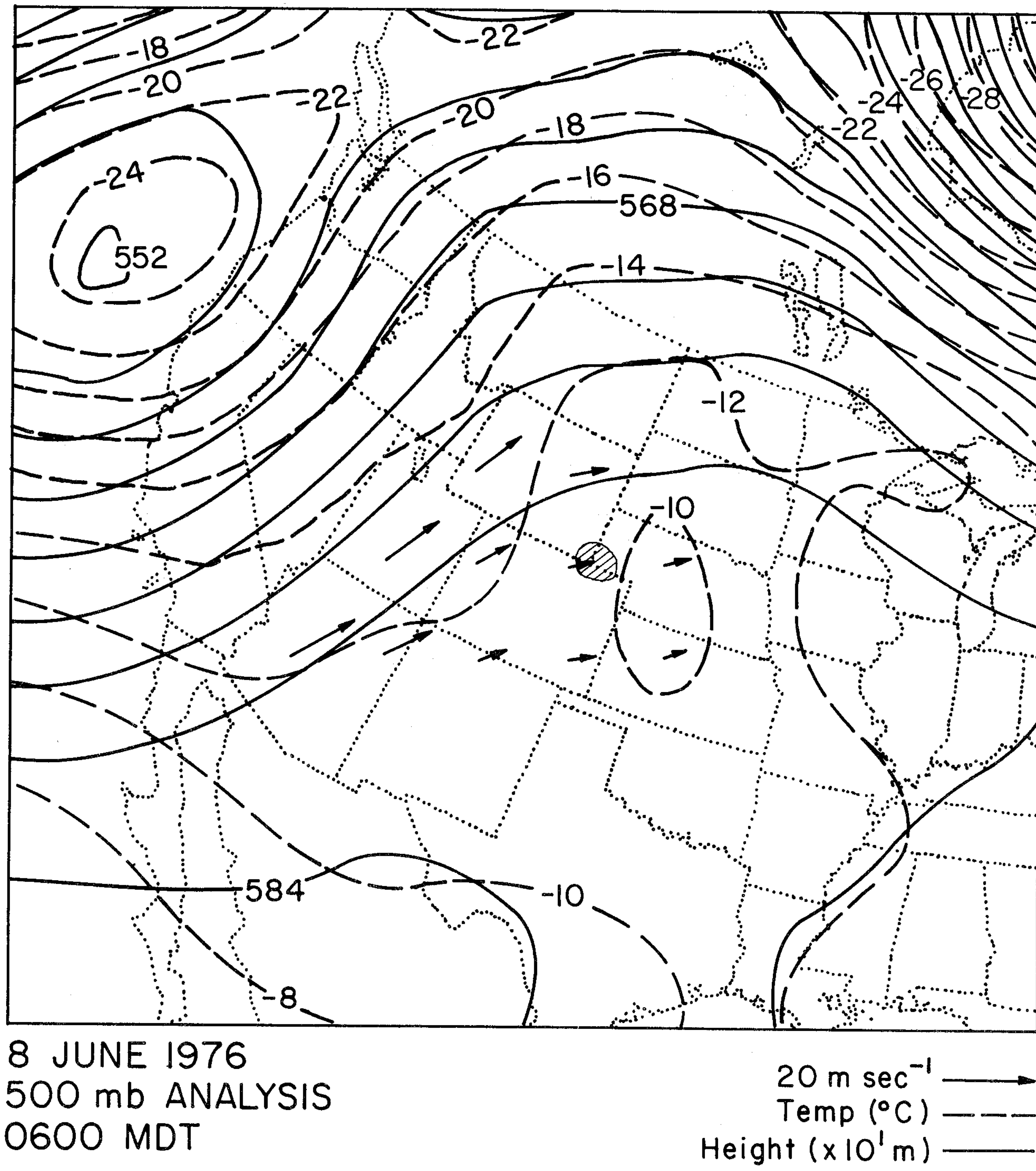

Fig. 2. 500 mb map of the western half of the U.S. for 0600 MDT on 8 June 1976 showing the early morning mid-level synoptic conditions. Solid lines are geopotential height contours (10^1 m) every 40 m; dashed lines are isotherms (°C) every 2°C; and wind vectors are plotted around the NHRE area (shaded).

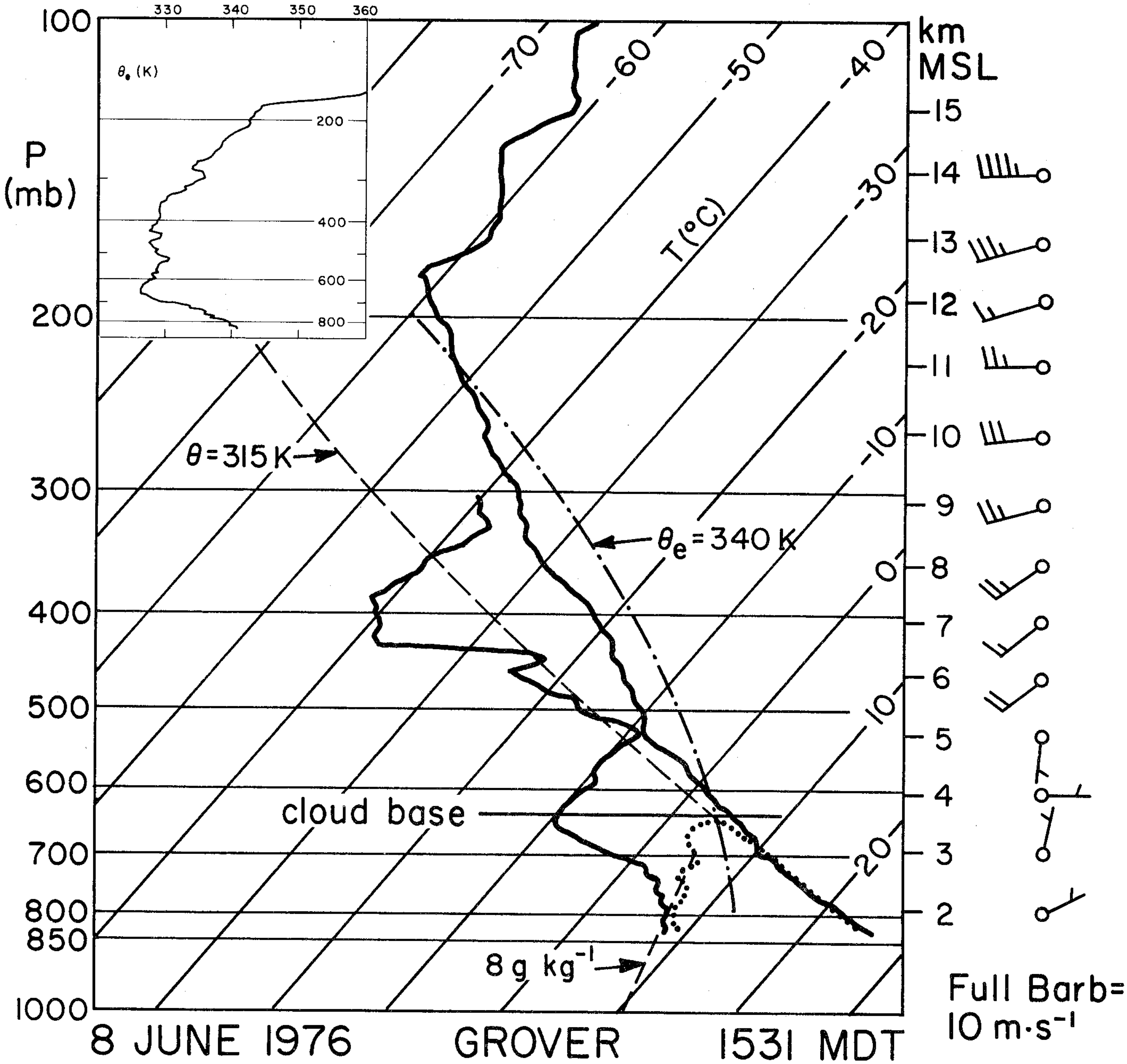

Fig. 3. Thermodynamic diagram showing the vertical distribution of temperature and dew point from the Grover 1531 sounding. Selected dry and moist adiabats and mixing ratio have been plotted as dashed lines and labeled. Dotted lines below cloud base are values of temperature and dew point obtained by Queen Air 304D in a descent sounding near Grover in general inflow conditions. Winds are plotted at 1 km intervals on the right; full barb is 10 m s^{-1}. Insert in the upper left shows θ_e vs. pressure for this sounding.

II. RADAR HISTORY

The storm investigated on this day was relatively long-lived with convective activity in the initial development area commencing around noon, development to > 50 dBZ at about the 5.0 km level[2] occurring around 1345, and continued activity past 1740 when radar surveillance was discontinued. Figures 4a through 4f show the history of the storm in PPI format from data obtained by the Grover (CP-2) radar. A number of individual cells in differing stages of growth were about to merge at 1340 (Fig. 4a). Some of the cells had formed and grown with little or no movement while the southern and south-western cells had formed ∿ 20 km farther to the west and moved into the area. The merger of cells 1 and 2, marked by arrows in Fig. 4a, initially formed the main body of the storm, with reflectivities of 15 dBZ in cell 1 already extending up to ∿ 12 km. Between 1340 and 1422 (Fig. 4b) cell 1, in the south-southeastern area of the storm, intensified to become the dominant feature of the storm, although other cells continued to develop as well. Overall storm motion was easterly at ∿ 6 m s^{-1} but individual cells seemed to move independently, a characteristic of airmass thunderstorms. Note that the high reflectivity gradients were on the southeastern and western edges of the storm, which were in the direction of the inflow (as identified by NCAR Queen Air 304D) and mid-level winds respectively. Around 1420, movement of the main storm center shifted to

[2]All altitudes are referenced to Mean Sea Level (MSL) unless otherwise indicated.

southeasterly at approximately 5 m s^{-1}. However, individual cells on the northern and northwestern flanks continued to move easterly or northeasterly before dissipating, effectively spreading the northern half of the storm mass. The South Dakota School of Mines and Technology's T-28, University of Wyoming's Queen Air 10UW, and 304D were all investigating the southern and southeastern area of the storm by 1455 (Fig. 4c). The cells to the west-southwest of the storm were growing vigorously and had an easterly component of motion. By 1534 (Fig. 4d), they had merged with the storm but had also weakened in intensity. The northern side of the storm had rotated southeastward while the main storm center, the high reflectivity region, moved at about 3 m s^{-1} during this time. Reflectivity gradients were still strong on the western and south-southeastern sides of the storm. By 1600, the investigating aircraft had left the area just as a major cell developed to the south-southwest and merged with the southeastward-propagating storm. Figure 4e shows the resultant storm structure after this merger. The active southeastern storm area continued to move southeastward at 7 m s^{-1}, maintaining its intensity through 1735 (Fig. 4f). Around this time, the radar azimuthal limits were shifted for surveillance of another storm.

During the first half of its lifetime, the storm was dominated by a single cell which apparently was in a favored area for continuous inflow. Many cells developed along the western flanks of this storm but moved with the mid-level winds rather than in the direction of the low-level inflow. Around 1600, a cell developed to the southwest and moved eastward into the main storm cell, maintaining its intensity while attaining the southeastward momentum of the storm. The storm was still active as it moved into the southern NHRE area. The variety of interactions on the storm scale and on smaller scales, as shown by the complicated motions of the radar cells, testify to the complexity of this storm.

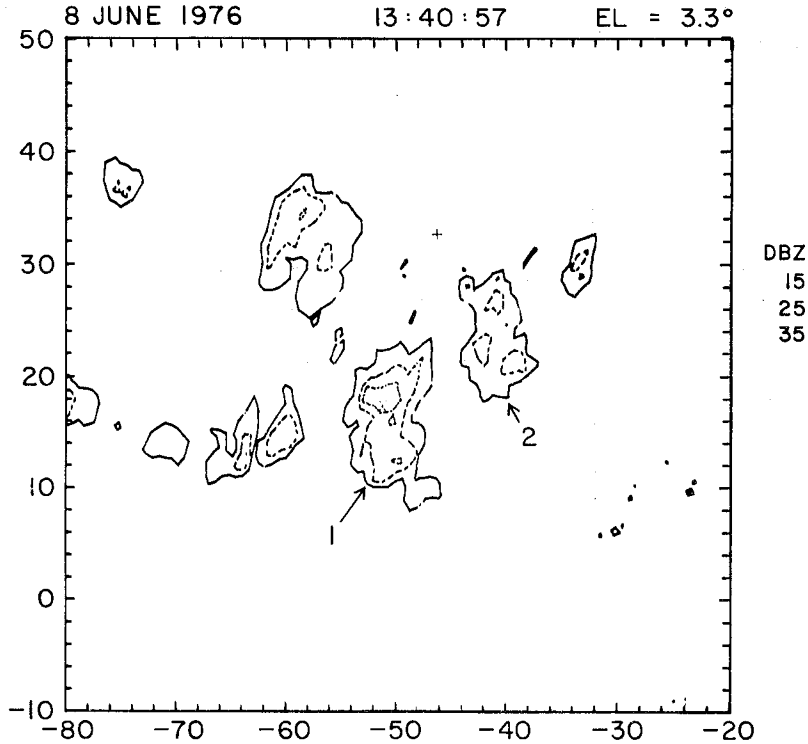

Fig. 4a. The 13:40:57 PPI radar scan on 8 June 1976 showing reflectivity contours on 60 km x 60 km map at 3.3 elevation angle. Contours are at 10 dBZ intervals from 15 dBZ. The Cheyenne VOR is marked with a cross.

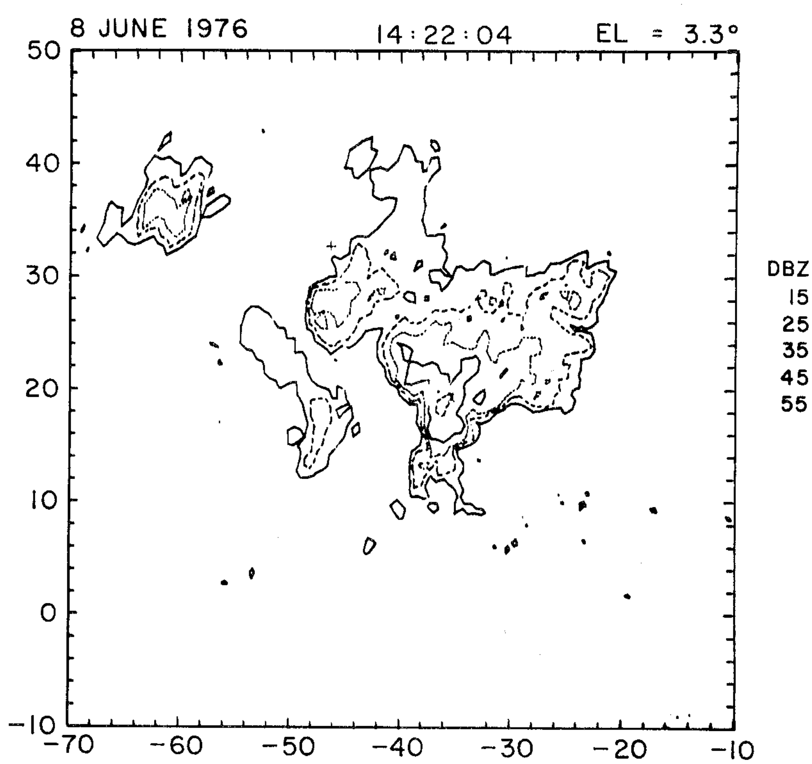

Fig. 4b. Same as Fig. 4a except at 14:22:04. The PPI area has shifted 10 km east from Fig. 4a.

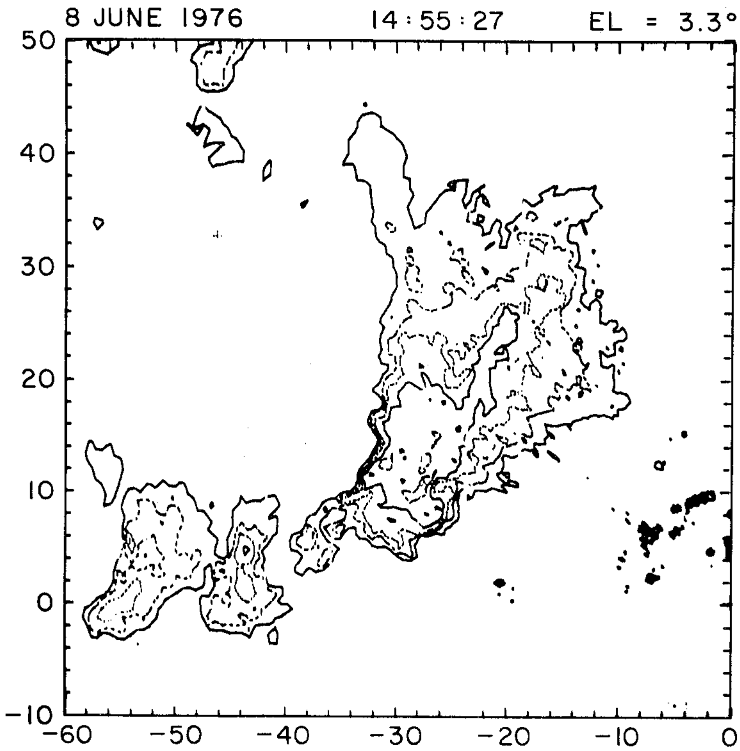

DBZ
15
25
35
45
55

Fig. 4c. Same as Fig. 4a except at 14:55:27. The PPI area has shifted 10 km east from Fig. 4b.

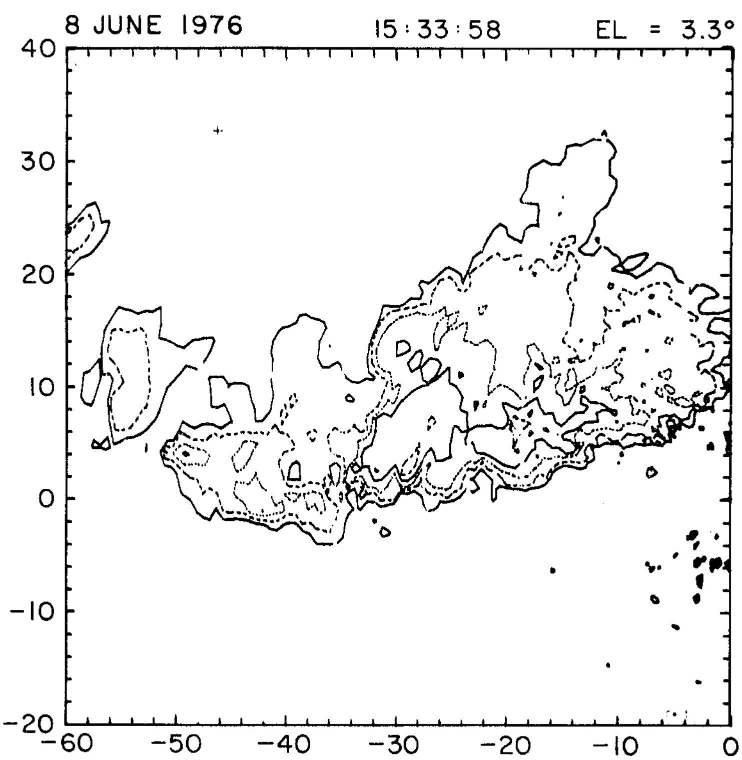

DBZ
15
25
35
45
55

Fig. 4d. Same as Fig. 4a except at 15:33:58. The PPI area has shifted 10 km south from Fig. 4c.

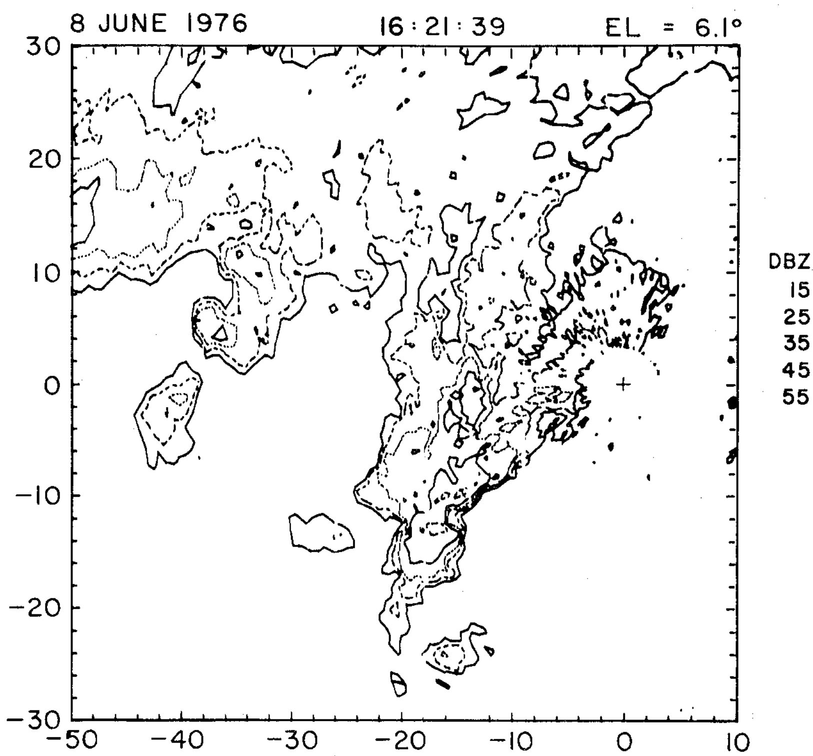

Fig. 4e. Same as Fig. 4a except at 16:21:39 and at 6.1° elevation angle. The radar location is marked with a cross. The PPI area has shifted 10 km east and 10 km south from Fig. 4d.

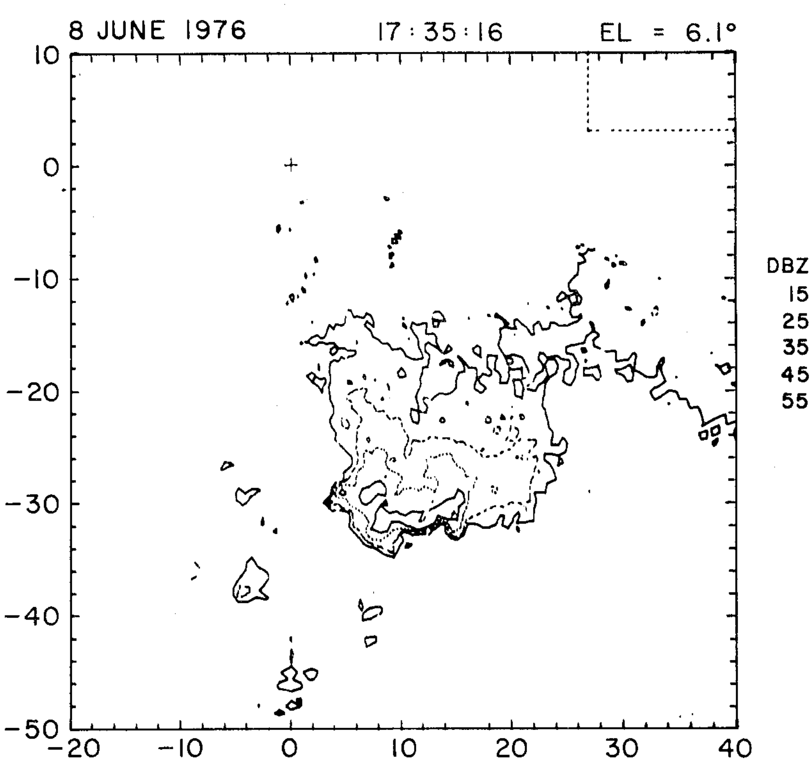

Fig. 4f. Same as Fig. 4e except at 17:35:16. Dashed rectangle in the upper right marks the southwest corner of the dense precipitation network. The PPI area has shifted 30 km east and 20 km south from Fig. 4e.

III. PENETRATING AIRCRAFT

A. WYOMING QUEEN AIR 10UW

The Wyoming Queen Air 10UW made approximately 11 passes on the southern and southeastern flanks of the storm on this day, starting at about 1420 and ending at 1542:30 when an aircraft power failure interrupted the recording of data. Figures 5a, 6a, ... 12a show 10UW's track for the cloud penetration passes in relation to the radar echo structure at the time of each pass. Care should be taken in interpreting the radar data since it is in PPI format (note the arcs of constant altitude) while the aircraft passes were nearly constant in altitude. Also, note that radar ground clutter and artifacts have not been removed from the data presented. There were 11 instances when the Grover radar detected the skinpaint of 10UW, and no consistent error in the track was evident. The tracks have been corrected for a storm motion of 5 m s^{-1} to the southeast until 1500, after which time a storm motion of 3 m s^{-1} to the southeast was used. The resulting track should be within 1-1.5 km of true position.

Aircraft operations on this day were coordinated about actively growing turrets at the southern apex of the storm. The 10UW penetrations were at the 4.5-5.0 km level except for passes 6, 7, and 8 which were at cloud base ($\sim$ 4.0 km). A number of penetrations were made through the same cell, both by 10UW and the T-28. Some of the 10UW data from the penetrations are presented in Figs. 5b, 6b,... 12b, and include pressure, temperature, equivalent potential temperature (θ_e), vertical velocity, hot-wire and ASSP-derived liquid water contents (LWC), and a summary of the 2-D ice particle data. Also included are occasional LWC and total droplet concentration data from soot-coated slides. The vertical velocity is determined from the aircraft rate of climb and aircraft flight characteristics (i.e., airspeed, power setting, etc.), and is then smoothed and filtered. Hence, the response time and sensitivity is greatly reduced and the data are presented here only as an approximation in time and magnitude of vertical velocity strength. Most of the updraft encounters were verified from voice notes of the pilot and observers. Before 1 July during the 1976 field season, the hot-wire LWC magnitudes were incorrect, but are included in this Note to show encounters with cloud water and to show relative fluctuations for comparison with other parameters. The ASSP-derived LWC magnitudes are also in error as described in the appendix on aircraft instrumentation, but the two LWC traces show consistent agreement in fluctuations if a small lag time correction is applied to the hot-wire data. The values from both LWC sources are too low, and have no quantitative validity. The 2-D data presented include the approximate time that ice particles were detected, an estimate of the predominant ice particle types, and estimates of the maximum sizes and concentrations when appropriate. The data periods selected for presentation included encounters of cloud water, ice particles, and significant updrafts or downdrafts that were in or in close proximity to the cloud penetrations.

Passes 1 through 4 were sequential penetrations in or near a developing turret or cell, identified in Fig. 5a by an arrow. This cell formed southwest of the main storm and southeast of a smaller northward-moving storm cell, with the first indication of a -5 dBZ contour occurring at about 1405 at approximately the 5.5 km level. As the cell moved eastward around the southern apex of the main storm, it intensified, developing strong gradients along its reflectivity boundaries which were distinguishable from the larger scale reflectivity structure. As the cell merged with the main reflectivity core of the storm, the boundary of these persistent reflectivity gradients became the only identifiable feature of the cell after about 1516. By 1525, even this feature had become diffuse and no longer identifiable. Although a strong reflectivity gradient existed on the eastern side of the cell, the eastern legs of passes 1, 2, and 3 showed weak, although consistent, updrafts with no distinct changes in θ_e values. Passes 1 through 4 of 10UW showed the strongest updrafts to be on the west side of the cell investigated and in the higher liquid water regions encountered. The increase of size and concentration of ice particles at 10UW's altitude is evident in the data of passes 1, 2, and 3.

The radar data show that fairly rapid growth occurred in the west-southwest area between the main storm echo and a storm cell (located in the southwest corner of Figs. 5a-8a) which was propagating northward into the western side of the main storm. Pass 5 data (Fig. 9b) show a strong updraft with a broad area of LWC and θ_e values to 334 K in 10UW's penetration of the echo area at the junction of the main storm and southwestern storm cell. This echo area developed to define the sharp reflectivity gradient on the southwest quadrant of the main storm, while the storm cell moving up from the south maintained some northerly momentum along the west side of the main storm. However, this area was not investigated in detail.

After a number of passes at and below cloud base, 10UW made an extended pass (Pass 9, Fig. 10b) through clouds on the southern edge of the main storm. A number of strong updrafts, with θ_e values of 335 to 338 K at 4.3 - 4.5 km, suggest that the growth occurring in this inflow region was cellular in nature. LWC does not show any large changes after the 1523-1524 cloud penetration, and ice particles were detected only in the highest reflectivity encountered during this pass; 15-20 dBZ between 1527 and 1528.

Passes 10 and 10' were in and near a developing storm element or cell south of the main storm at the approximate coordinates (-30,-12) in Figs. 11a and 12a. This cell had reflectivities to 5 dBZ at the 6.0 km level by 1525. Reflectivities spread quickly vertically and horizontally with an overall movement of the cell to the east-northeast. The vertical spread was most rapid upwards, and the initial horizontal spread was most rapid at the 6.5 - 7.0 km level. New turrets continued to form on the west side as this cell grew and organized with the main storm. Pass 10 (Fig. 11b) was a penetration through growing turrets west of the reflectivity region of the cell. A fairly strong updraft was encountered at the penetration altitude of about 4.8 km, with θ_e values of $\sim$335 K and indications of moderately high LWC. No ice particles were detected by the 2-D probe. Pass 10' (Fig. 12b) skirted the southwest side of the echo area of the cell (see Fig. 12a) in coordination with the T-28. The updraft-downdraft gradient at about 1541 coincides with the penetration of the -5 dBZ contour, but no ice particles were detected at 10UW's altitude. About 1545, 10UW exited the

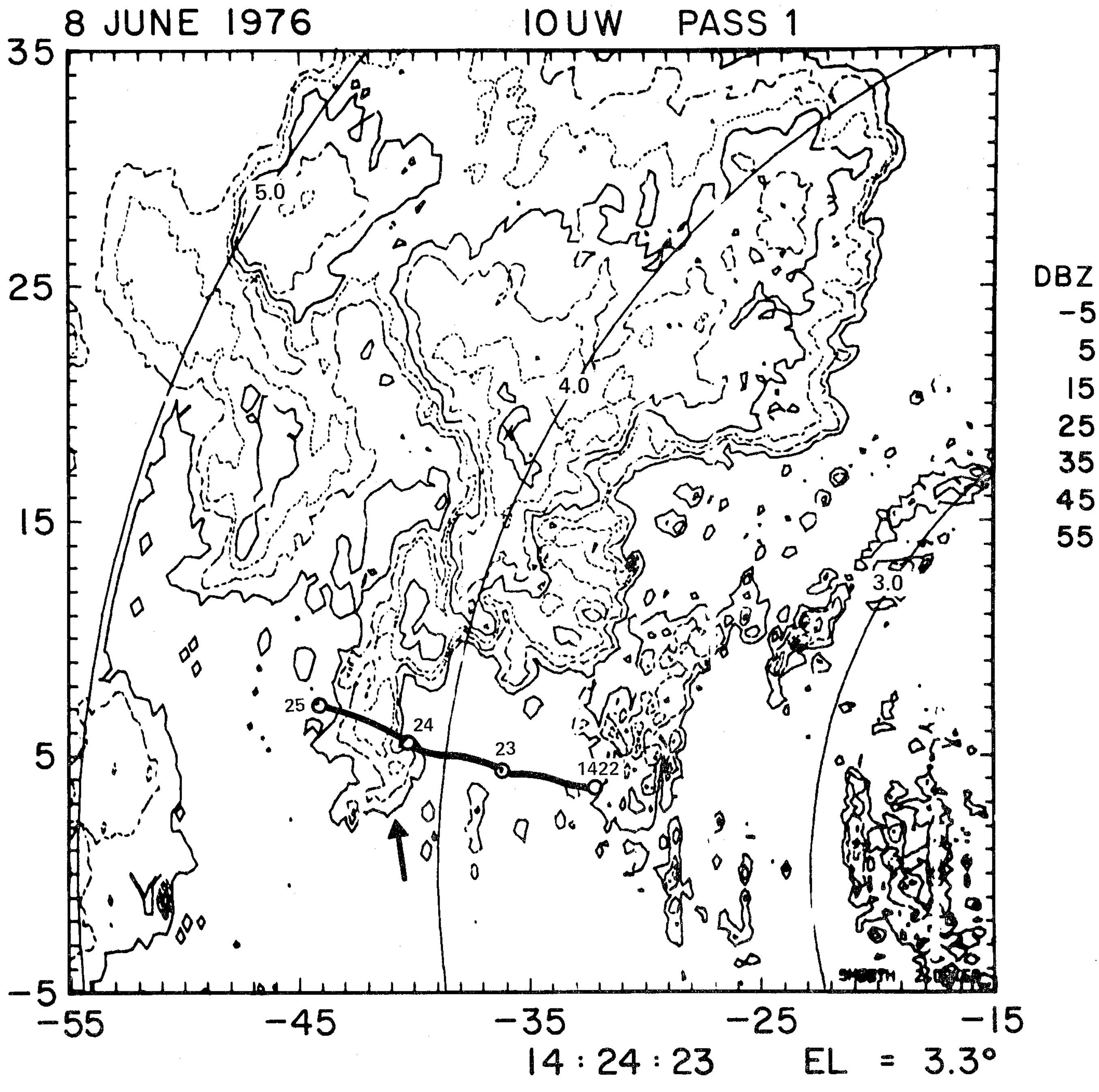

Fig. 5a. Radar reflectivity on 40 km x 40 km PPI map at 14:24:23 and 3.3° elevation angle showing corrected 10UW track (heavy line) for Pass 1 from 1422 to 1425. Altitude of 10UW is 4.7 - 4.8 km. Track is marked and labeled every minute. Reflectivity contours are every 10 dBZ beginning at -5 dBZ. Constant altitude arcs are at 3.0 km, 4.0 km and 5.0 km.

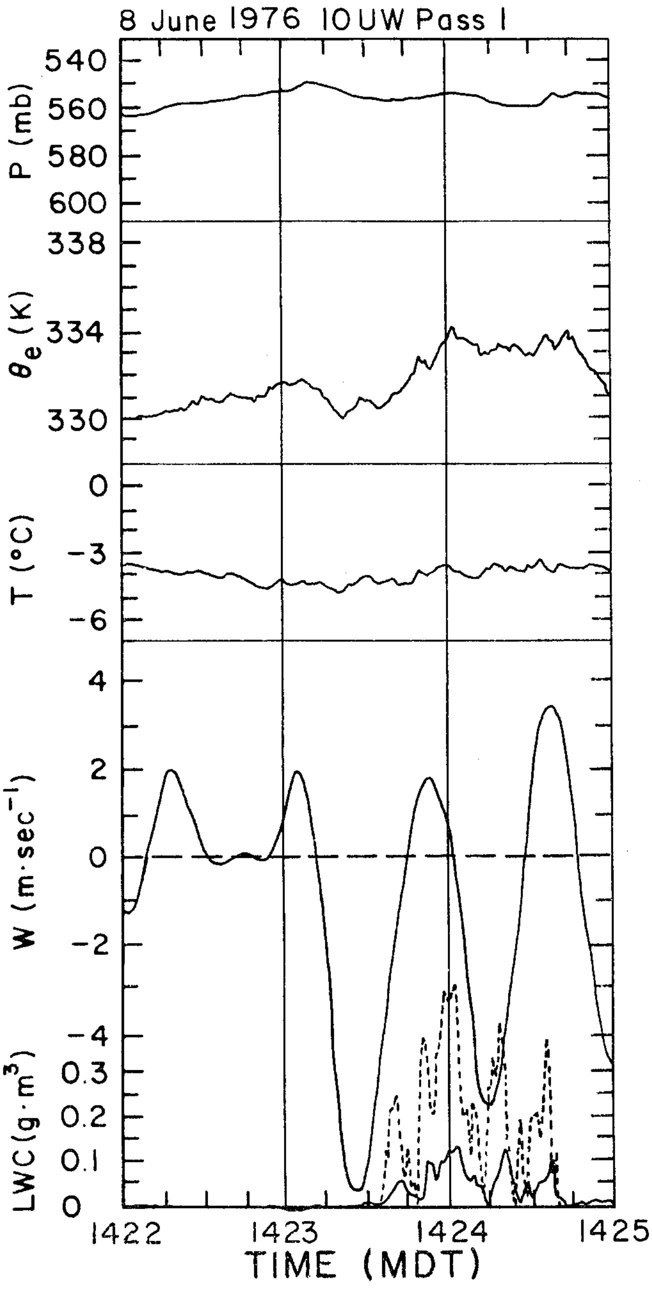

Fig. 5b. Data from 10UW for Pass 1 from 1422 to 1425 showing pressure, θ_e, temperature, vertical airspeed, and liquid water content from the J-W probe (solid line) and the integrated FSSP spectra (dashed lines). Time ticks are every 15 seconds.

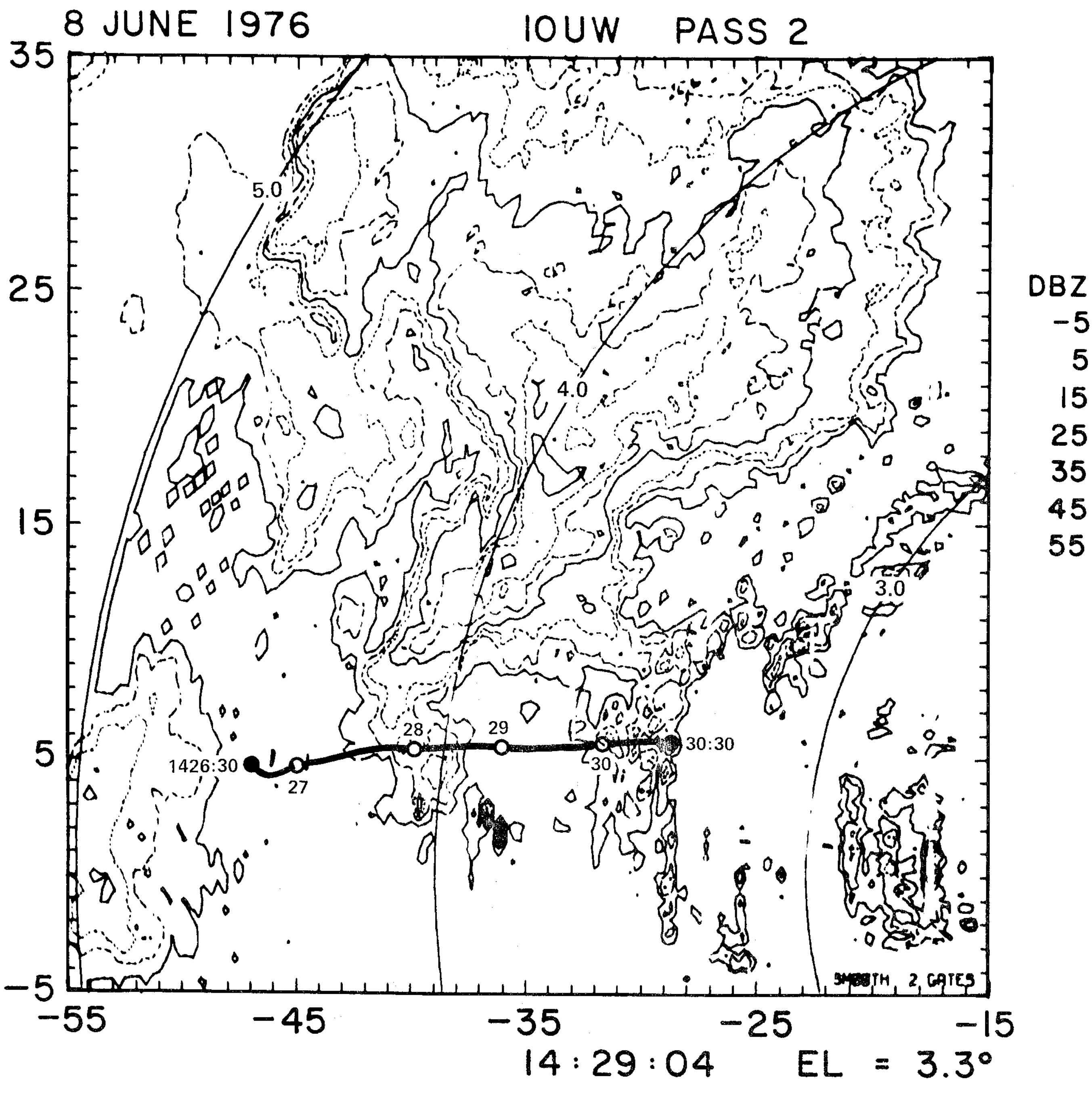

Fig. 6a. Same as Fig. 5a except PPI is at 14:29:04, and track is for Pass 2 from 14:26:30 to 14:30:30. Altitude of 10UW is 4.6 - 4.9 km.

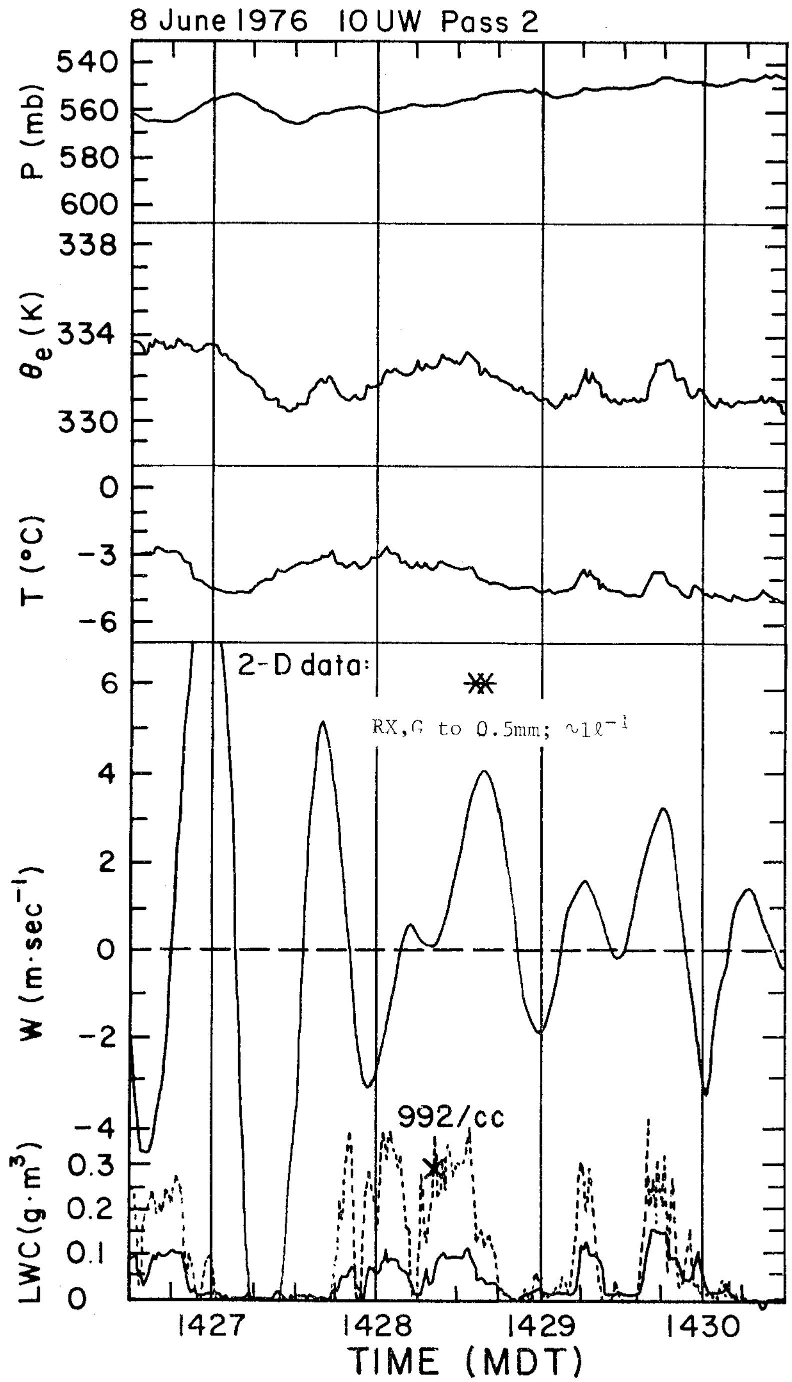

Fig. 6b. Same as Fig. 5b except for Pass 2 from 14:26:30 to 14:30:30. Data summary from the 2-D probe is plotted below the temperature trace with the following key: UX, unrimed crystals; LX, lightly rimed crystals; RX, rimed crystals; D, dendritic crystal; A, aggregate; G, graupel. Size of the largest particle diameter and a rough estimate of concentration are given when appropriate. A soot-coated cloud droplet slide sample is plotted on the LWC trace with the total droplet concentration given.

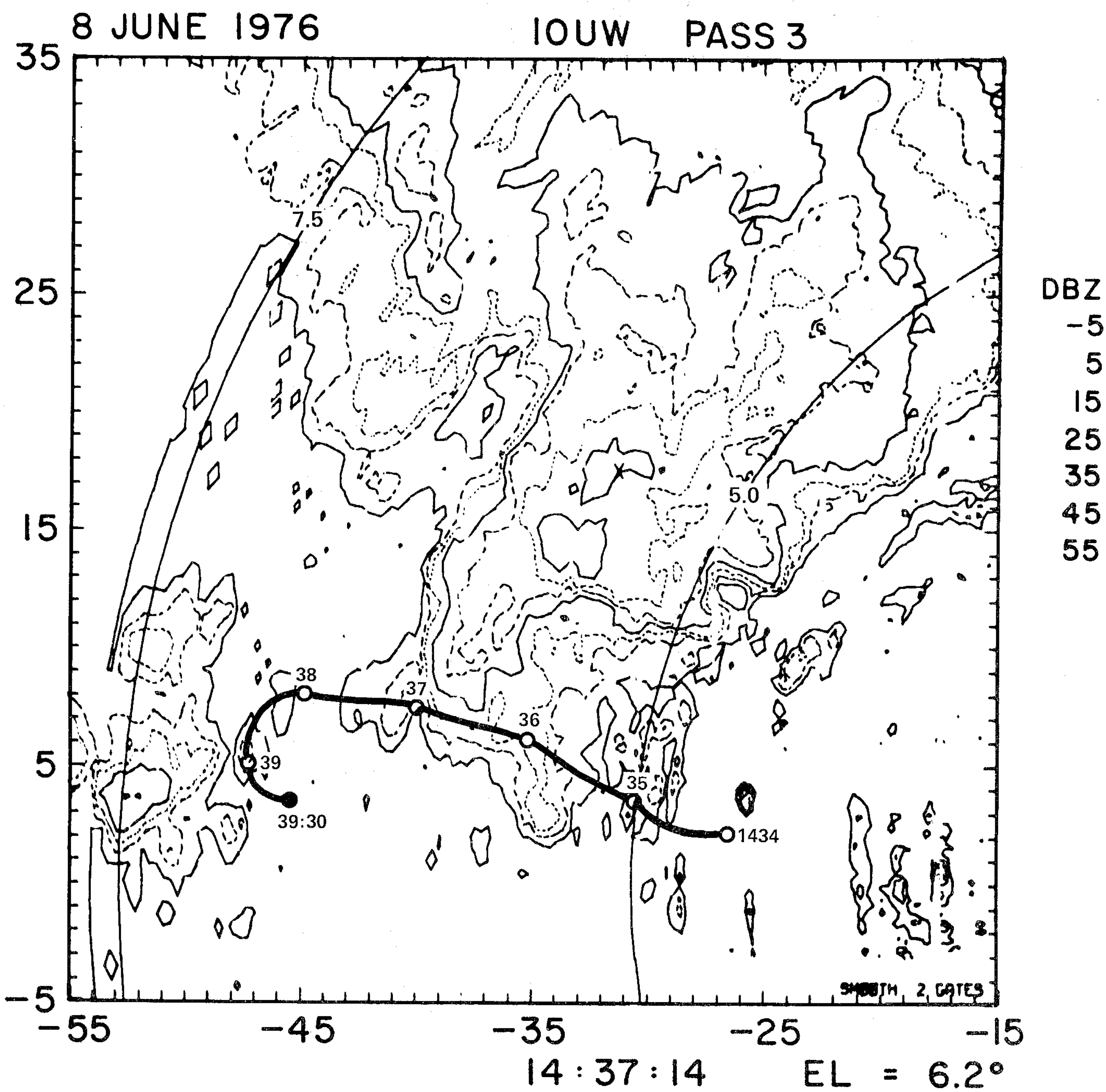

Fig. 7a. Same as Fig. 5a except PPI is at 14:37:14 and 6.2° elevation angle, and track is for Pass 3 from 14:34:00 to 14:39:30. Altitude of 10UW is 4.9 - 5.1 km. Constant altitude arcs are at 5.0 km and 7.5 km.

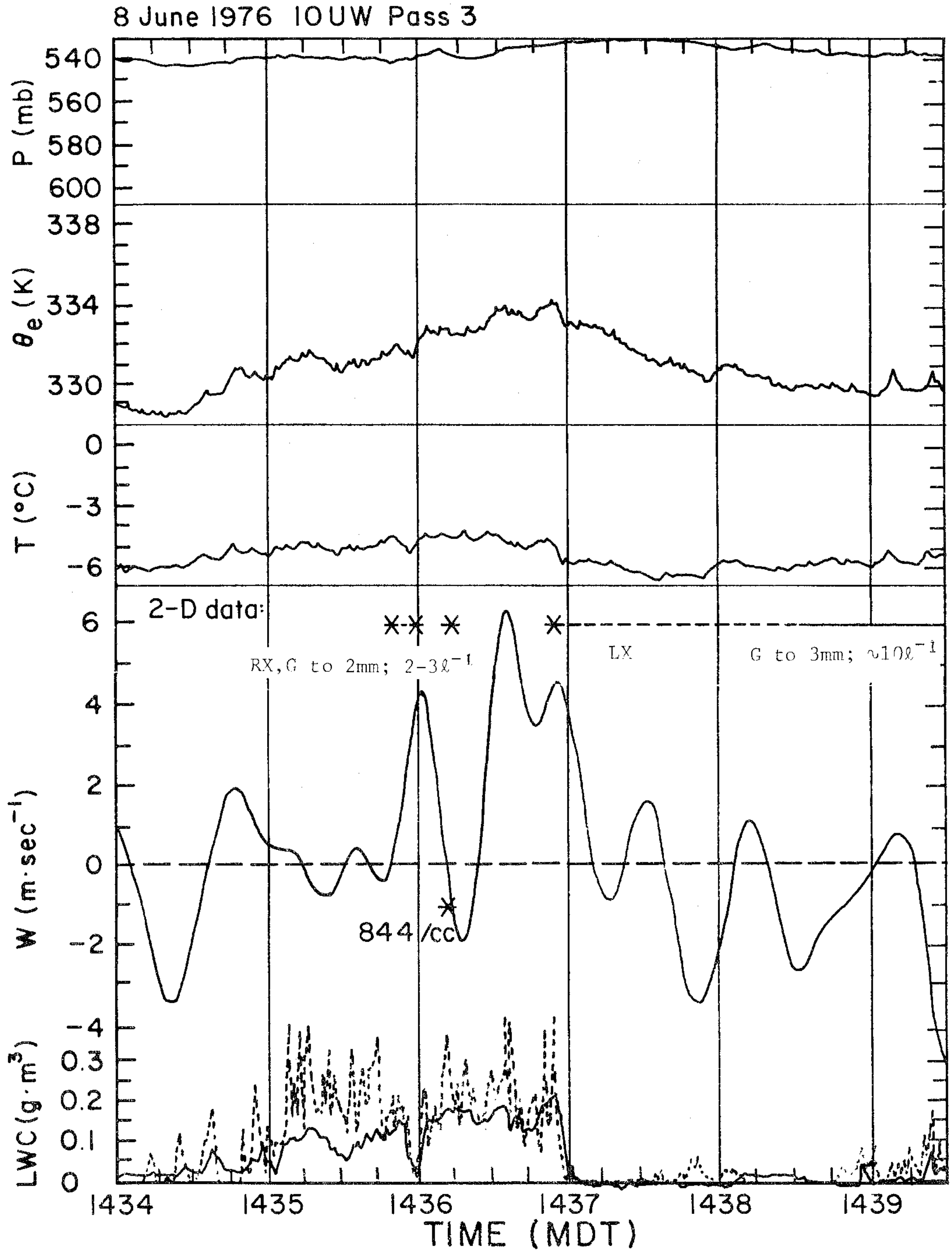

Fig. 7b. Same as Fig. 6b except for Pass 3 from 14:34:00 to 14:39:30.

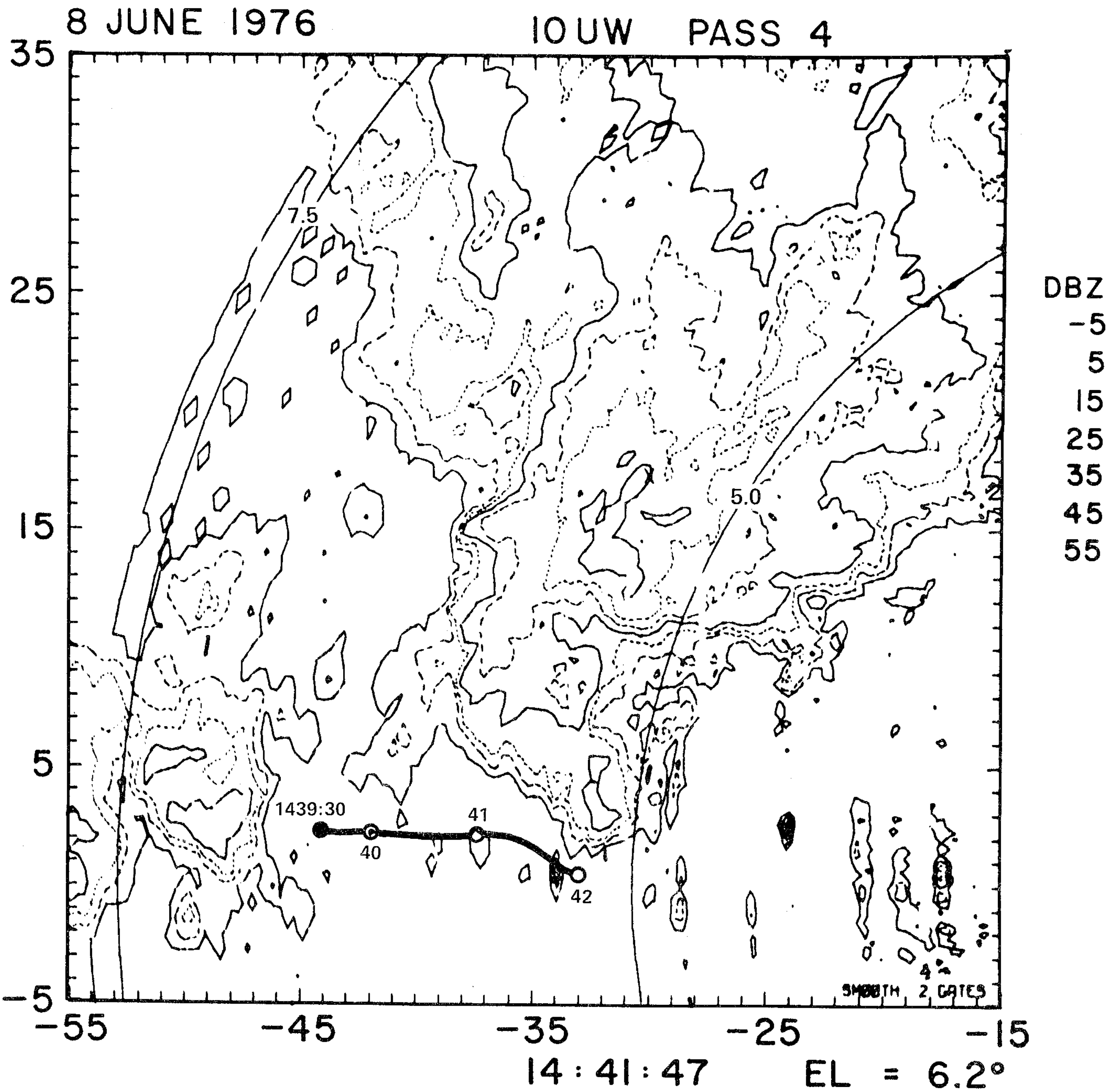

Fig. 8a. Same as Fig. 7a except PPI is at 14:41:47, and track is for Pass 4 from 14:39:30 to 14:42:00. Altitude of 10UW is 5.0 - 5.1 km.

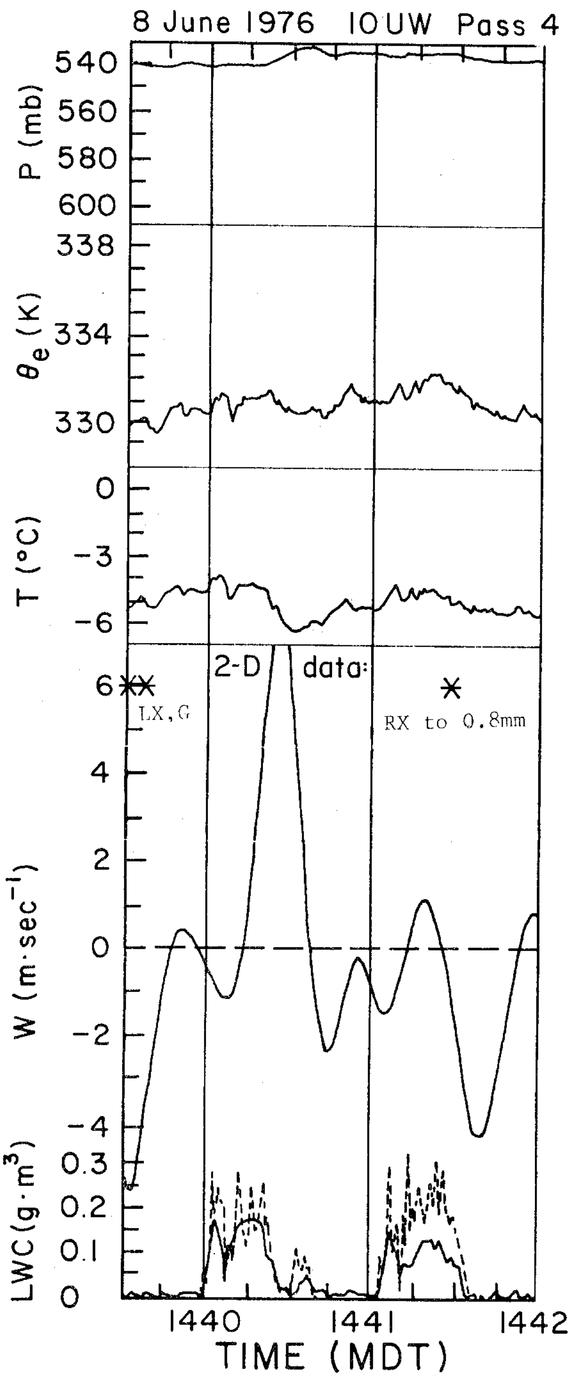

Fig. 8b. Same as Fig. 6b except for Pass 4 from 14:39:30 to 14:42:00.

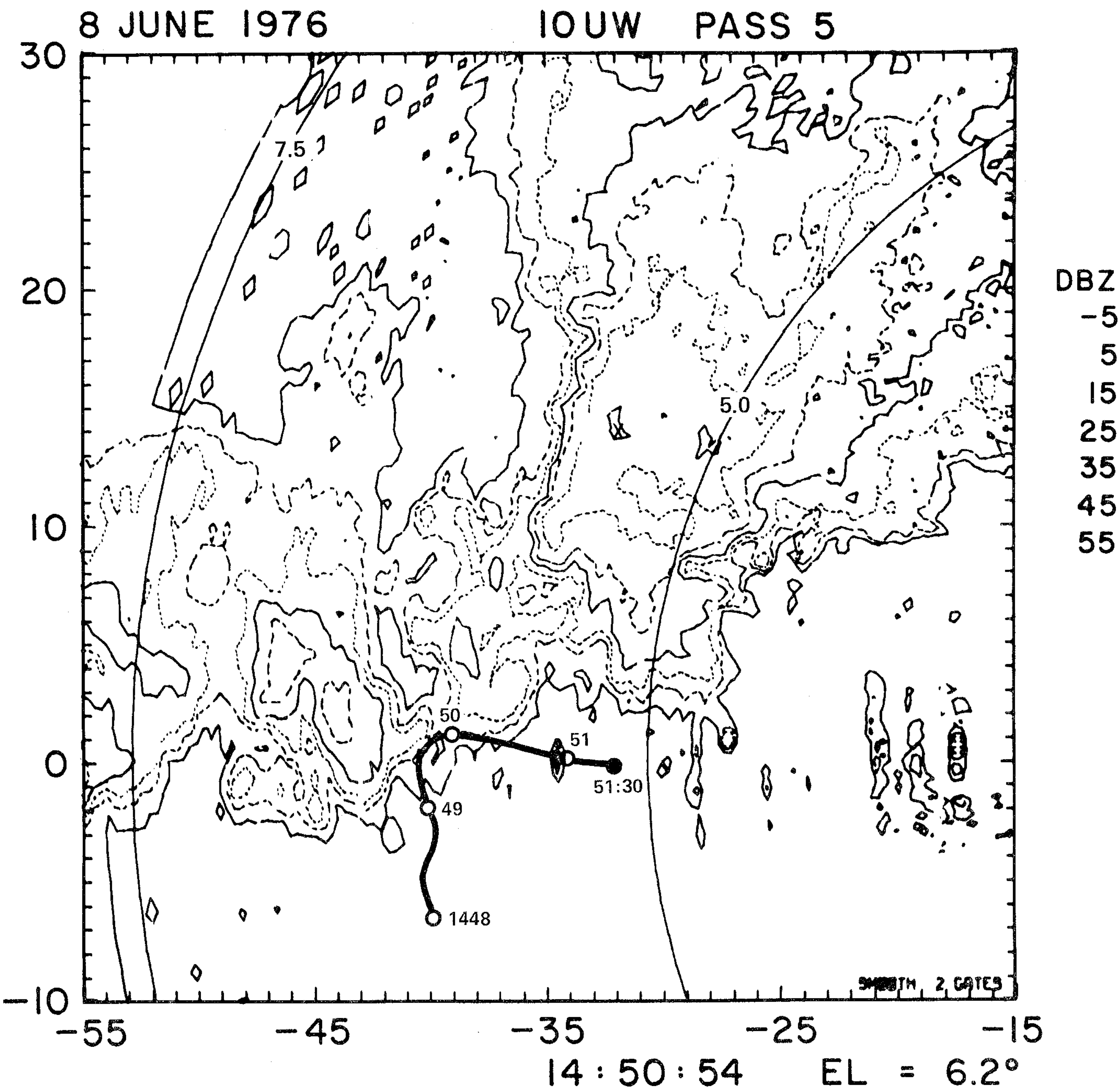

Fig. 9a. Same as Fig. 7a except PPI is at 14:50:54, and track is for Pass 5 from 14:48:00 to 14:51:30. Altitude of 10UW is 4.9 - 5.0 km. PPI area has shifted 5 km south from Fig. 8a.

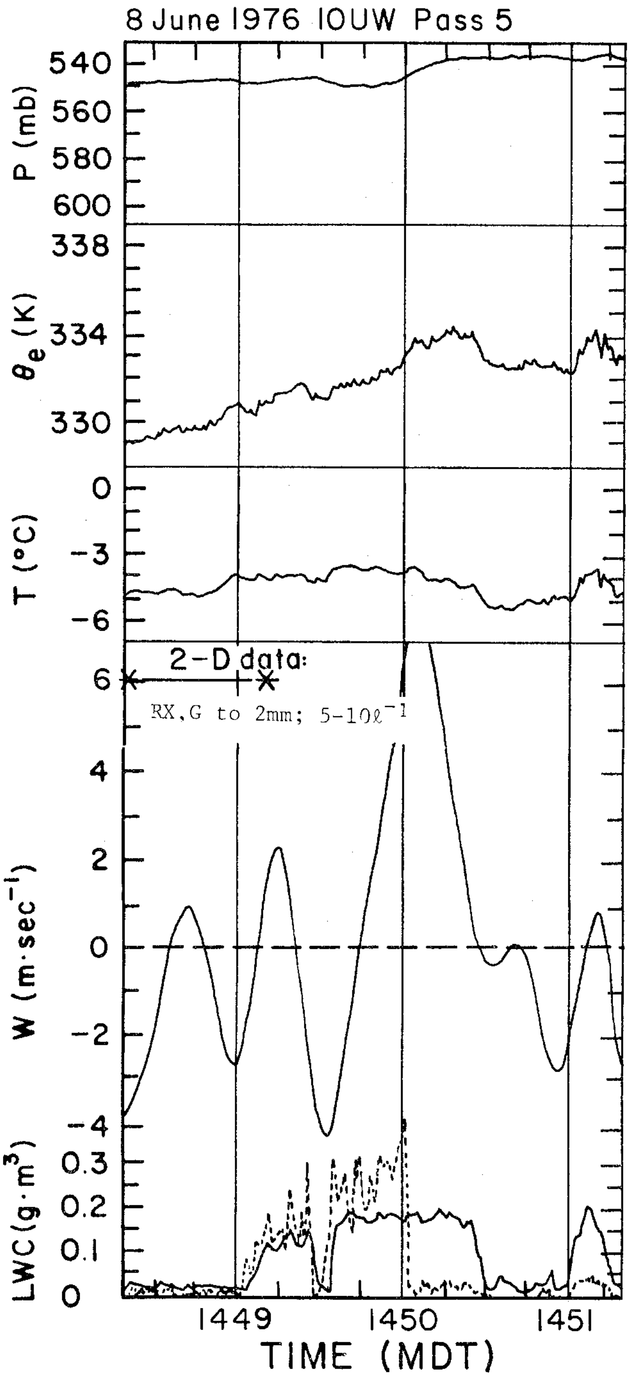

Fig. 9b. Same as Fig. 6b except for Pass 5 from 14:48:15 to 14:51:20.

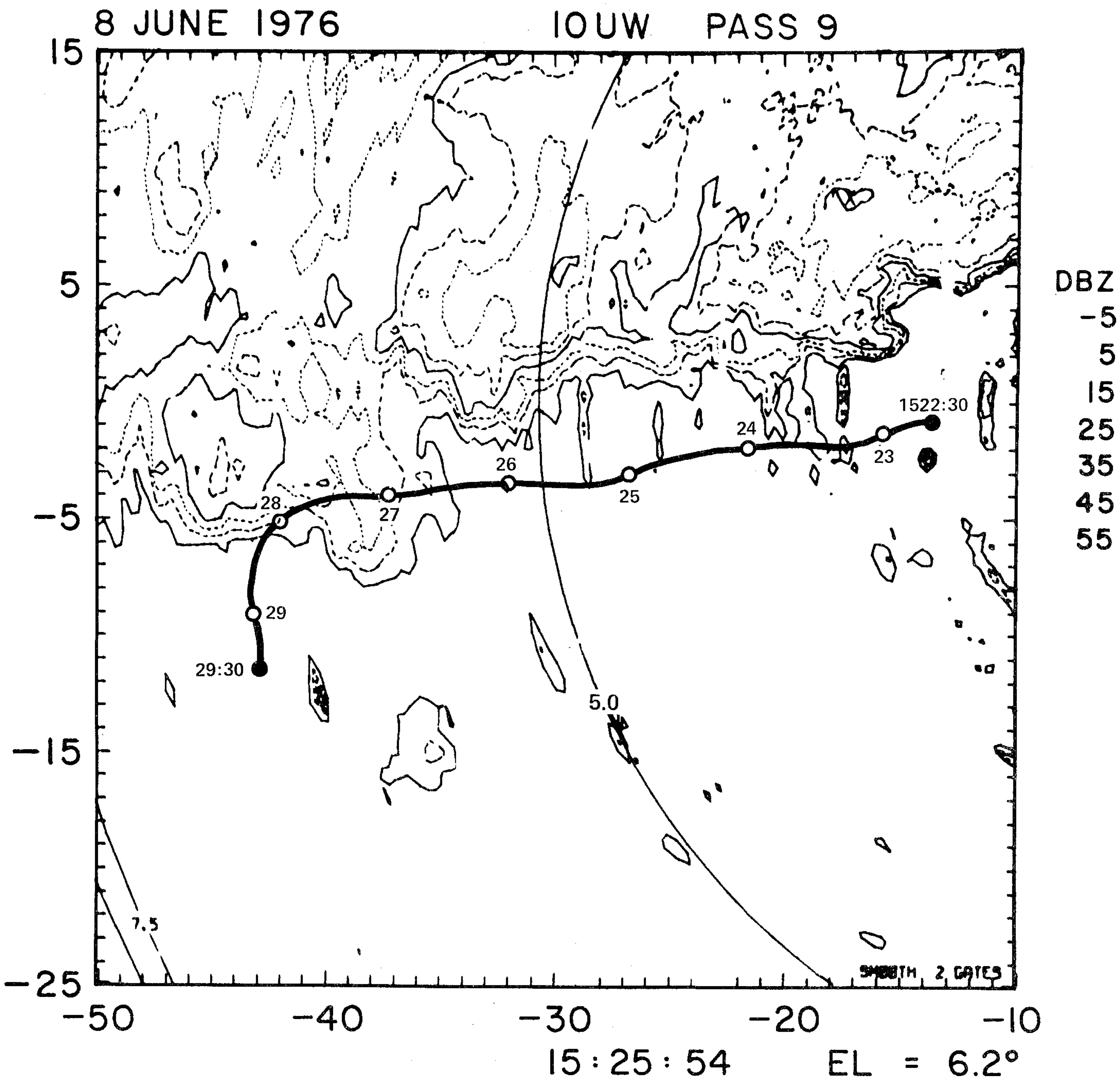

Fig. 10a. Same as Fig. 7a except PPI is at 15:25:54, and track is for Pass 9 from 15:22:30 to 15:29:30. Altitude of 10UW is 4.0 - 4.3 km. PPI area has shifted 5 km east and 15 km south from Fig. 9a.

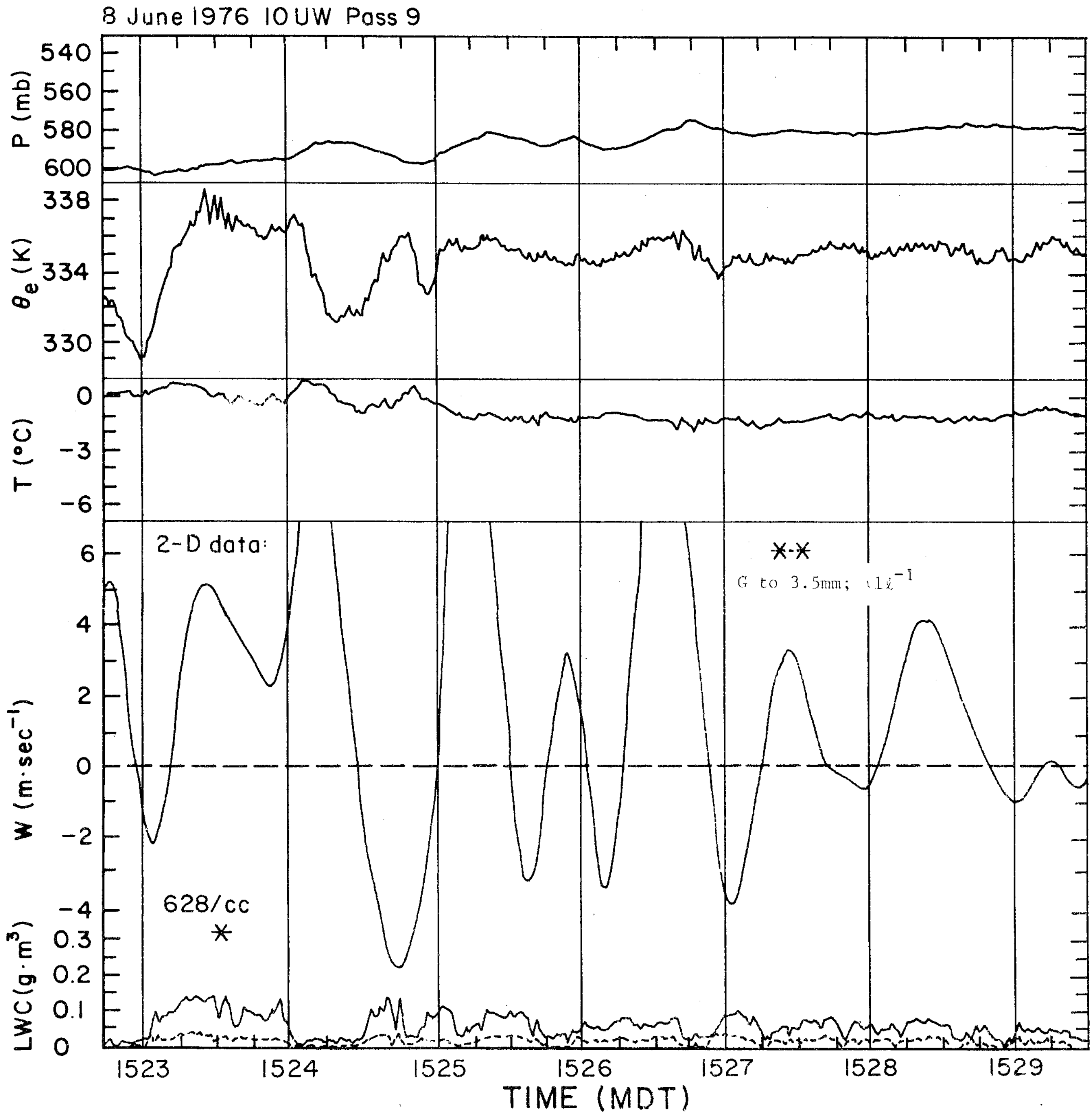

Fig. 10b. Same as Fig. 6b except for Pass 9 from 15:22:45 to 15:29:30.

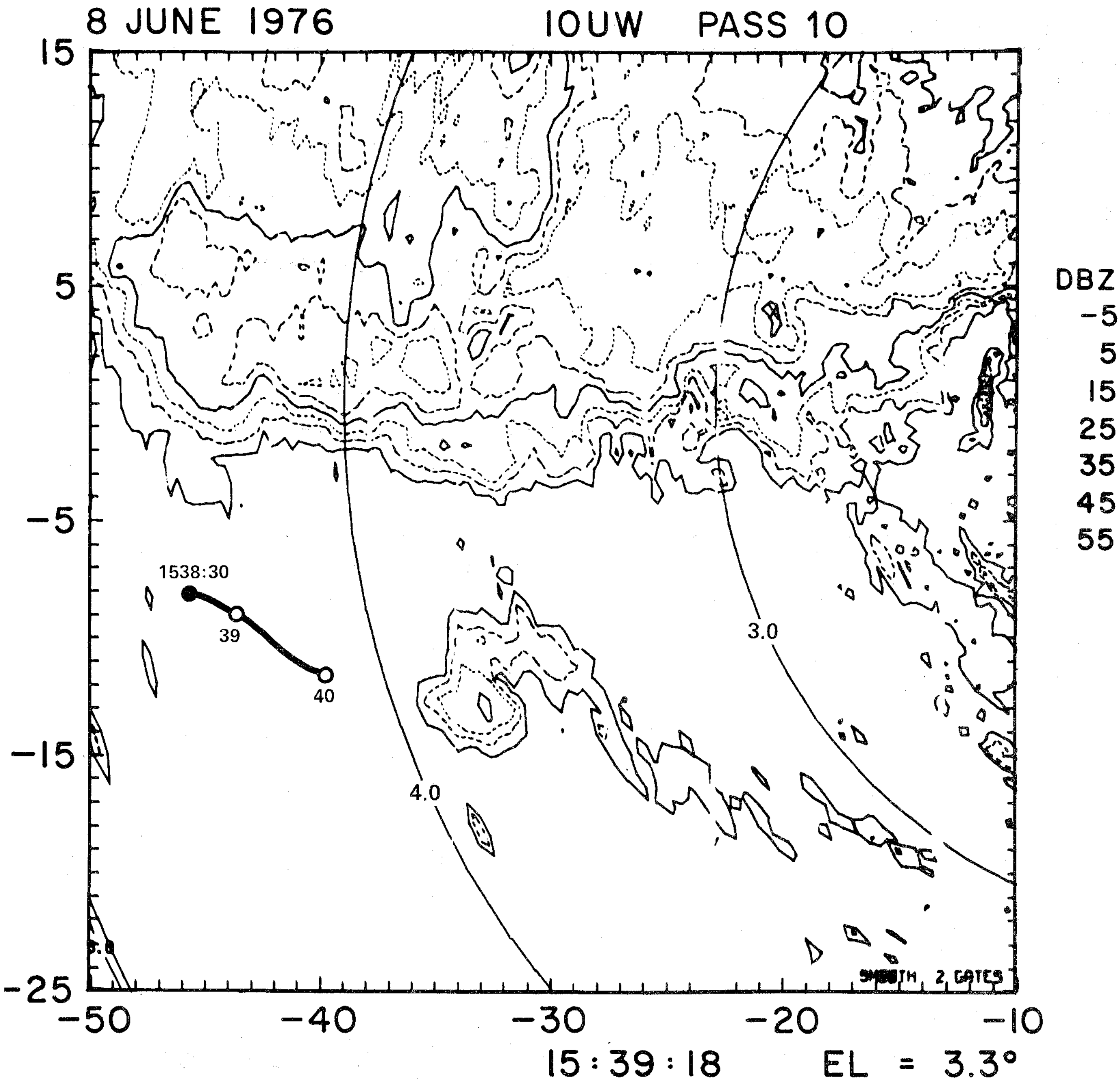

Fig. 11a. Same as Fig. 7a except PPI is at 15:39:18 and 3.3° elevation angle, and track is for Pass 10 from 15:38:30 to 15:40:00. Altitude of 10UW is 4.7 - 4.8 km. Constant altitude arcs are at 3.0 km and 4.0 km.

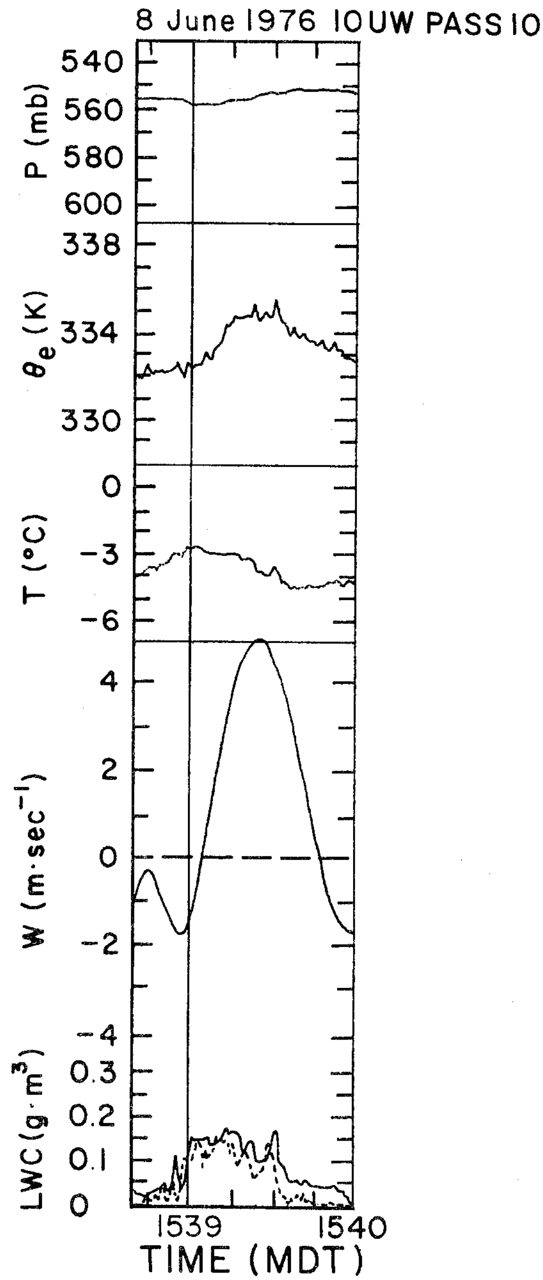

Fig. 11b. Same as Fig. 5b except for Pass 10 from 15:38:40 to 15:40:00.

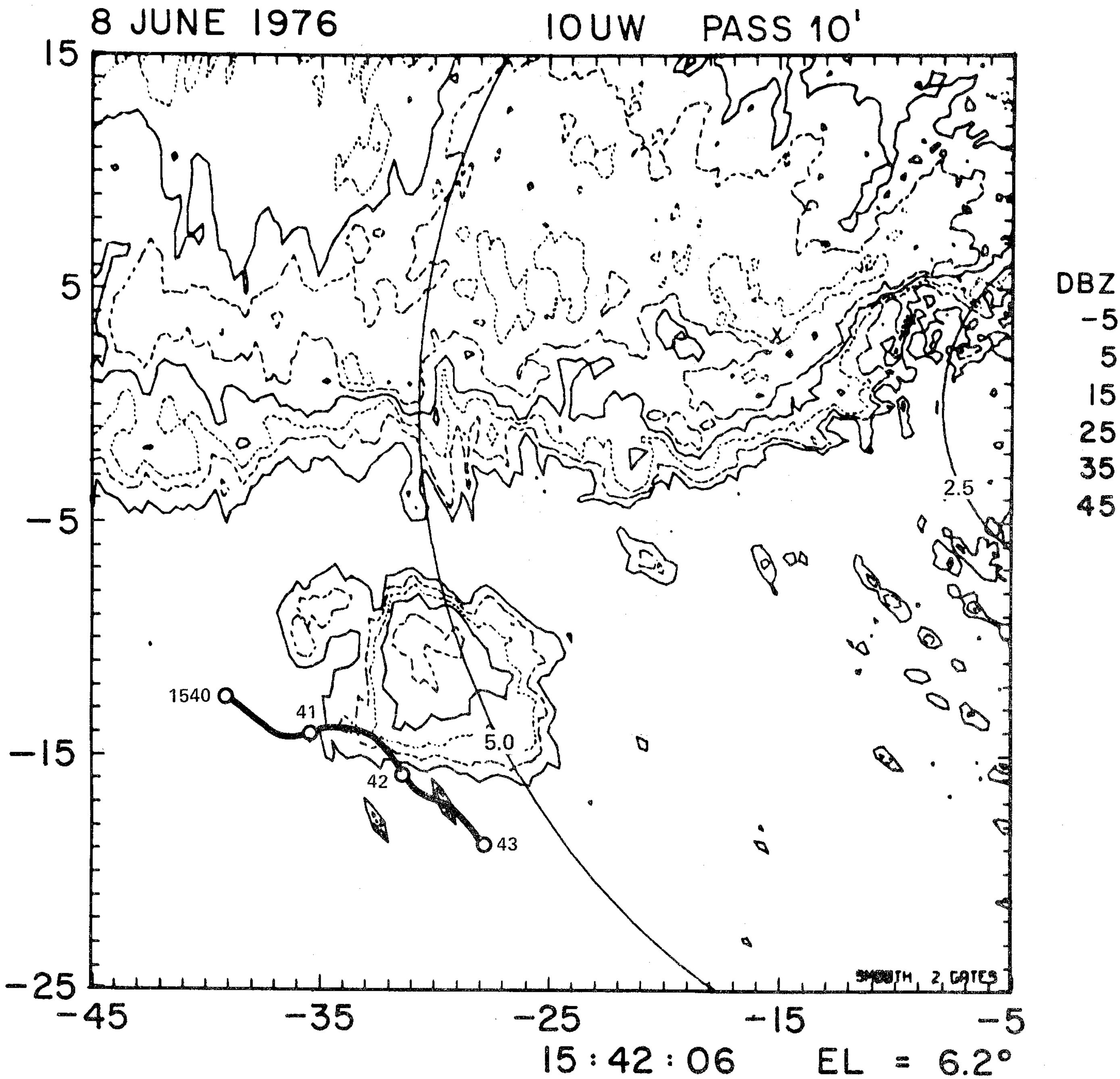

Fig. 12a. Same as Fig. 7a except PPI is at 15:42:06, and track is for Pass 10' from 1540 to 1543. Altitude of 10UW is 4.7 - 4.9 km. PPI area has shifted 5 km east from Fig. 11a.

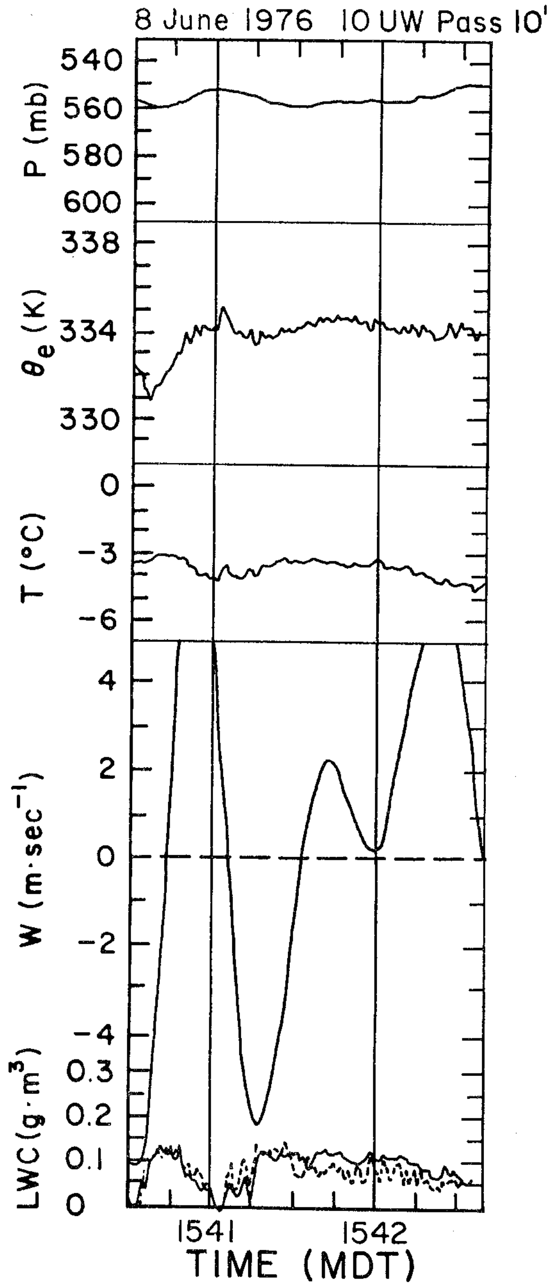

Fig. 12b. Same as Fig. 5b except for Pass 10' from 15:40:30 to 15:42:40.

area due to a power failure, collecting precipitation samples enroute to Laramie.

B. SOUTH DAKOTA SCHOOL OF MINES & TECHNOLOGY T-28 510MH

The T-28 made eight passes of the southern flank of the main storm and of smaller storm cells in the vicinity of the main storm. The first pass began at about 1433 and the eighth pass ended at about 1544. The tracks of the passes, presented in Figs. 13a, 14a, ... 20a, did not show any consistent error from occasions of radar skinpaint, but have been corrected for a southeastern storm motion of 5 m s^{-1} to 1500 and a southeastern motion of 3 m s^{-1} after that time. The resulting track should be within 1 km of true position. As with the 10UW tracks, the radar data plotted with the tracks are in PPI format while the T-28 was close to constant altitude. Ground clutter and artifacts have not been removed from the radar data presented.

Pressure, temperature, θ_e (assuming 100% relative humidity), vertical airspeed, J-W and FSSP liquid water contents, and a coarse summary of ice particle data from the 2-D probe are presented in Figs. 13b, 14b, ... 20b. Only in-cloud θ_e values greater than 330 K are plotted, since 100% relative humidity is assumed. The J-W probe appeared to work well this day, within its accuracy limitations, and the FSSP LWC values plotted with the J-W LWC have been corrected for the coincidence error mentioned in the aircraft instrumentation appendix. The 2-D probe data summary is similar to that presented with 10UW data. As with 10UW, the data times presented were chosen to include encounters with cloud water, ice particles, and/or significant updrafts or downdrafts in or near the clouds penetrated.

Passes 1, 3, 4, and 5 were made through the same cell as 10UW's passes 1-4, with T-28's passes 3-5 taking place after 10UW's investigation of the cell. Between passes 1 and 3, the T-28 made an investigative excursion into a developing storm element to the southwest of the main storm. By 1500, this element had begun to intensify and merge with the main storm. While a line of cells developed to the west, this element was the only one to organize with the main storm until around 1600. Passes 2 and 2' (Figs. 14b and 14c) detected relatively strong updrafts and fairly high LWC on the south-southwest side of this storm element. Peak updrafts and LWC in pass 2 were 20 m s^{-1} and 1.4 g m^{-3} respectively, with 7 m s^{-1} and 1.0 g m^{-3} in pass 2'. Ice particles were present in the early part of pass 2, in and near the higher reflectivity area of the storm, and through the strong updraft that occurred prior to 1439. The shift from unrimed to rimed crystals as the LWC increased was notable. No ice particles were detected in the weaker conditions of pass 2' except for a couple of small, unrimed dendrites in the updraft at 1442:25.

Pass 1 (Fig. 13b) by the T-28 was coordinated with 10UW's pass 3. Although the T-28 was farther south than 10UW, its data also show that the strongest updrafts ($\sim$ 6 m s^{-1}) occurred on the western side of the cell. The 2-D data show larger ice particles in the updraft at the -15°C level ($\sim$ 6.0 km) than at 10UW's altitude (-5°C at $\sim$ 5.0 km). Values of θ_e were a few degrees lower than those measured by 10UW. Passes 3, 4, and 5 (Figs. 15b - 17b) were made as the cell was merging with the main reflectivity core of the storm after $\sim$ 1450. The strongest updraft in pass 3 (13 m s^{-1} maximum) was located on the east side of the cell's reflectivity boundary, with LWC's greater than 1.0 g m^{-3} in that area. Values of θ_e in the updraft were nearly 334 K, and no ice particles were present in the updraft core. Pass 4 was along a nearly identical flight path as pass 3. In this pass the updraft, though still present, was much weaker and the LWC's were slightly lower. Also, a low concentration of ice particles was detected through most of the updraft. Calculated θ_e values were about the same as in pass 3. Pass 5 was a north-south penetration of the area east of the cell which by this time was rather diffuse. Early in the pass where reflectivities were greater than -5dBZ (see Fig. 17a), ice particles were detected that were mostly unrimed. Liquid water contents reached 1.0 g m^{-3} maximum in weak updrafts, but were generally less than 0.4 g m^{-3}. After about 1516:50, liquid water contents were consistently higher and ice particles were no longer present. Two updrafts were encountered between 1517 and 1518, with a maximum strength of $\sim$ 17 m s^{-1}, and θ_e values peaked at $>$ 335 K. These features occurred in the same area east of the cell discussed in the two earlier passes, and showed signs of continued growth in this region.

Passes 6 and 7 by the T-28 were investigations of clouds developing along the southern boundary of the main storm mass. These passes were made shortly after 10UW's pass 9 and about 5 km farther south. Conditions were weak with mostly downdrafts and very little ice as evident from the pass 6 data in Fig. 18b. Data from pass 7 (Fig. 19b) are not significantly different except for increased ice particles, particularly in size. The radar data at $\sim$ 1530 show reflectivities to 15 dBZ at the 8.5 km level, indicating that the ice particles detected on pass 7 could have originated above the T-28's altitude (6.0 km).

In coordination with 10UW's Pass 10', the T-28 made a penetration (Pass 8) through turrets on the west side of the developing storm element described in the 10UW section. Data from this pass, presented in Fig. 20b, show moderate updrafts (5-7 m s^{-1}), with small concentrations of graupel and unrimed crystals. Cloud water was lacking in most of the reflectivity area of the penetration, but did peak at 1.3 g m^{-3} in the updraft prior to 1542. A notable feature is the 20 m s^{-1} downdraft at 1541:30 which is well-correlated with a similar feature in the 10UW data. Values of θ_e from the T-28's pass were 2-3 degrees lower than those in 10UW's Pass 10'

In summary, 10UW and the T-28 coordinated their efforts on the southern flanks of the mature storm complex on this day. Although both aircraft consistently detected updrafts and inflow conditions in this general area, there appeared to be favored regions where developing cells were able to organize with the main storm. One example is the cell penetrated by 10UW in Passes 1-4 and by the T-28 in Passes 1, 3, 4, and 5. The first pass of 10UW was 15-20 minutes after the cell's initial radar echo, but an updraft related to this cell was detected up to one hour after this first pass. The ice particle data show continual development of the ice phase precipitation process, with some ice particles detected in updrafts encountered by both aircraft. However, the cell's reflectivity maximum merged early in its development with the main storm's core, complicating possible connections between updrafts and reflectivity structure. Another example of development in a favored region for larger scale organizations is the cell penetrated by both aircraft just before leaving the area. This cell merged with the

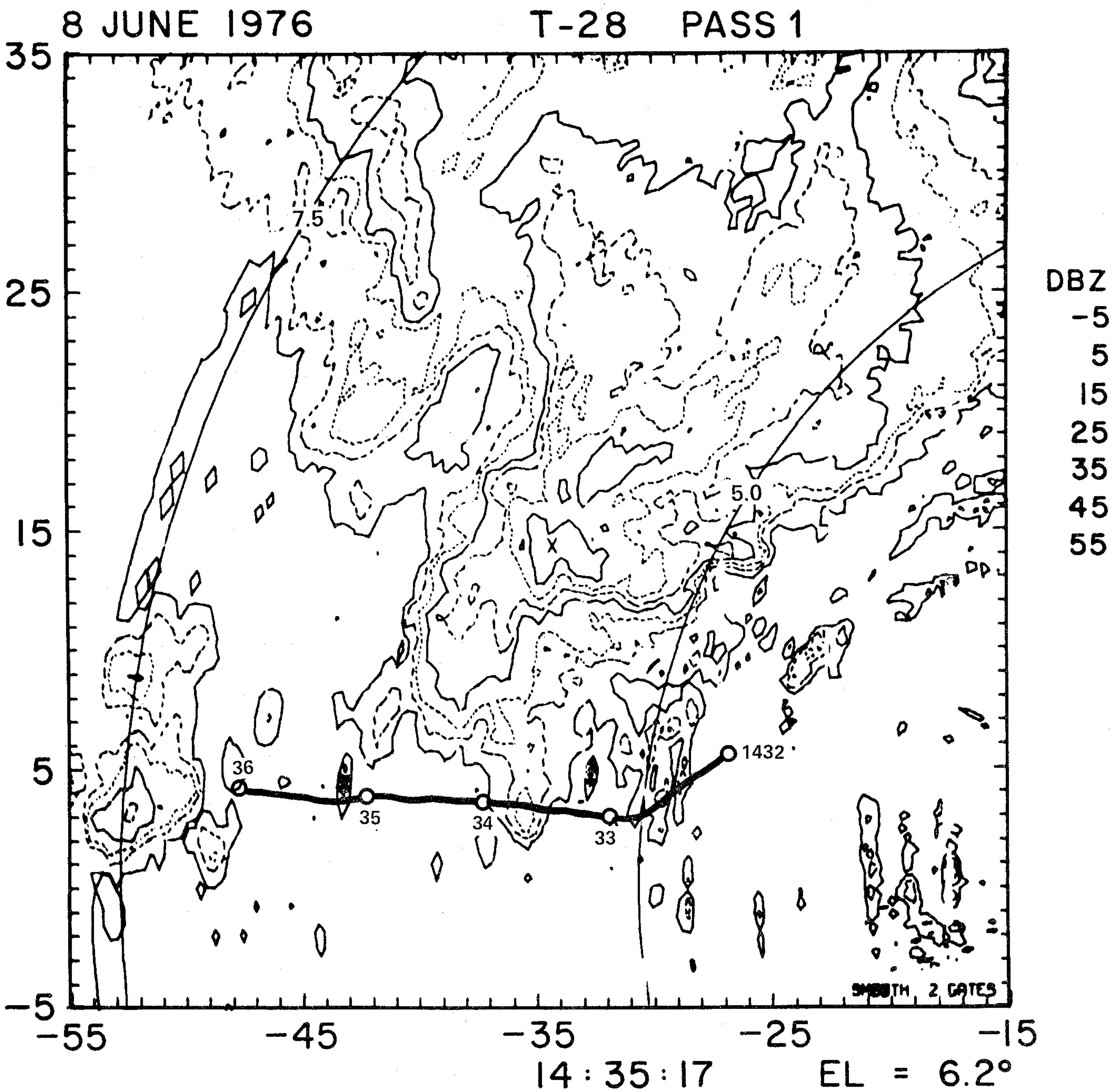

Fig. 13a. Radar reflectivity on 40 km x 40 km PPI map at 14:35:17 and 6.2° elevation angle showing corrected T-28 track (heavy line) for Pass 1 from 1432 to 1436. Altitude of T-28 is 6.2 - 6.3 km. Track is marked and labeled every minute. Reflectivity contours are every 10 dBZ beginning at -5 dBZ. Constant altitude arcs are at 5.0 km and 7.5 km.

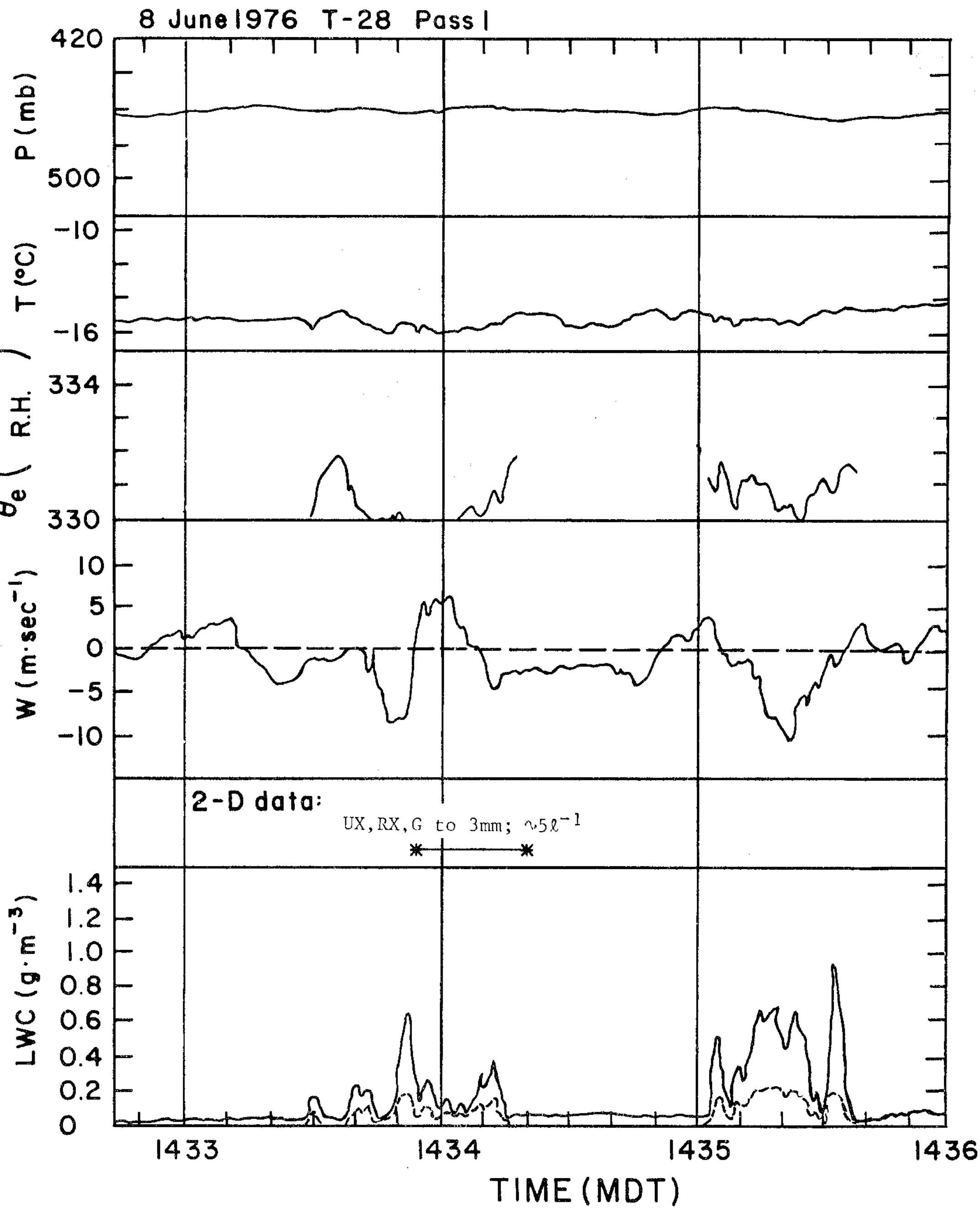

Fig. 13b. Data from T-28 for Pass 1 from 14:32:45 to 14:36:00 showing pressure, temperature, θ_e greater than 330 K (at 100% relative humidity), vertical airspeed, 2-D data summary, and liquid water content from the J-W probe (solid line) and the integrated FSSP spectra (dashed line). The 2-D data key is: UX, unrimed crystals; LX, lightly rimed crystals; RX, rimed crystals; D, dendritic crystals; A, aggregates; G, graupel. Size of the largest particle diameter, and a rough concentration are given when appropriate. Time ticks are every 10 seconds.

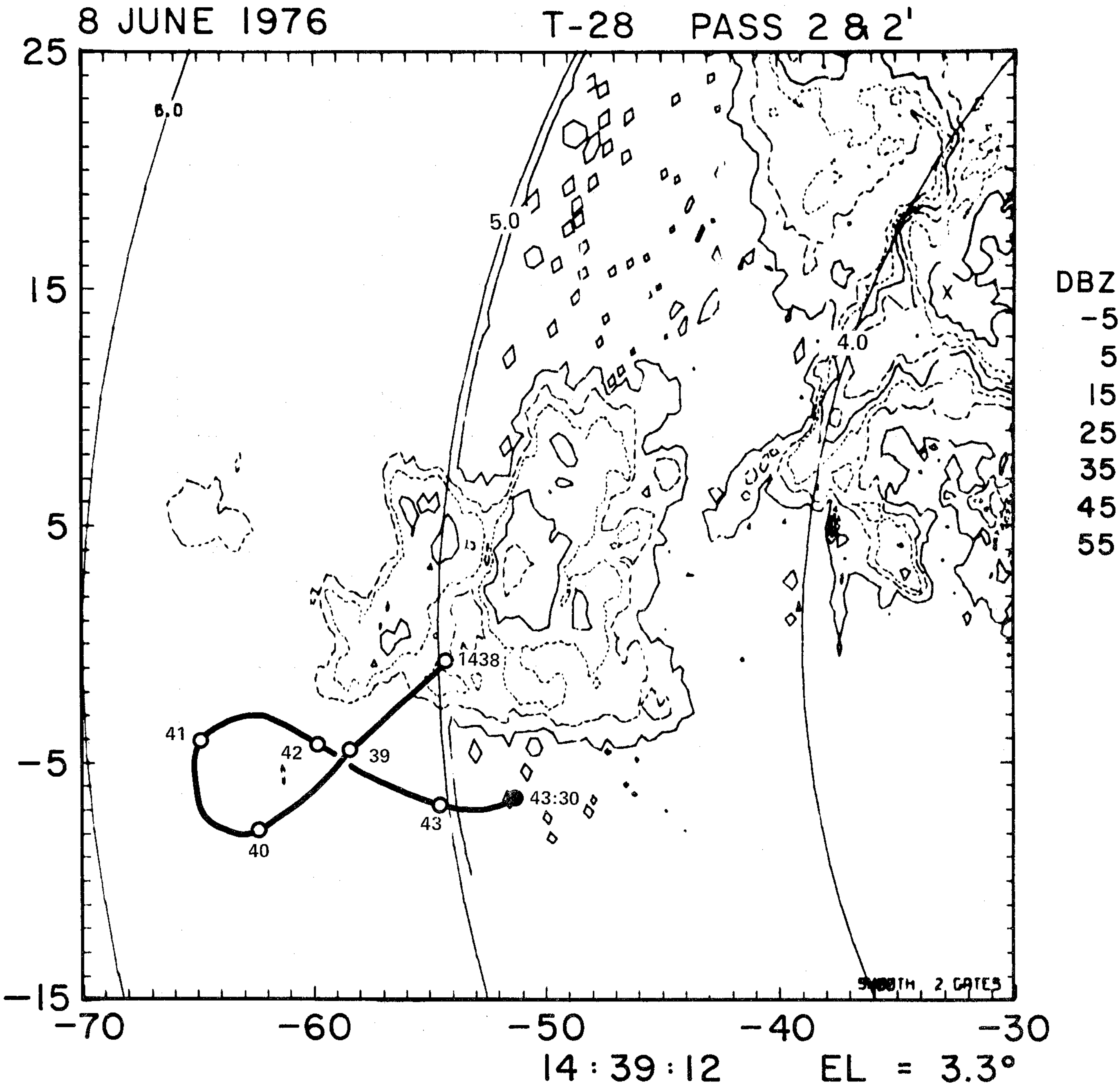

Fig. 14a. Same as Fig. 13a except PPI is at 14:39:12 and 3.3° elevation angle, and track is for Passes 2 and 2' from 14:38:00 to 14:43:30. Altitude of T-28 is 6.0 - 6.1 km. Constant altitude arcs are at 4.0 km, 5.0 km, and 6.0 km. PPI area has shifted 15 km west and 10 km south from Fig. 13a.

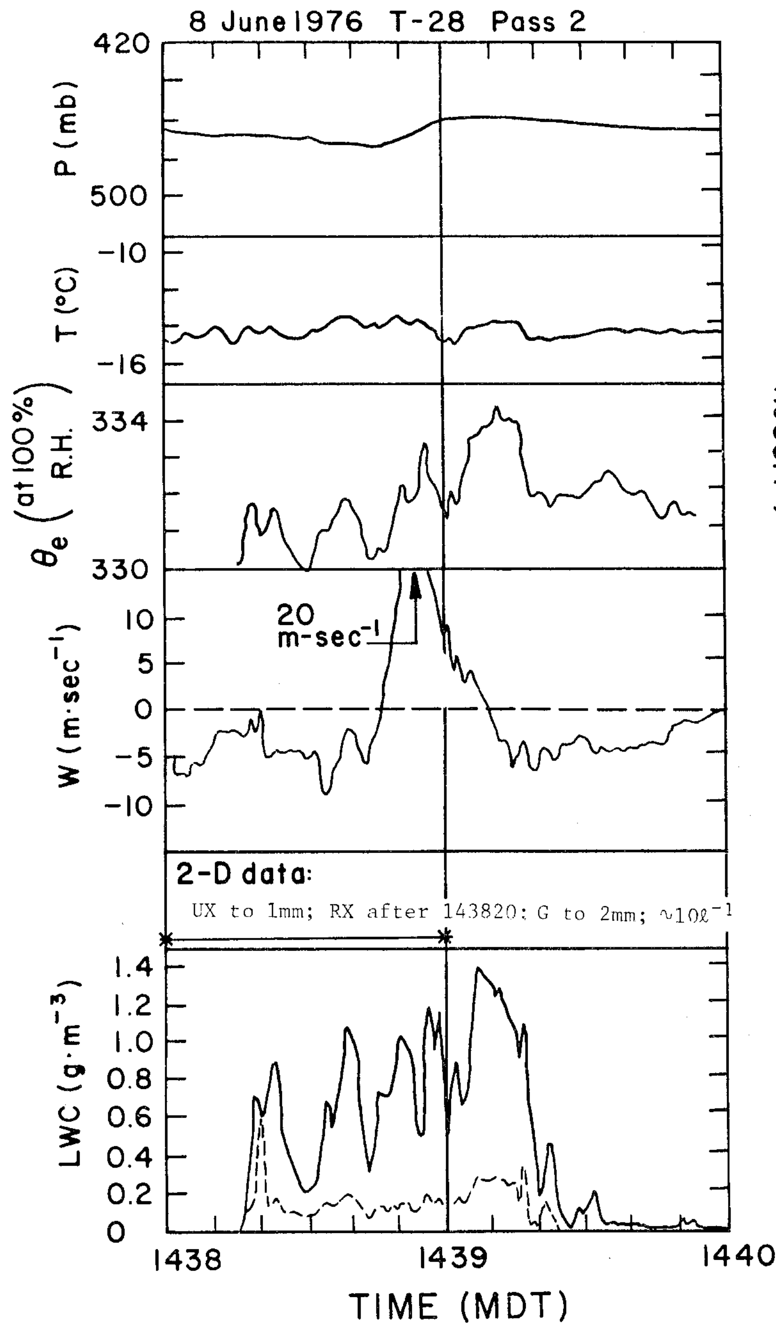

Fig. 14b. Same as Fig. 13b except for Pass 2 from 1438 to 1440.

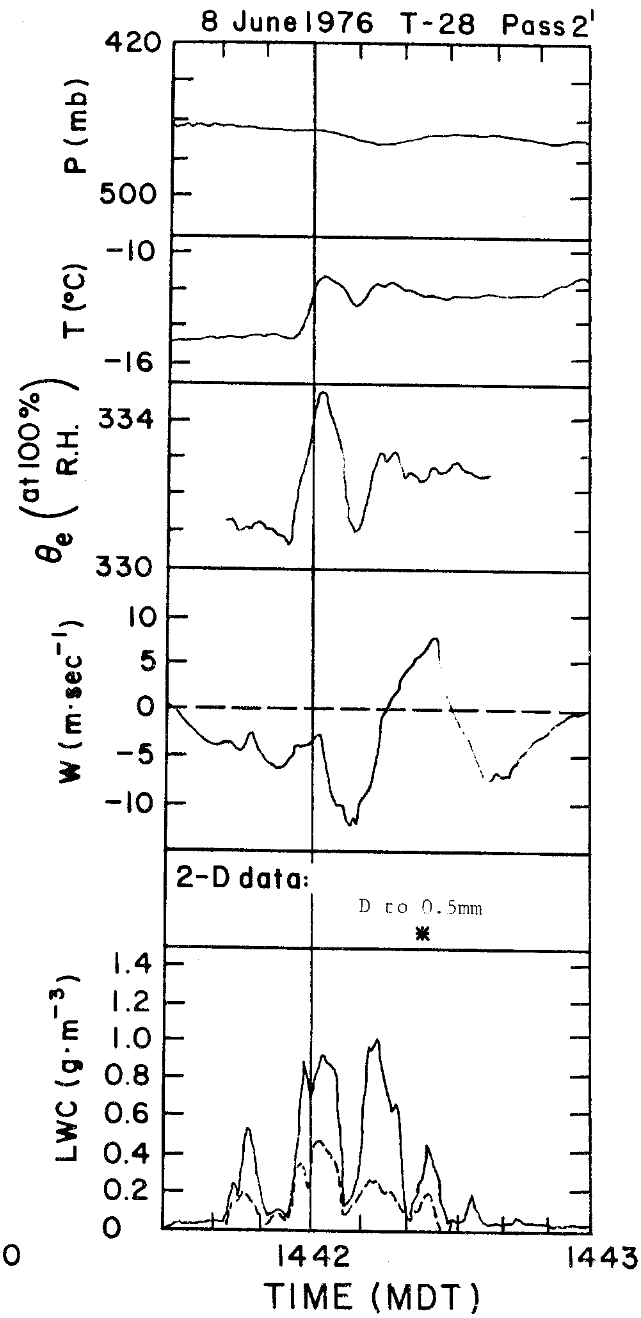

Fig. 14c. Same as Fig. 13b except for Pass 2' from 14:41:30 to 14:43:00.

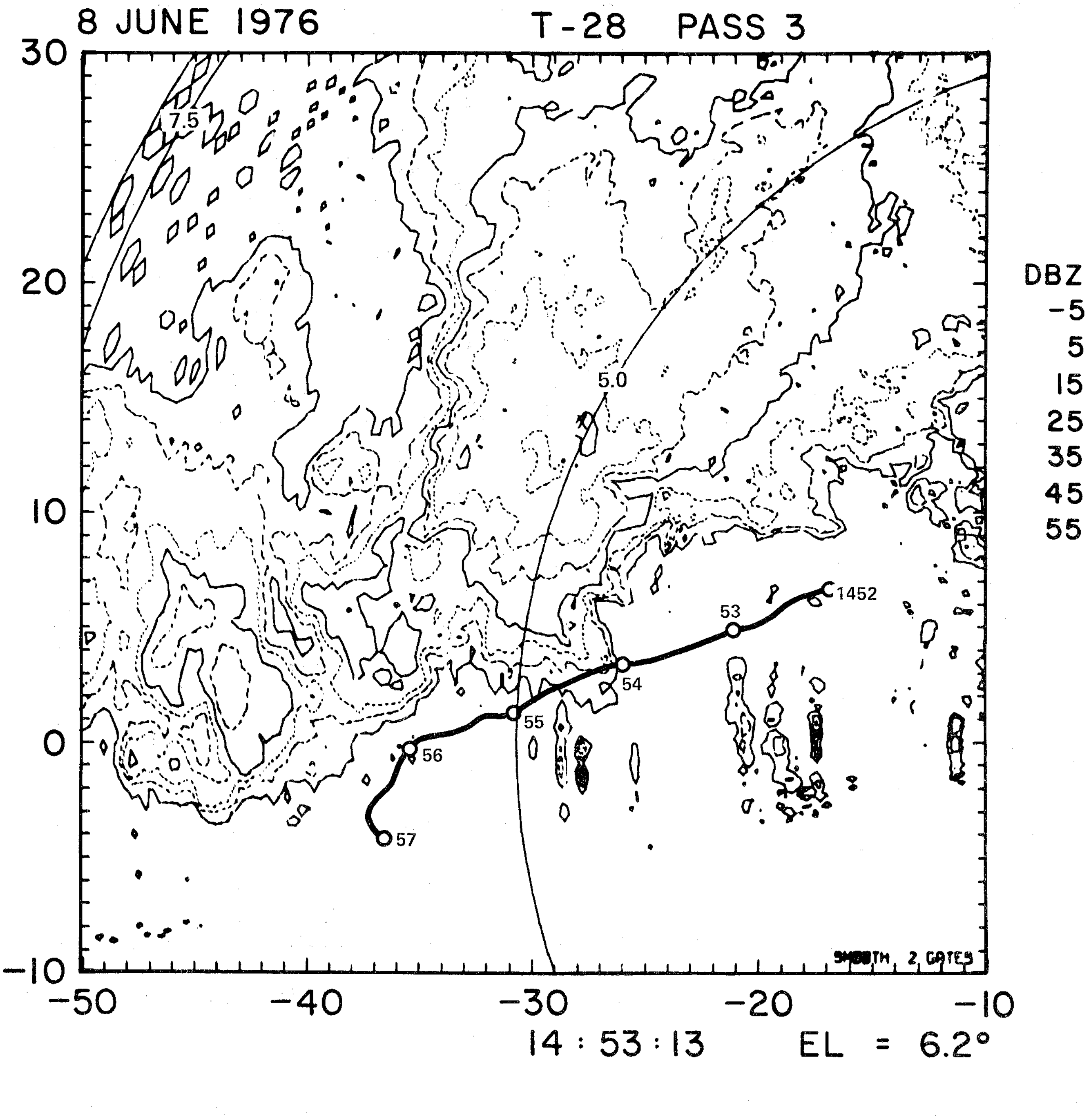

Fig. 15a. Same as Fig. 13a except PPI is at 14:53:13, and track is for Pass 3 from 1452 to 1457. Altitude of T-28 is 5.8 to 6.0 km. PPI area has shifted 20 km east and 5 km north from Fig. 14a.

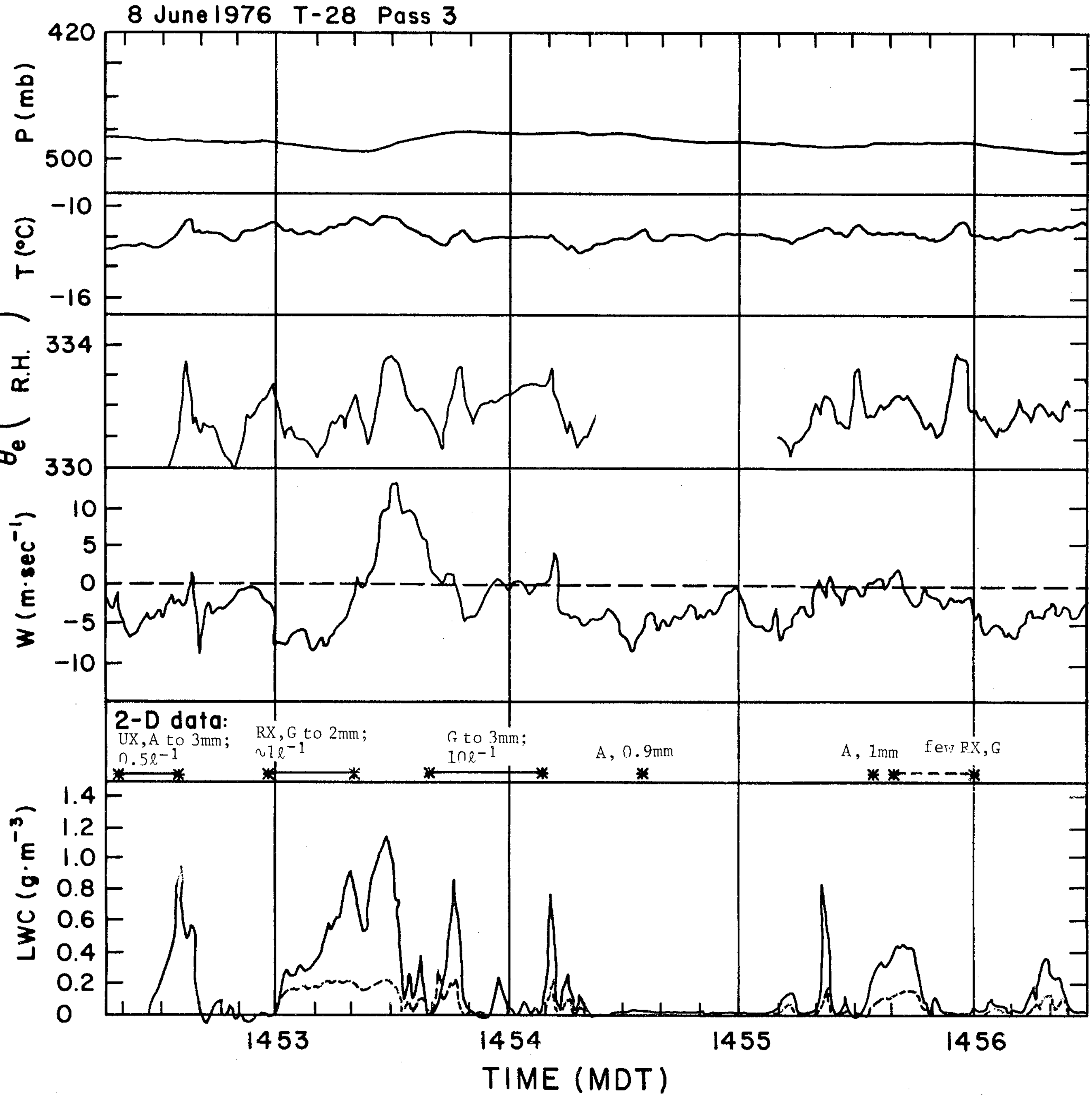

Fig. 15b. Same as Fig. 13b except for Pass 3 from 14:52:15 to 14:56:30.

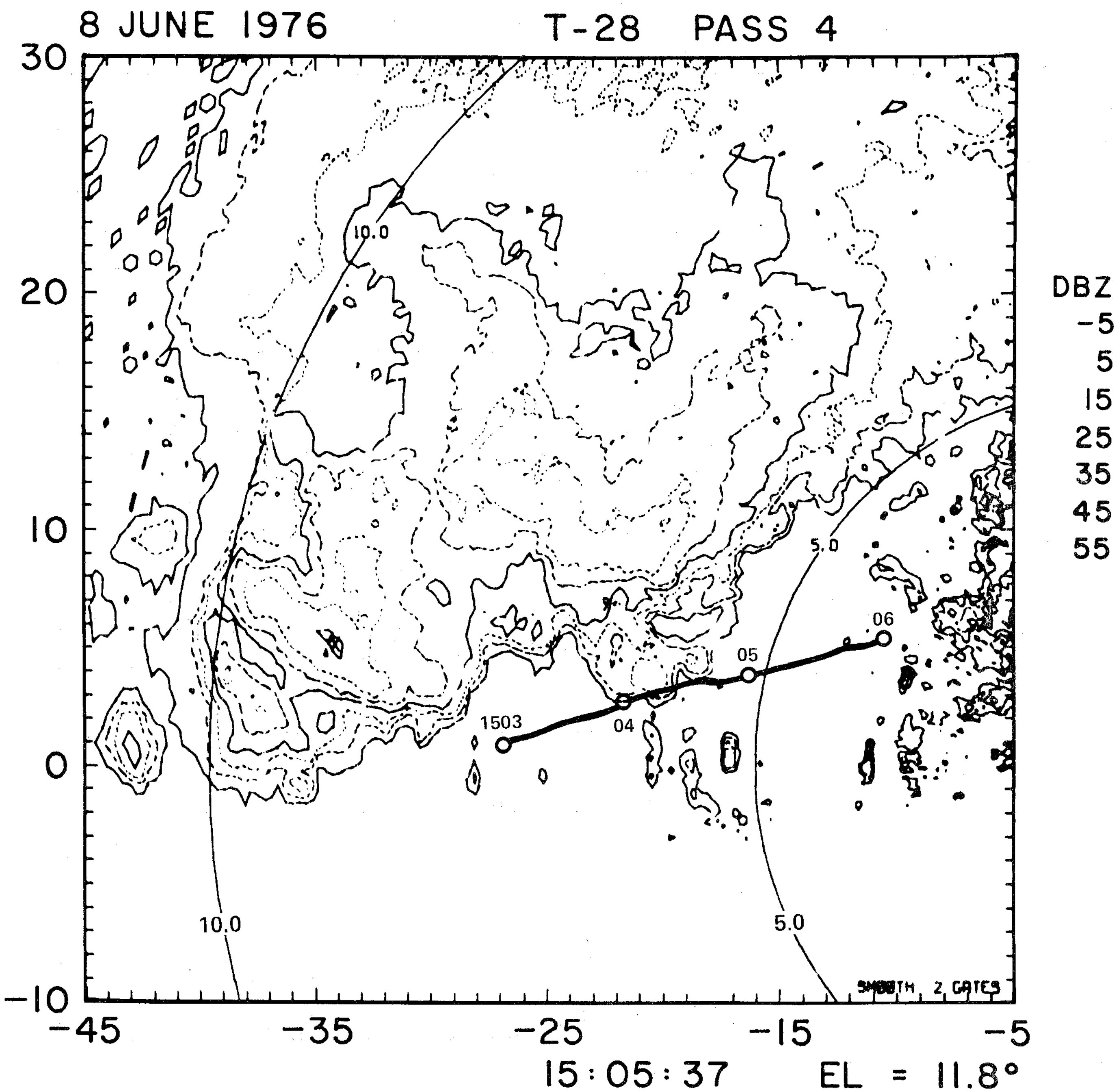

Fig. 16a. Same as Fig. 13a except PPI is at 15:05:37 and 11.8° elevation angle, and track is for Pass 4 from 1503 to 1506. Altitude of T-28 is 5.8 - 6.1 km. Constant altitude arcs are at 5.0 km and 10.0 km. PPI area has shifted 5 km east from Fig. 15a.

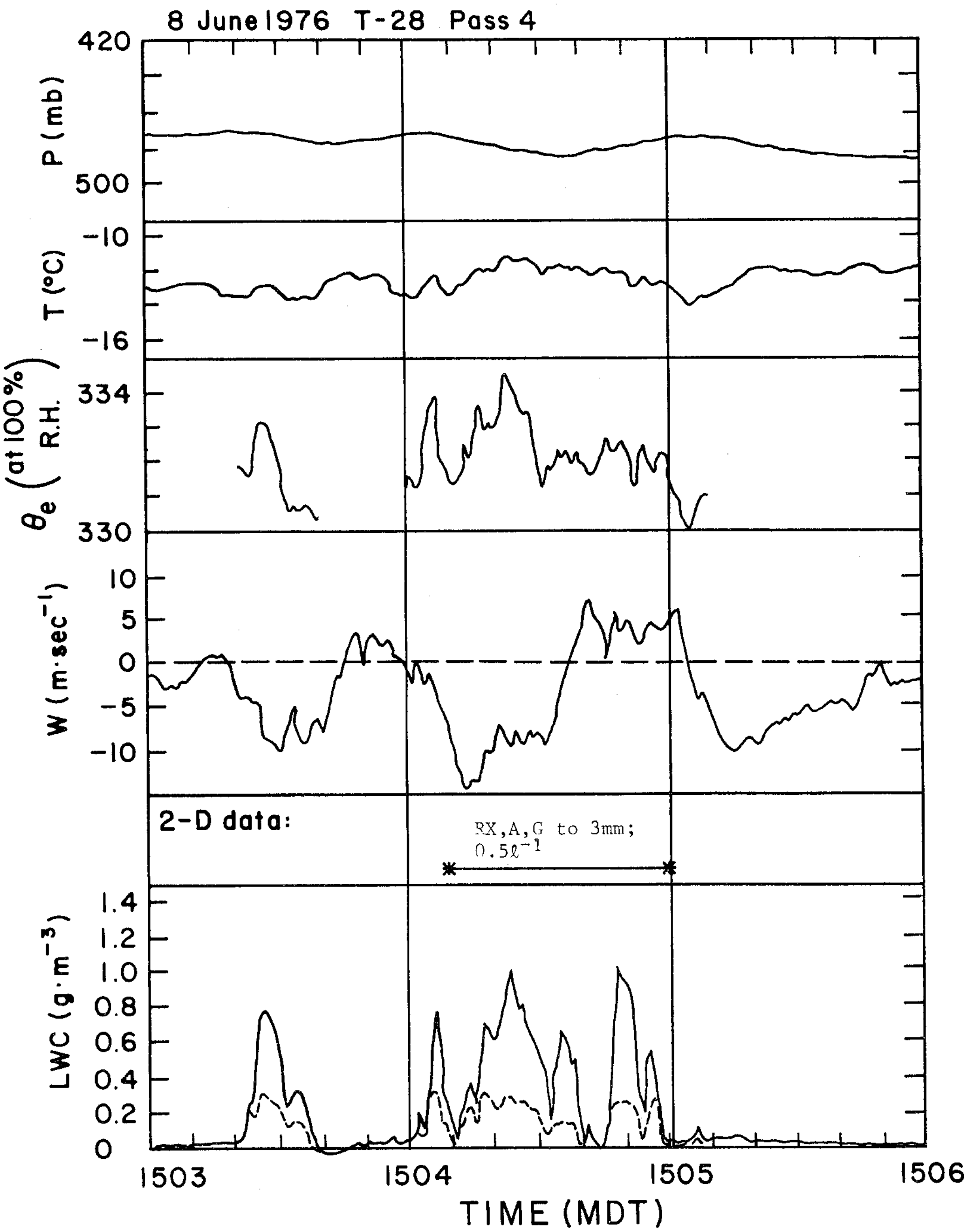

Fig. 16b. Same as Fig. 13b except for Pass 4 from 1503 to 1506.

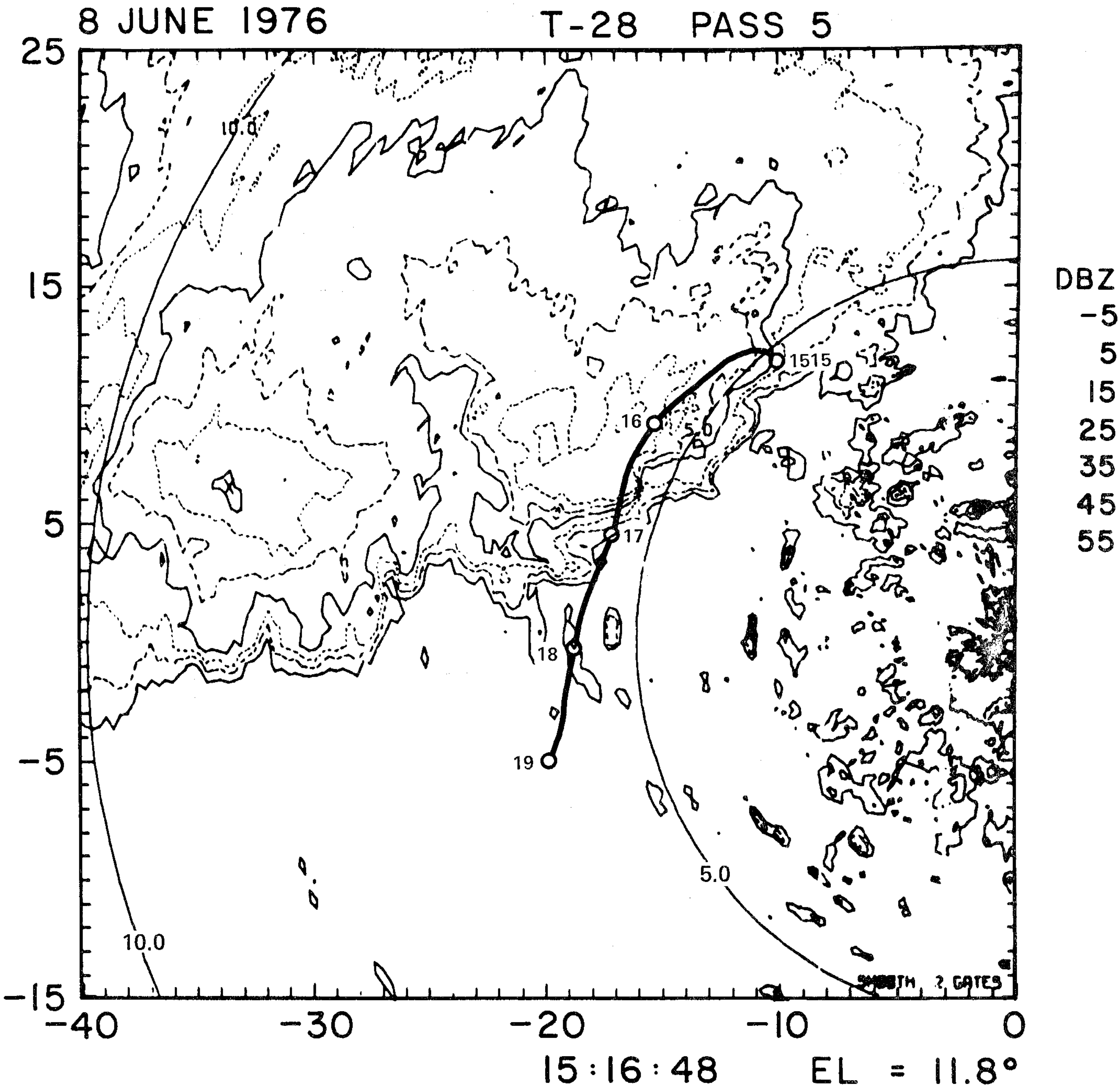

Fig. 17a. Same as Fig. 16a except PPI is at 15:16:48, and track is for Pass 5 from 1515 to 1519. Altitude of T-28 is 5.7 - 6.1 km. PPI area has shifted 5 km east and 5 km south from Fig. 16a.

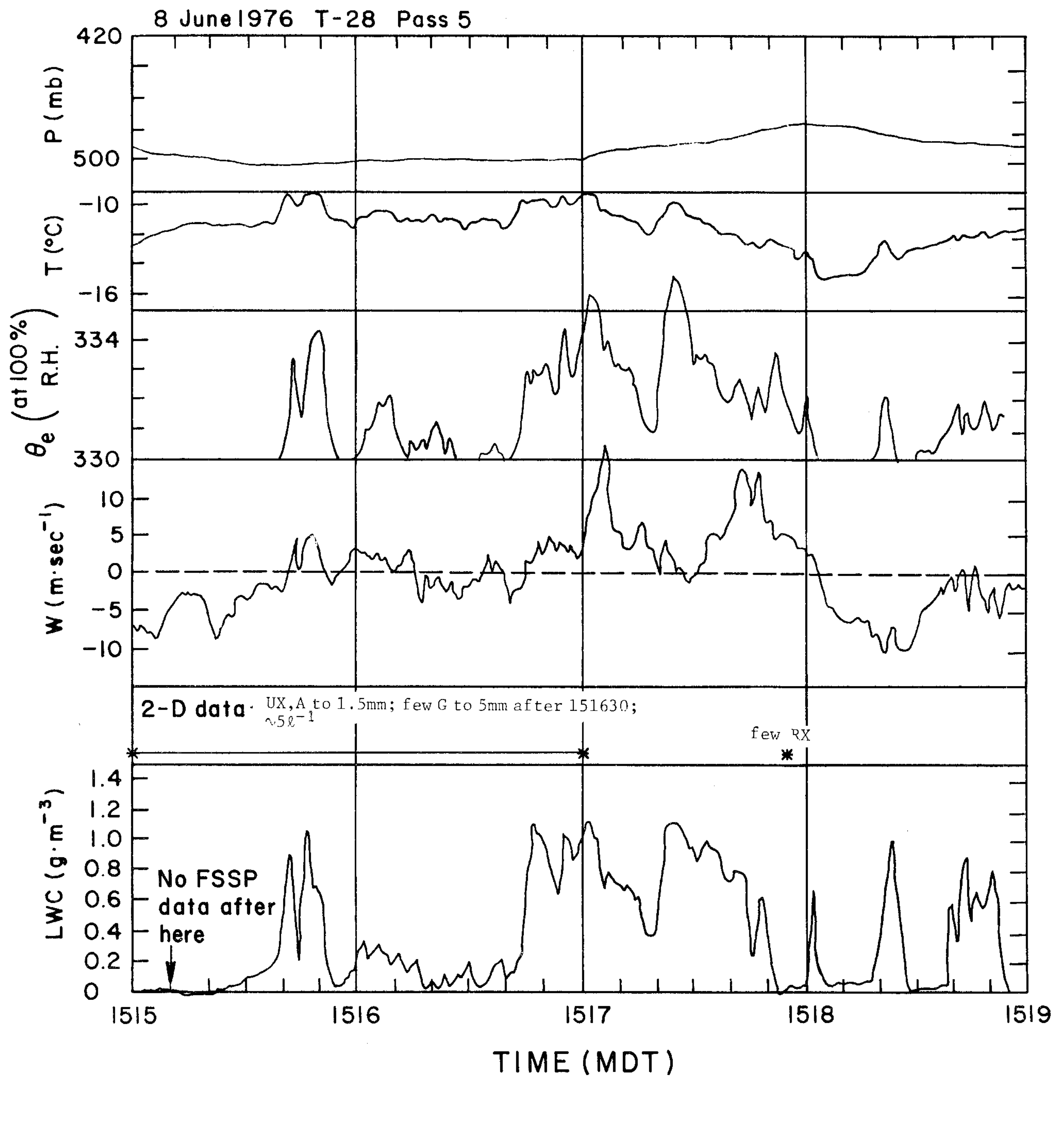

Fig. 17b. Same as Fig. 13b except for Pass 5 from 1515 to 1519. An FSSP recording failure occurred at 15:15:10.

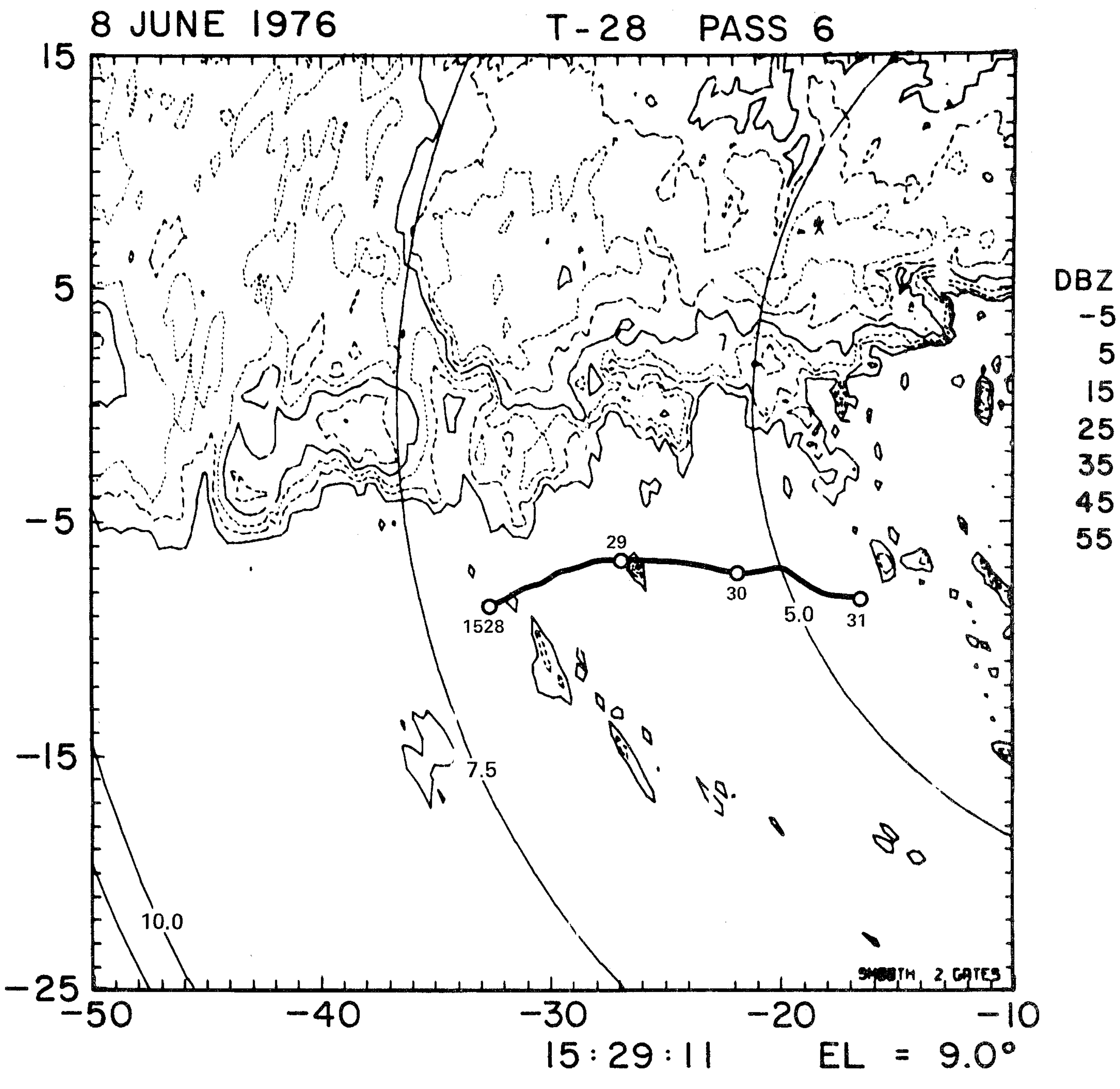

Fig. 18a. Same as Fig. 16a except PPI is at 15:29:11 and 9.0° elevation angle, and track is for Pass 6 from 1528 to 1531. Altitude of T-28 is 5.9 - 6.2 km. Constant altitude arcs are at 5.0, 7.5, and 10.0 km. PPI area has shifted 10 km east and 10 km south from Fig. 17a.

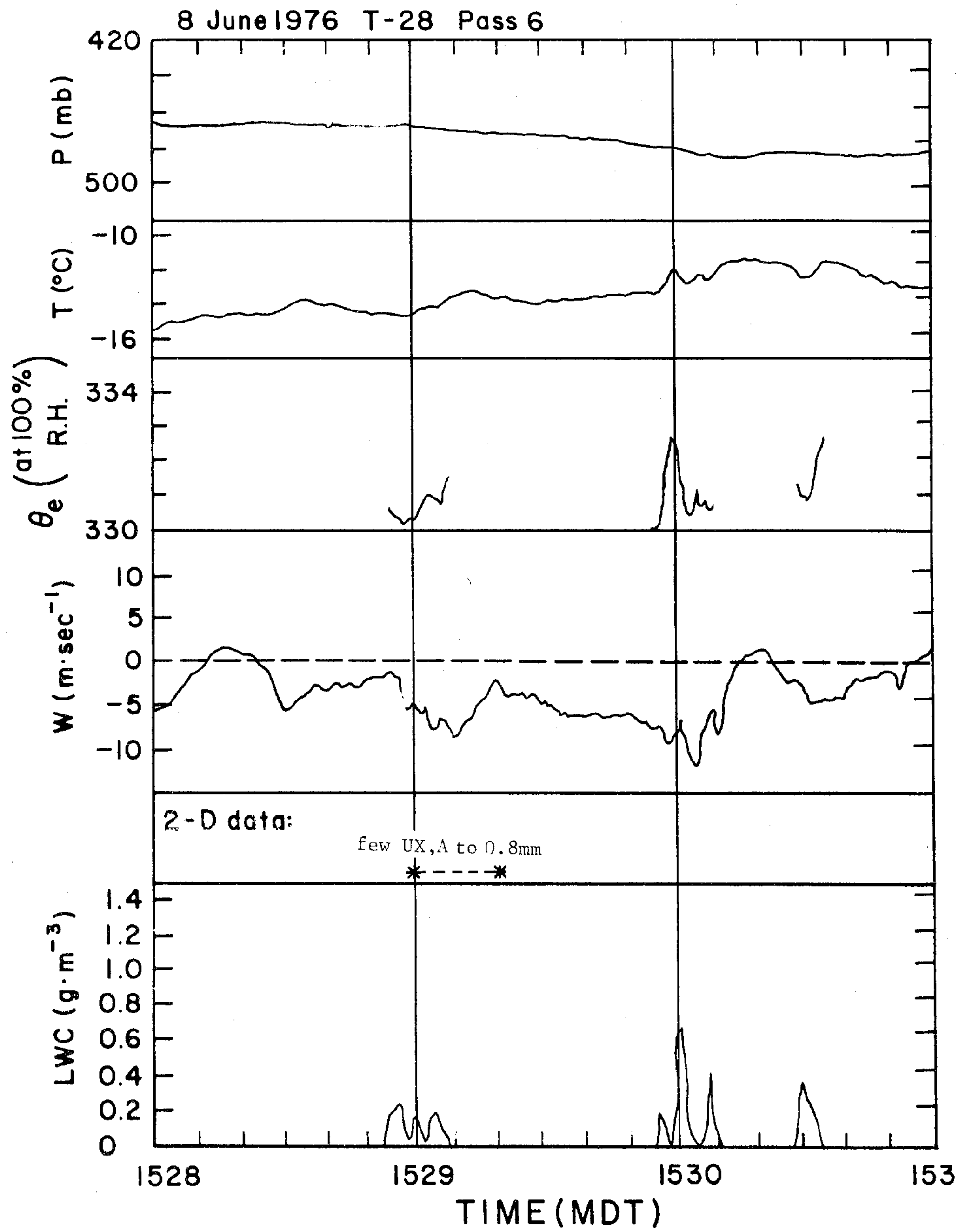

Fig. 18b. Same as Fig. 13b except for Pass 6 from 1528 to 1531.

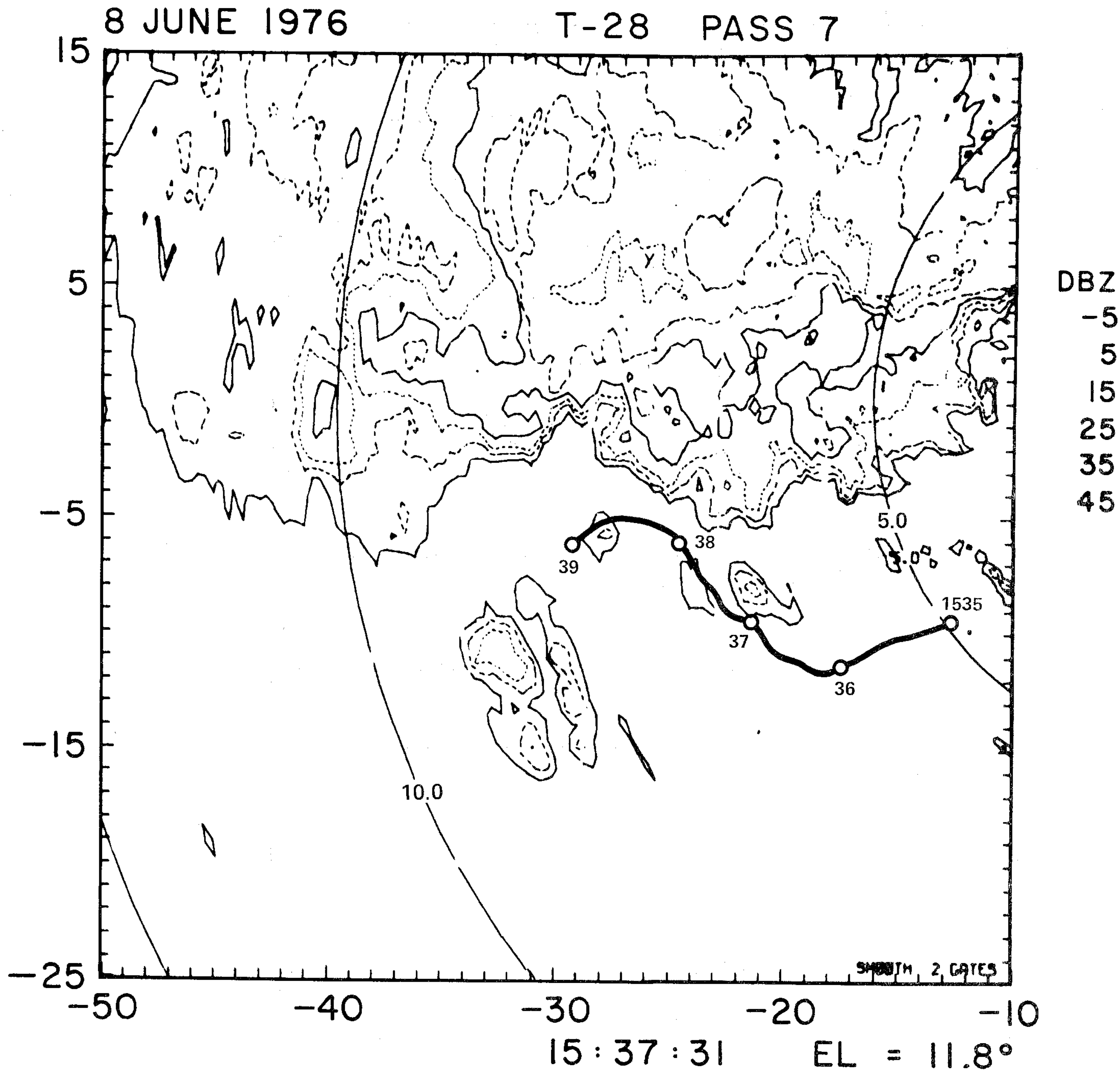

Fig. 19a. Same as Fig. 16a except PPI is at 15:37:31, and track is for Pass 7 from 1535 to 1539. Altitude of T-28 is 5.9 - 6.3 km.

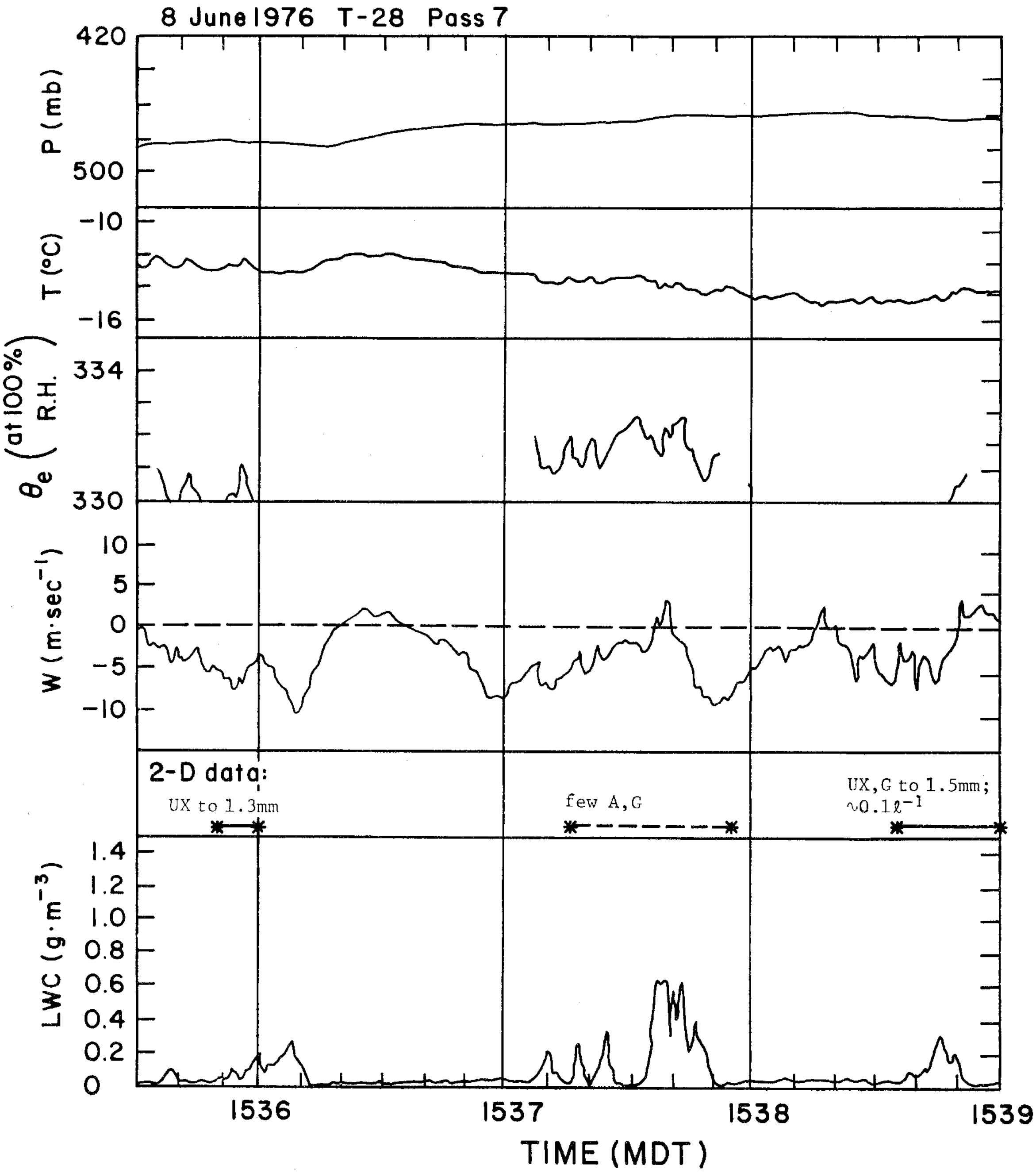

Fig. 19b. Same as Fig. 13b except for Pass 7 from 15:35:30 to 15:39:00.

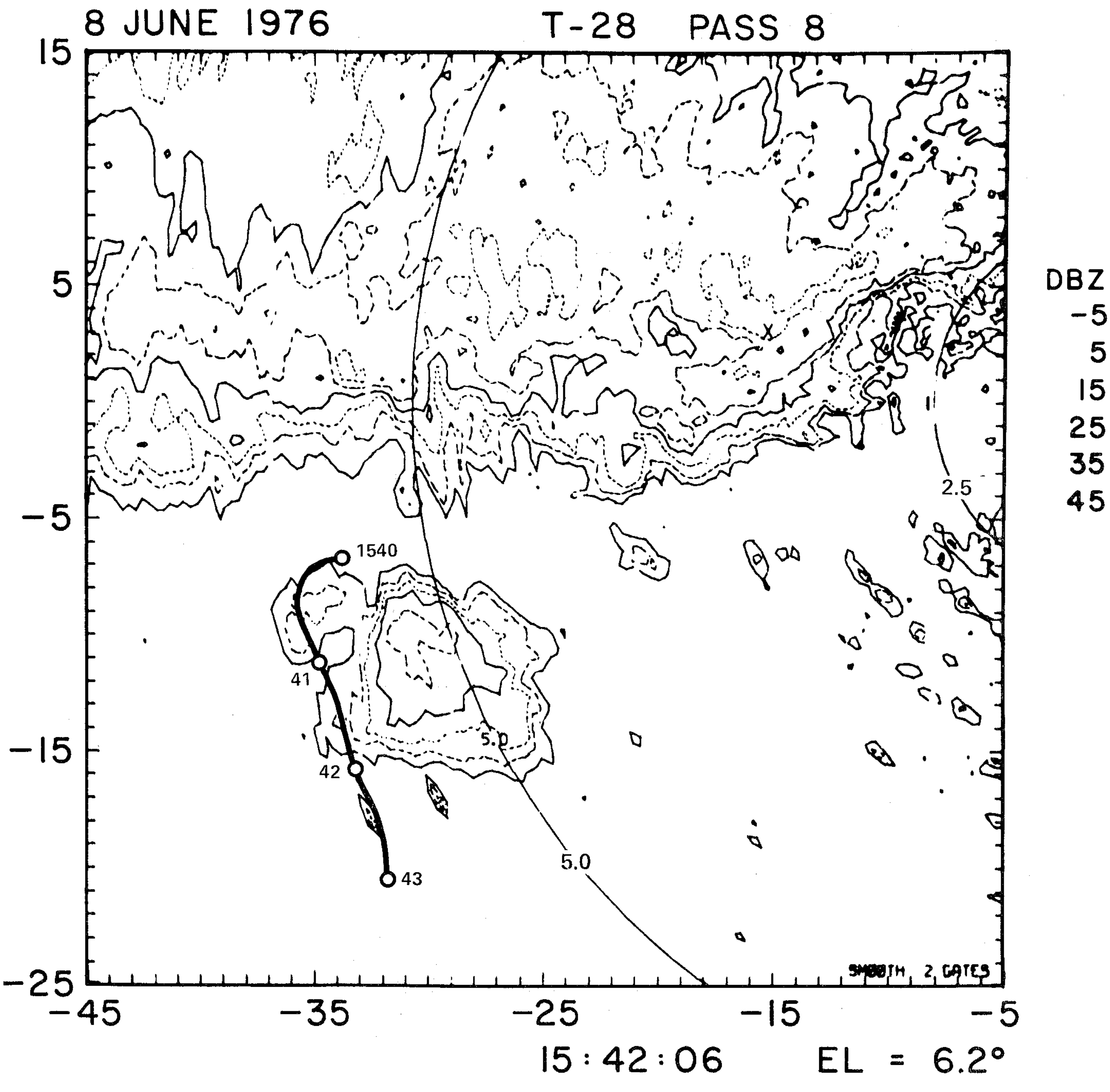

Fig. 20a. Same as Fig. 13a except PPI is at 15:42:06, and track is for Pass 8 from 15:40:00 to 15:43:00. Altitude of T-28 is 5.9 - 6.2 km. PPI area has shifted 5 km east from Fig. 19a.

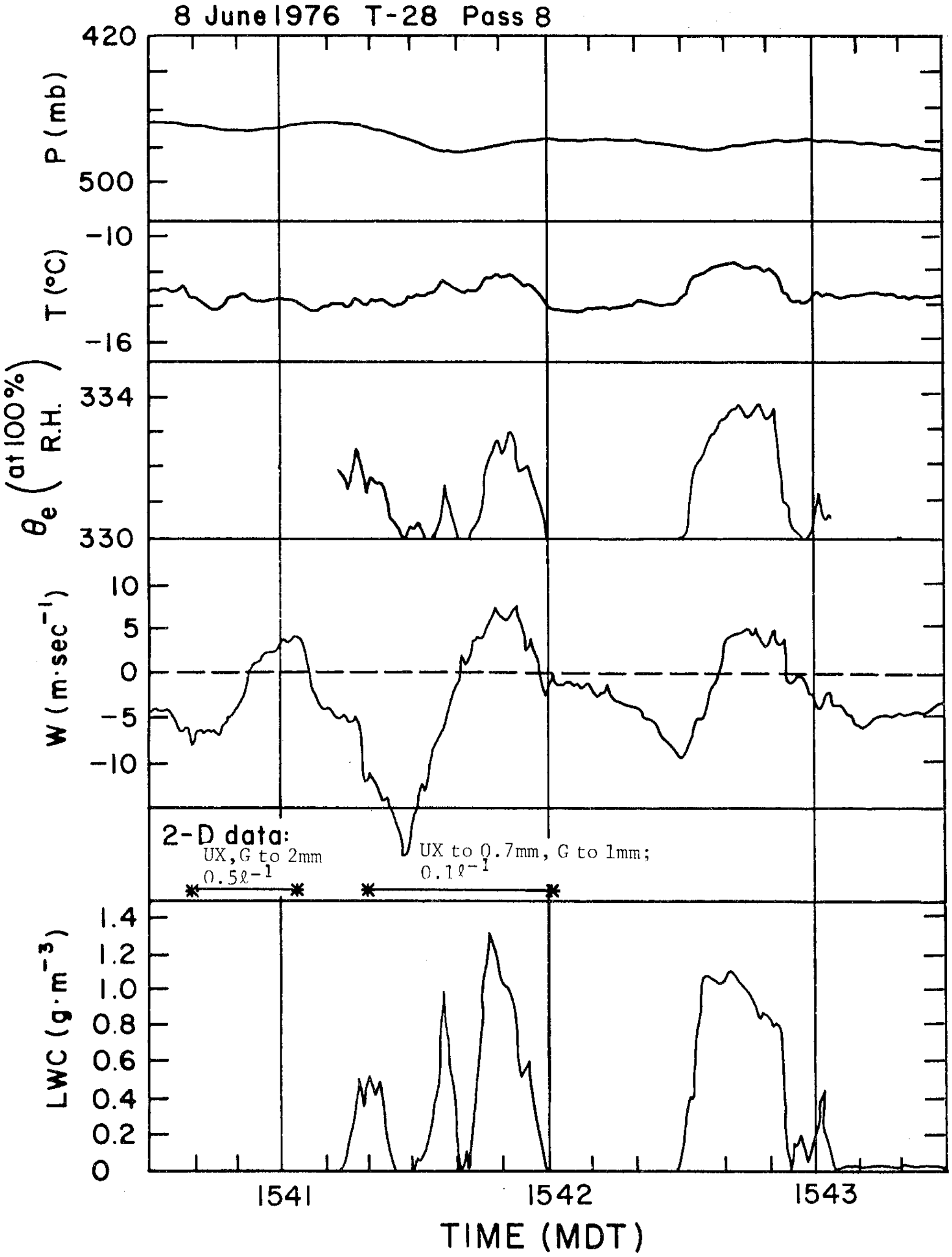

Fig. 20b. Same as Fig. 13b except for Pass 8 from 15:40:30 to 15:43:30.

main storm and intensified the southern end of the complex, as described in the radar history section.

IV. SUBCLOUD AIRCRAFT

A. NCAR QUEEN AIR 304D

The NCAR Queen Air 304D operated below cloud base in the southern and southeastern areas of the storm on this day from about 1405 to 1530. The aircraft tracks for this time period are plotted on radar PPI's in Figs. 21a-d. These tracks have been corrected for the mean error observed from 10 occurrences of radar skinpaint and for storm motion, which was 6 m s^{-1} to the east in Fig. 21a, 5 m s^{-1} to the southeast in Fig. 21b, and 3 m s^{-1} to the south-southeast in Figs. 21c and 21d. The resulting accuracy of the tracks should be ±1.5 km, although this may be worse near the end times of the different plots due to variations in the echo motion and development. The PPI's presented show reflectivities closest to 304D's altitude, which varied between 2.0 and 4.1 km but was generally 3.7 - 3.8 km. Ground clutter in the radar data gets rather severe in the south and southeast corner of the plots near the radar. However, it has not been removed in order to show the influence it may have on the reflectivity structure of the storm as it propagates southeastward.

Selected parameters from 304D data are presented in Figs. 22a-i for the time period 1400-1530. These include pressure, temperature, mixing ratio, potential temperature (θ), equivalent potential temperature (θ_e), vertical velocity, and horizontal wind speed and direction. The aircraft instrumentation involved in obtaining these values is described in the appendix. The vertical velocity calculations are based on departures from a post-determined reference level, which is about +1.5 m s^{-1} on this day. The relative zero should be displaced upward about 1.5 m s^{-1} on the vertical velocity plots in Figs. 22a-i.

The 304D operations were concentrated along the southern boundary of the storm in coordination with the penetrating aircraft, with an early excursion along the eastern boundary to determine the extent of the inflow in that direction. The three primary parameters used for distinguishing inflow from outflow on this day are vertical velocity, θ_e, and the horizontal wind. The horizontal wind vectors are plotted on the aircraft tracks in Figs. 21a-d. These vectors are roughly 10-second averages, centered at the time of the plotted vector. Notable features of the wind data are the strong southeasterlies at the southern end of the storm, the changing structure of the winds with time and altitude along the east-southeast boundary of the storm, and the convergence field at the southern end of the storm that is evident at 1409-1414, at 1437-1445, and strongly at 1518-1524. These features correlate well with vertical velocity and θ_e data.

The strongest updraft velocities occurred in the same relative position at the south-southeast boundary of the storm throughout the investigative period, but most notably at about 1424-1426, 1437-1439, and 1442-1444. In this updraft area, mean values were 3-5 m s^{-1} with maxima to 10 m s^{-1}. Values of θ_e in inflow areas were about 337 K or higher, compared with surface values of about 341 K. Indications of mixing below cloud base are evident in the short-term fluctuations in the vertical velocity during the lower passes of 304D (e.g., 1500-1510). Outflow or environmental air encounters are evident in the θ_e drops at 1420:00 - 1420:20 and 1433:00 - 1436:15. These agree with changes in

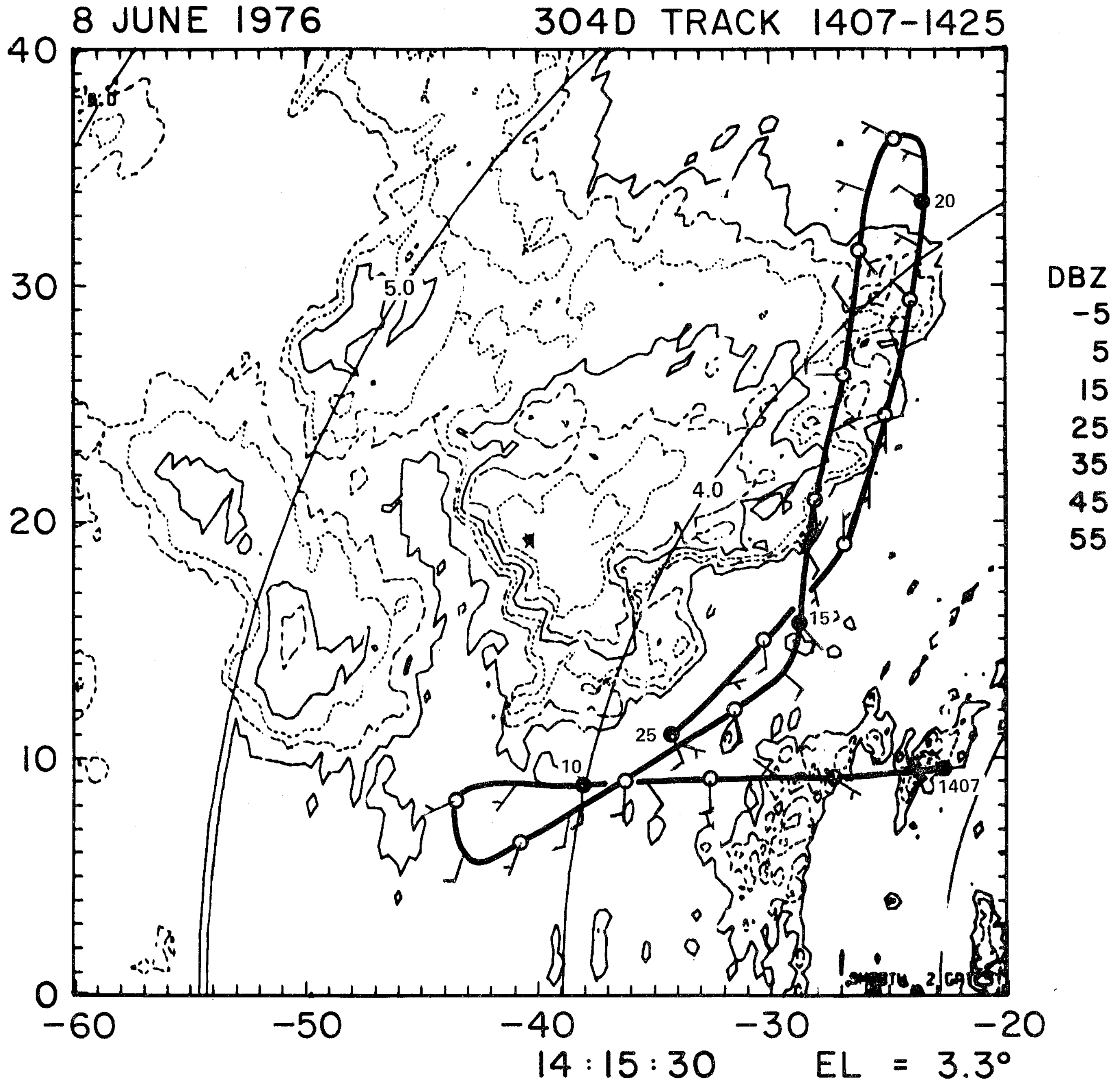

Fig. 21a. Radar reflectivity on 40 km x 40 km PPI map at 14:15:30 and 3.3° elevation angle showing corrected 304D track (heavy line) from 1407 to 1425. Altitude of 304D is 3.6 - 4.1 km. Track is marked every minute and labeled every 5 min. 10 second averaged winds are plotted every 30 seconds, with a full barb equal to 5 m s^{-1}. Reflectivity contours are every 10 dBZ beginning at -5 dBZ. Constant altitude arcs are at 4.0 and 5.0 km.

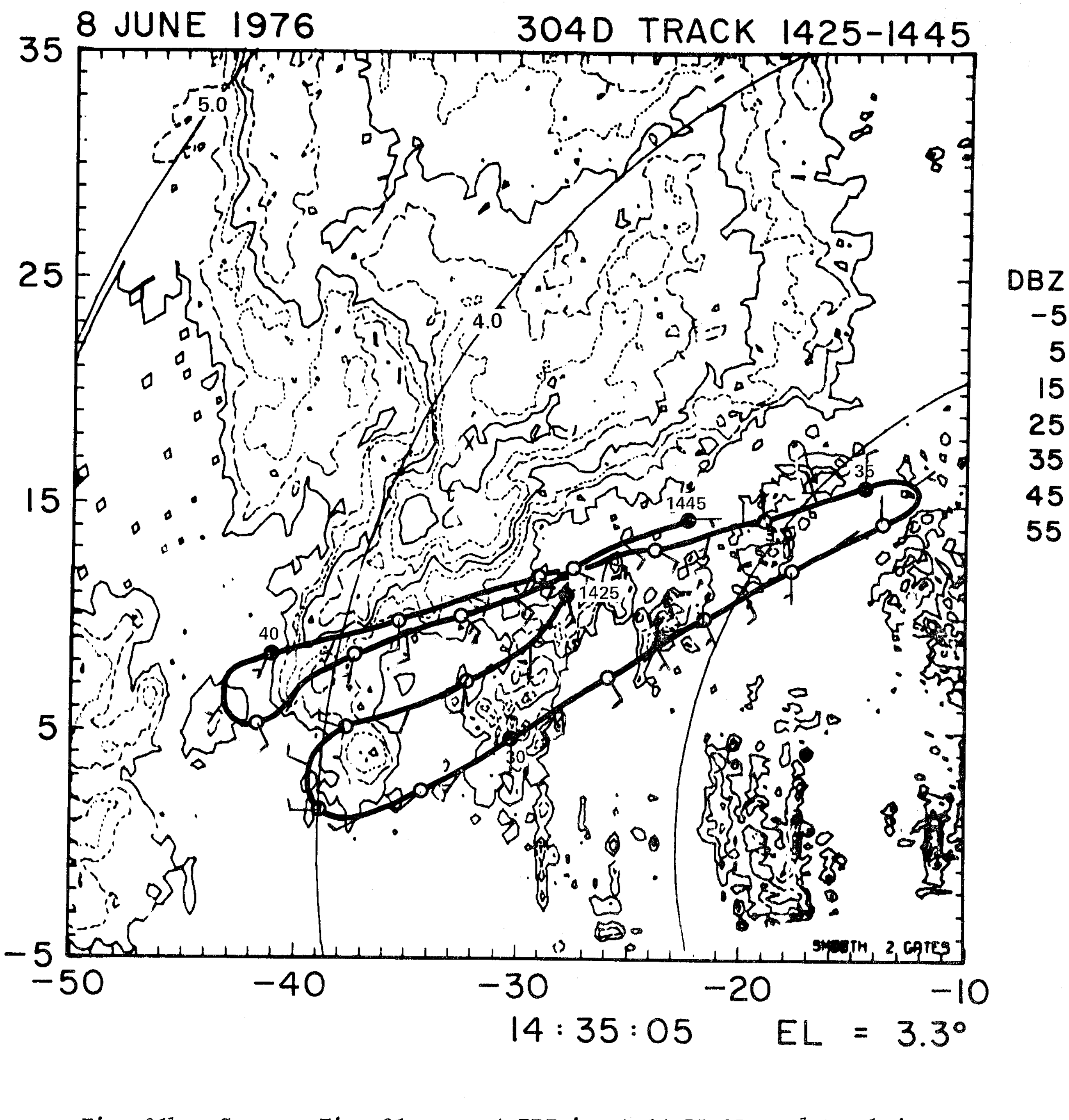

Fig. 21b. Same as Fig. 21a except PPI is at 14:35:05, and track is from 1425 to 1445. Altitude of 304D is 3.8 km. PPI area has shifted 10 km east and 5 km south from Fig. 21a. The 3.0 km altitude arc has been added.

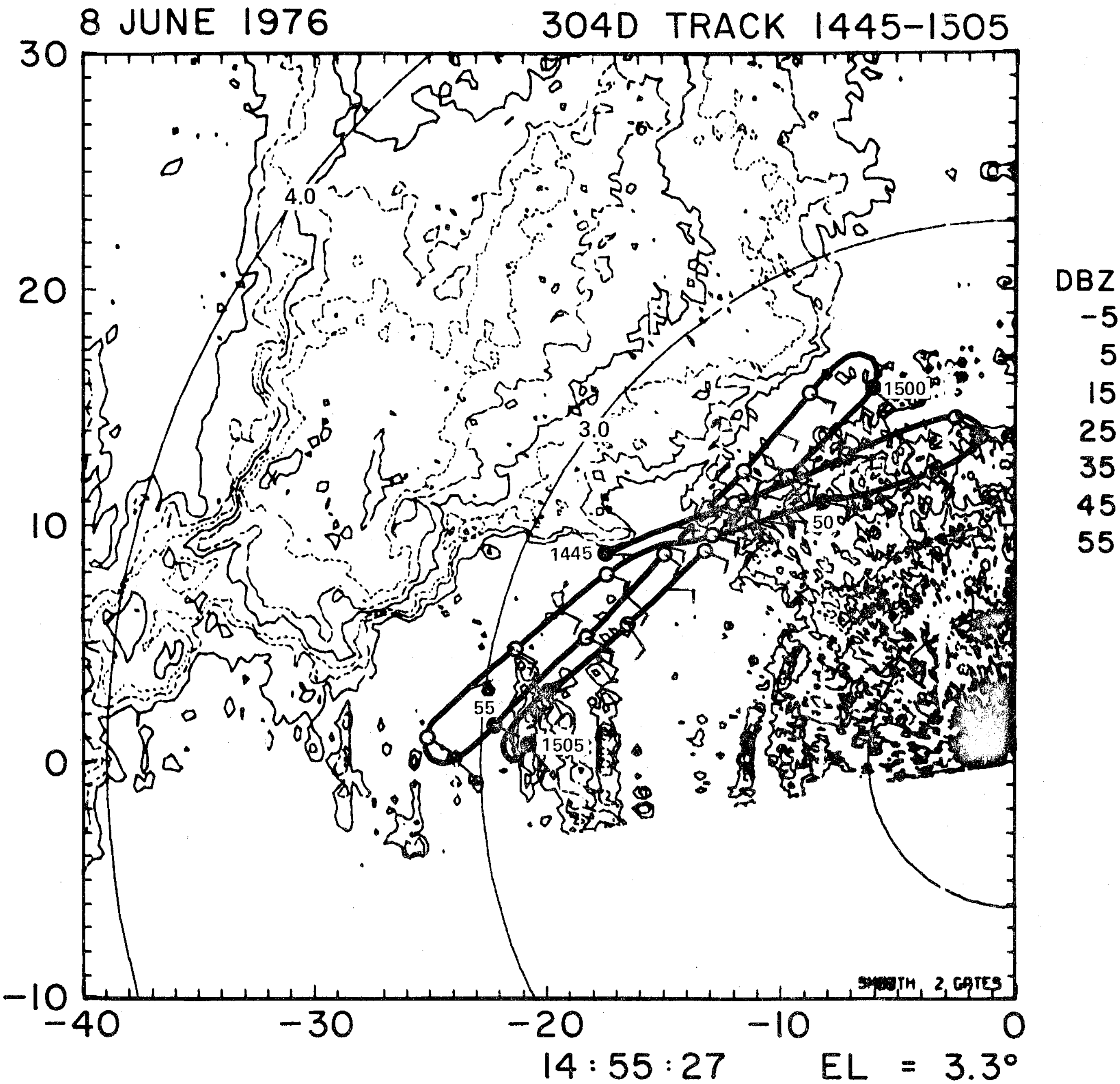

Fig. 21c. Same as Fig. 21a except PPI is at 14:55:27, and track is from 1445 to 1505. Altitude of 304D is 2.0 - 2.6 km. PPI area has shifted 10 km east and 5 km south from Fig. 21b.

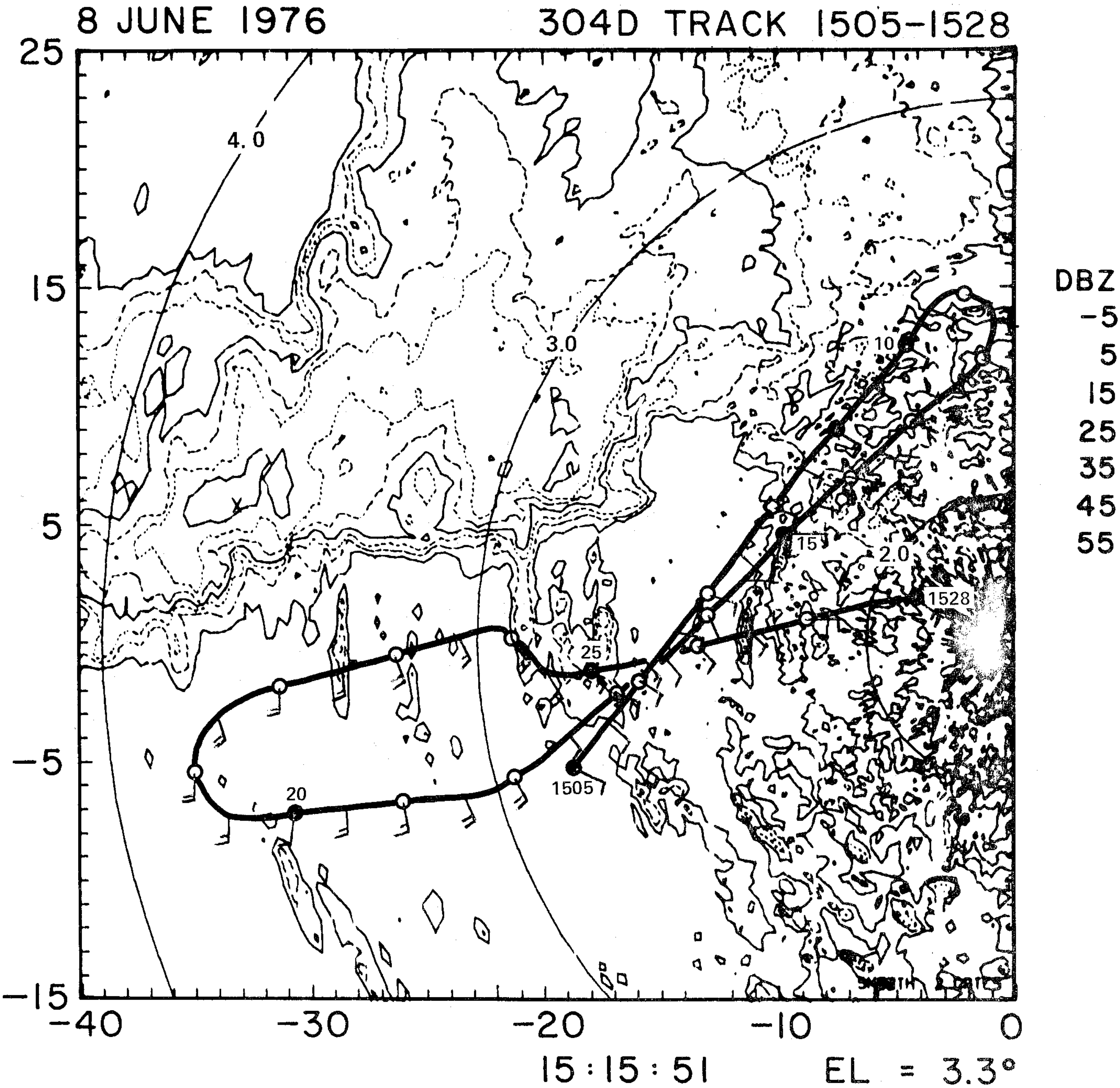

Fig. 21d. Same as Fig. 21a except PPI is at 15:15:51, and track is from 1505 to 1528. Altitude of 304D is 2.0 - 3.8 km. PPI area has shifted 5 km south from Fig. 21c. The 2.0 km altitude arc has been added.

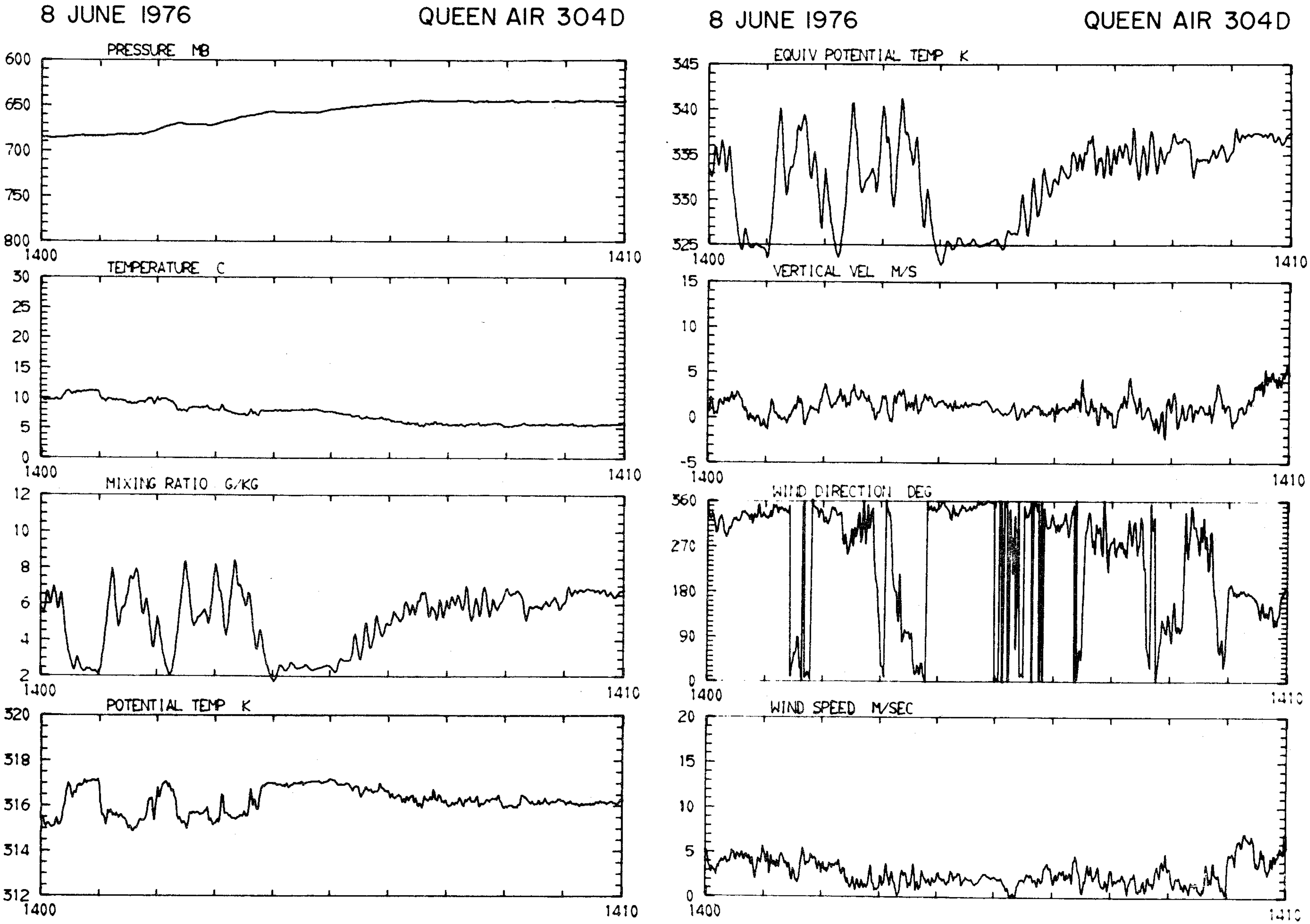

Fig. 22a. Data from 304D for time period 1400-1410 showing pressure, temperature, mixing ratio, and potential temperature on the left, and equivalent potential temperature, vertical velocity, horizontal wind direction, and horizontal wind speed on the right. The reference zero for vertical velocity is actually +1.5 m s^{-1} on this day. Time ticks are every minute.

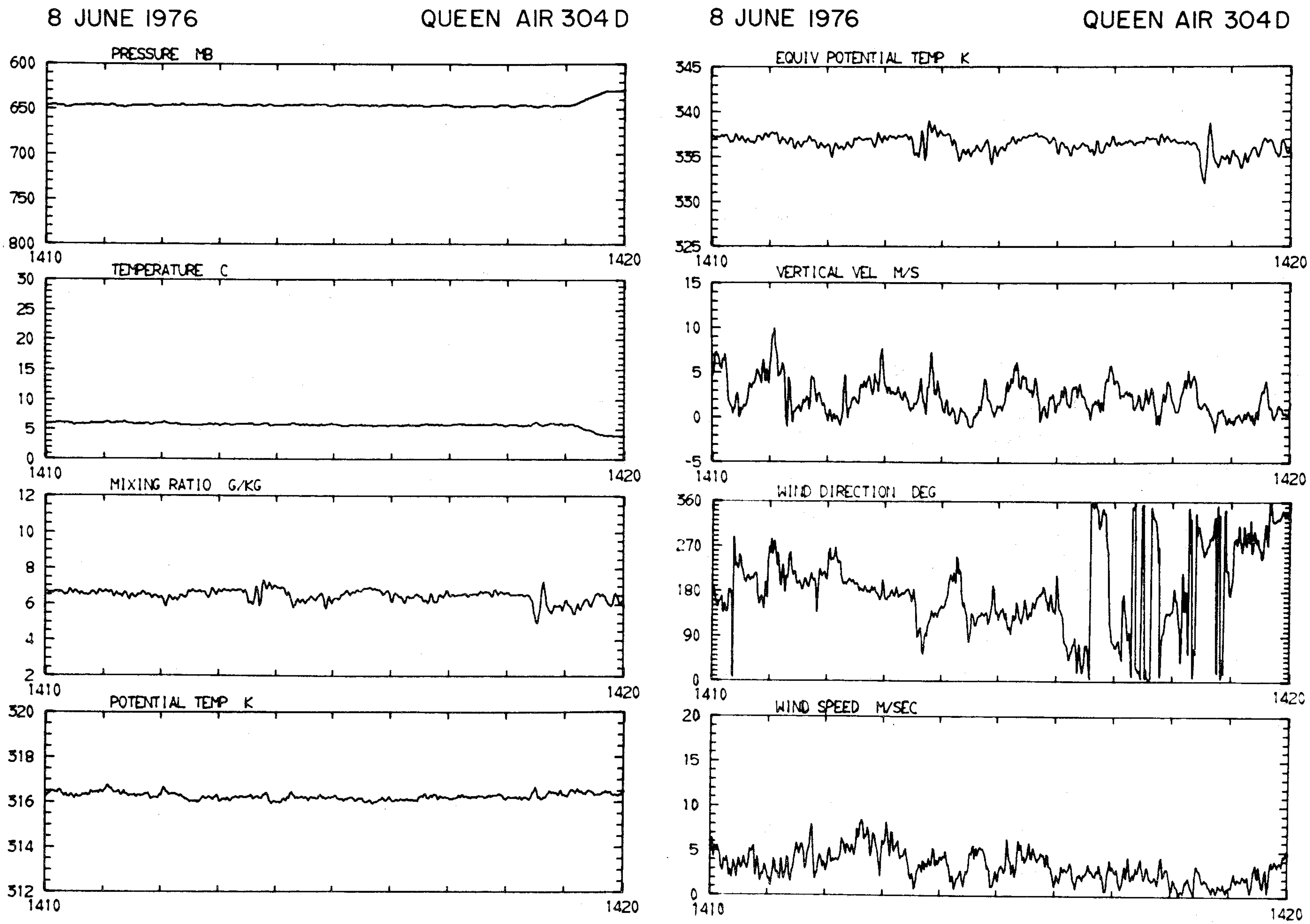

Fig. 22b. Same as Fig. 22a except from 1410 to 1420.

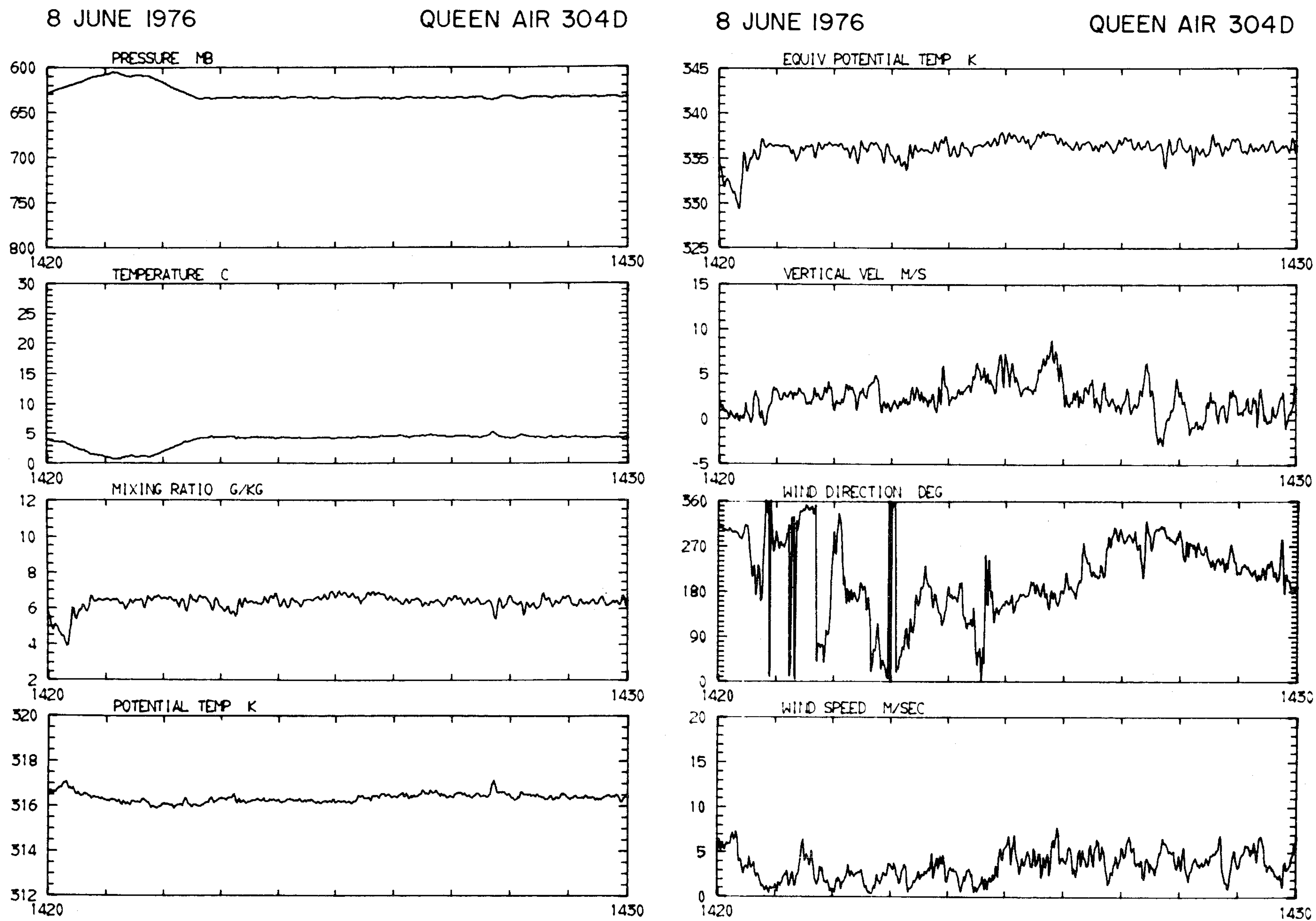

Fig. 22c. Same as Fig. 22a except from 1420 to 1430.

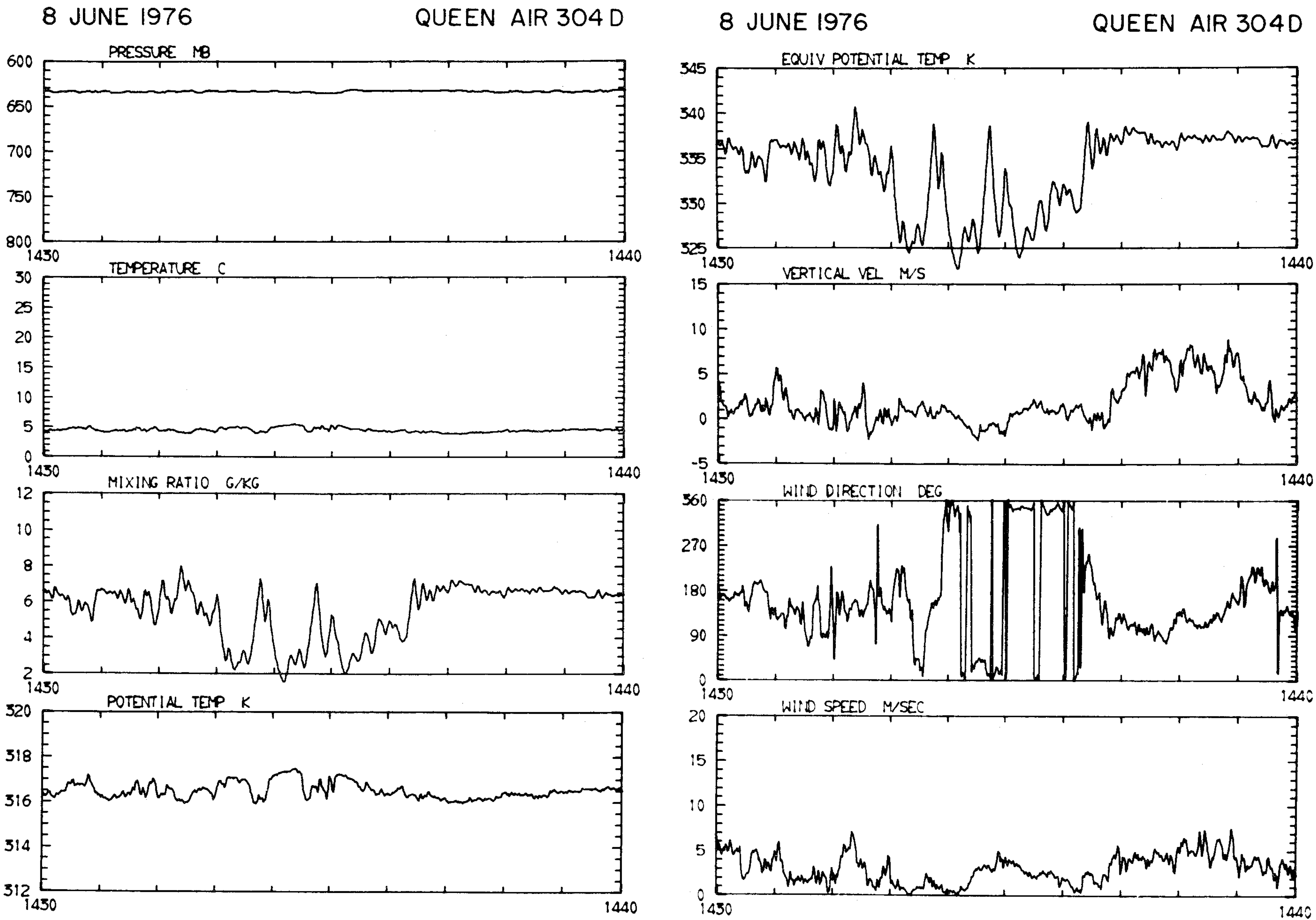

Fig. 22d. Same as Fig. 22a except from 1430 to 1440.

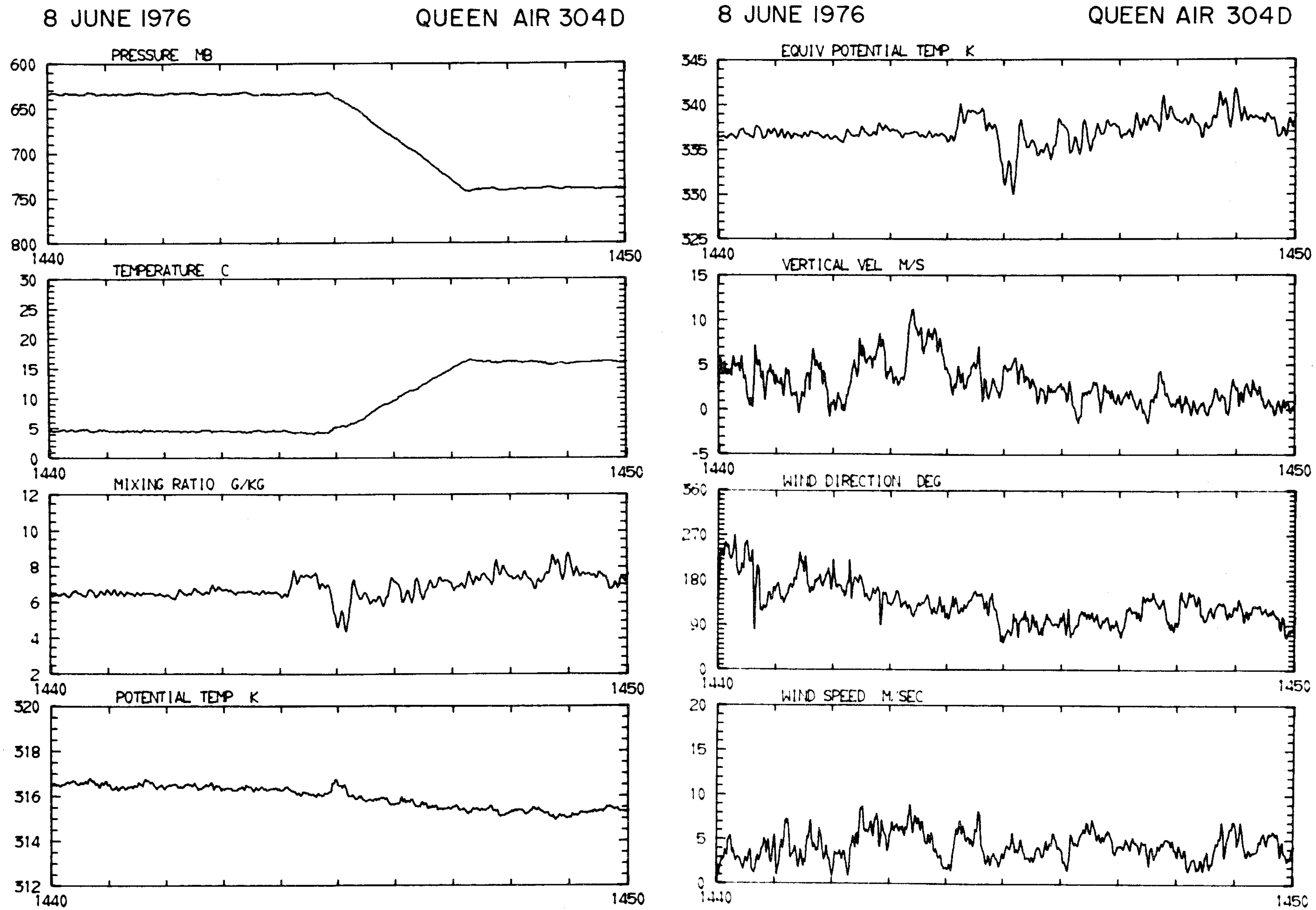

Fig. 22e. Same as Fig. 22a except from 1440 to 1450.

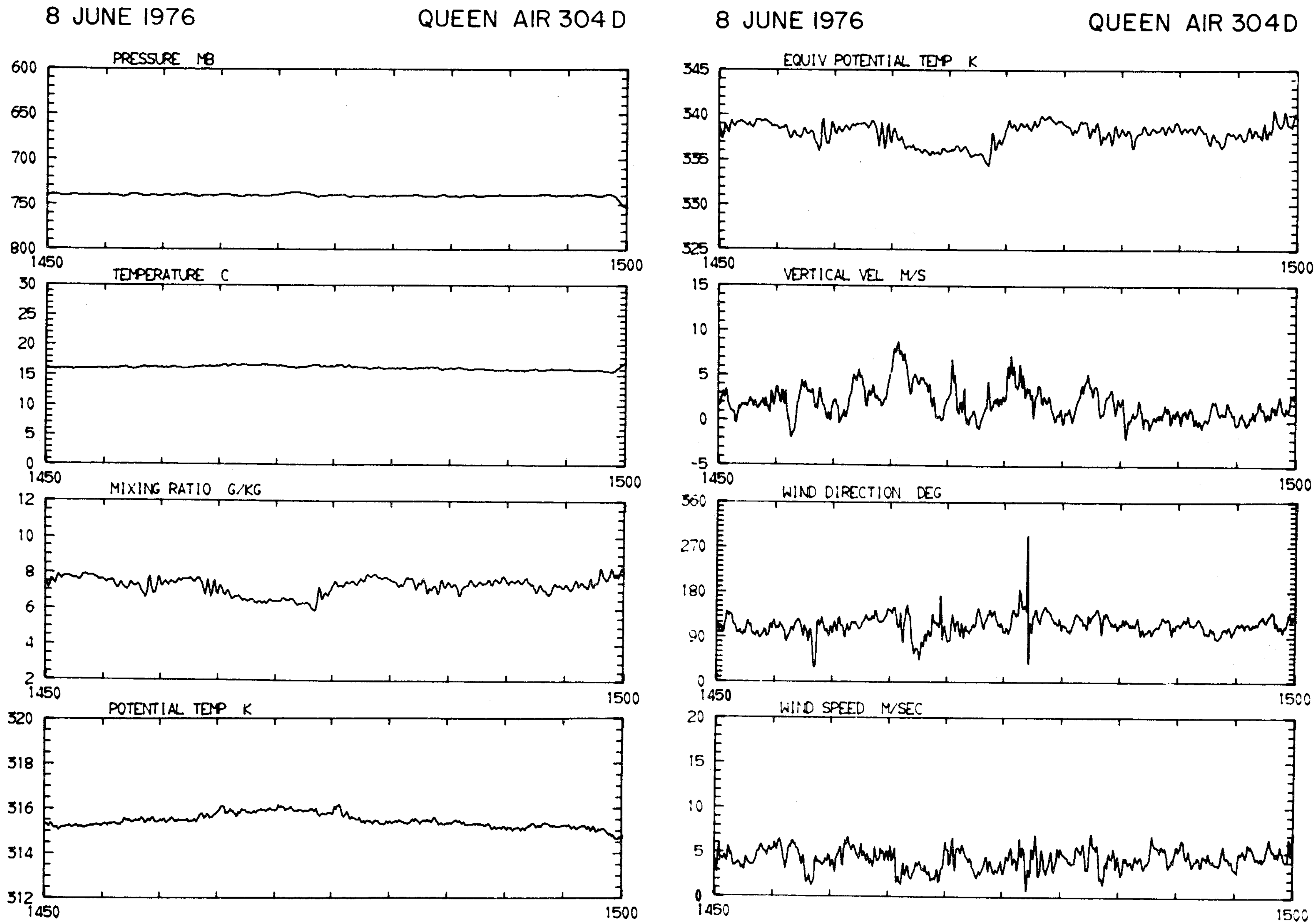

Fig. 22f. Same as Fig. 22a except from 1450 to 1500.

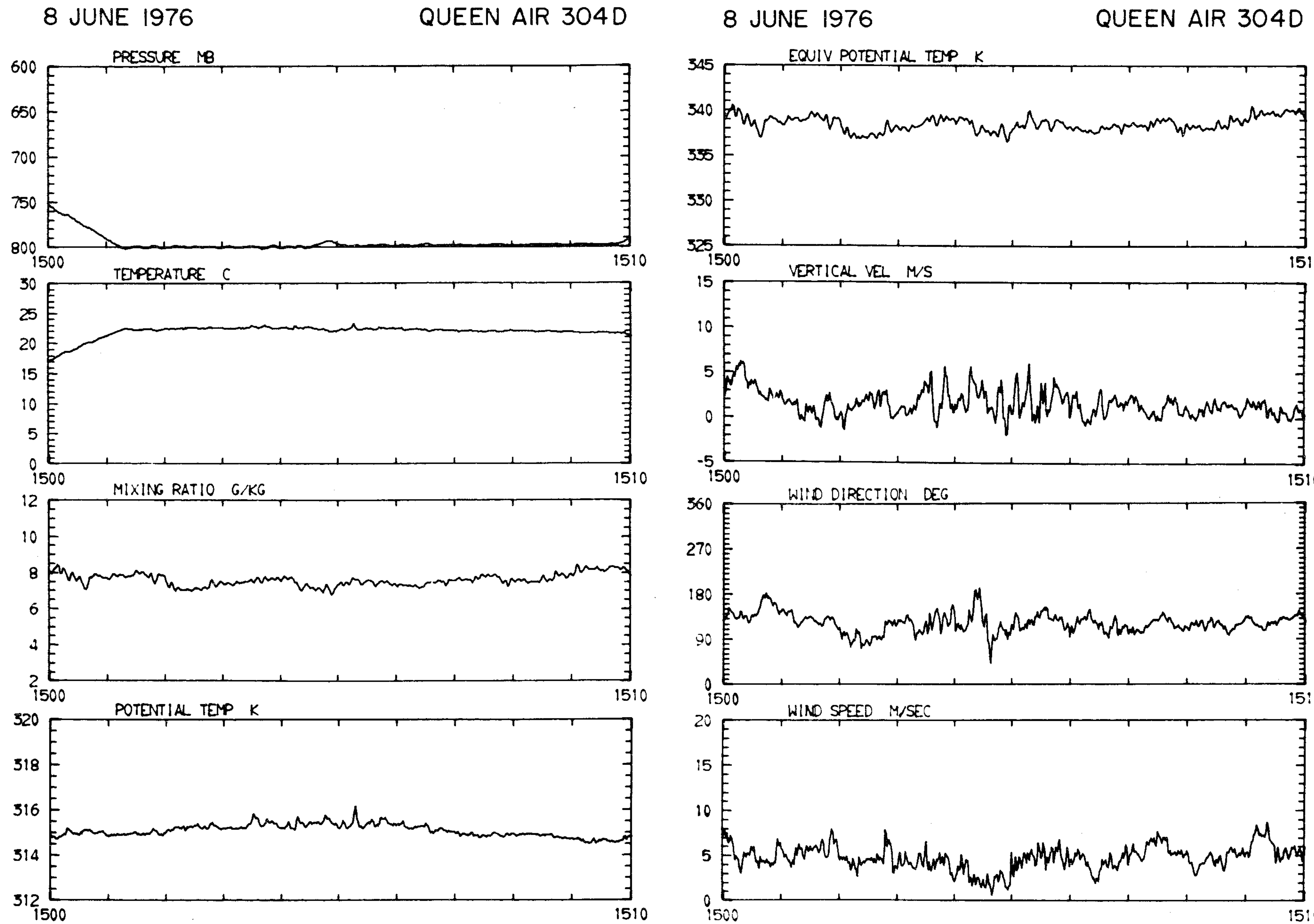

Fig. 22g. Same as Fig. 22a except from 1500 to 1510.

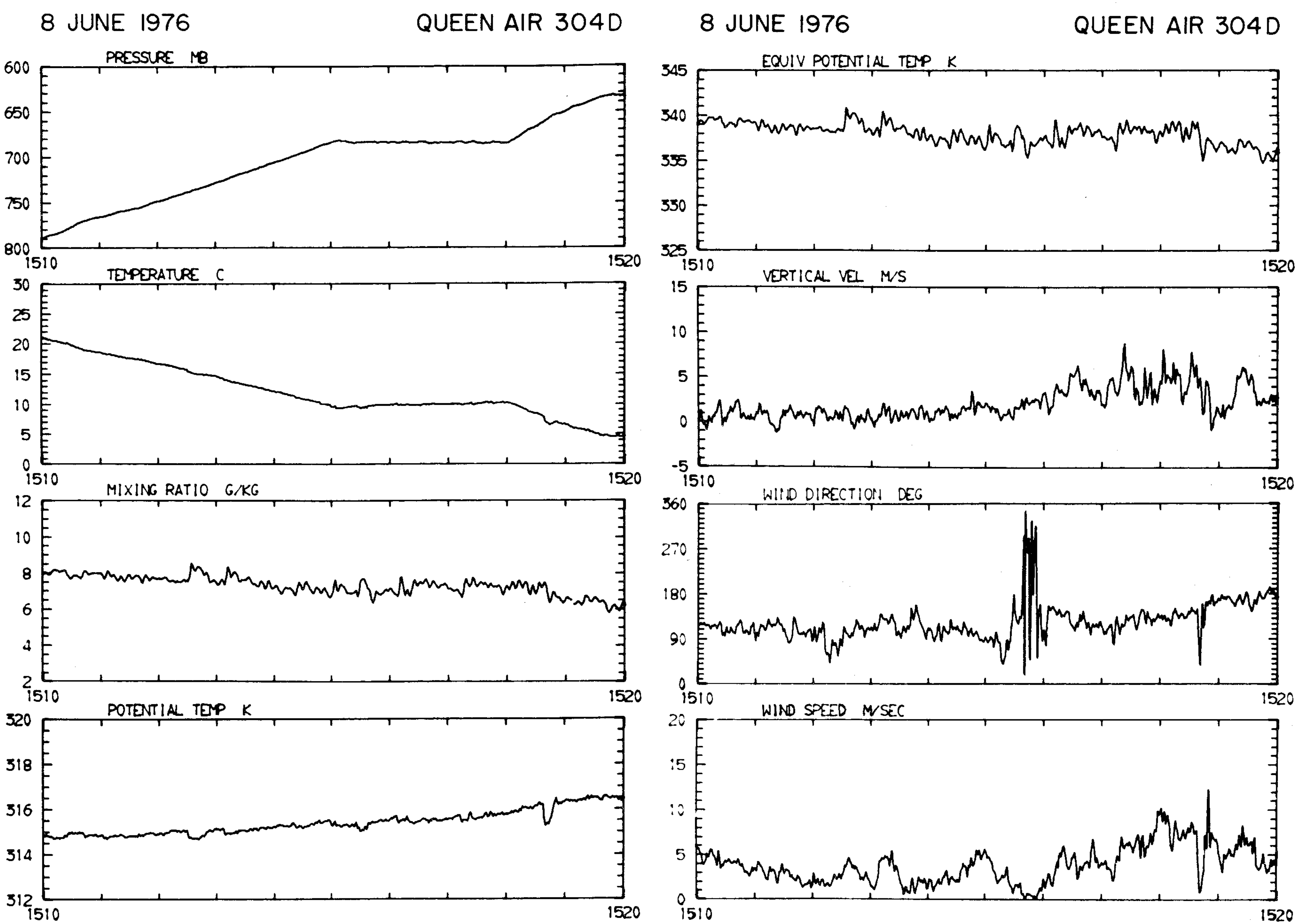

Fig. 22h. Same as Fig. 22a except from 1510 to 1520.

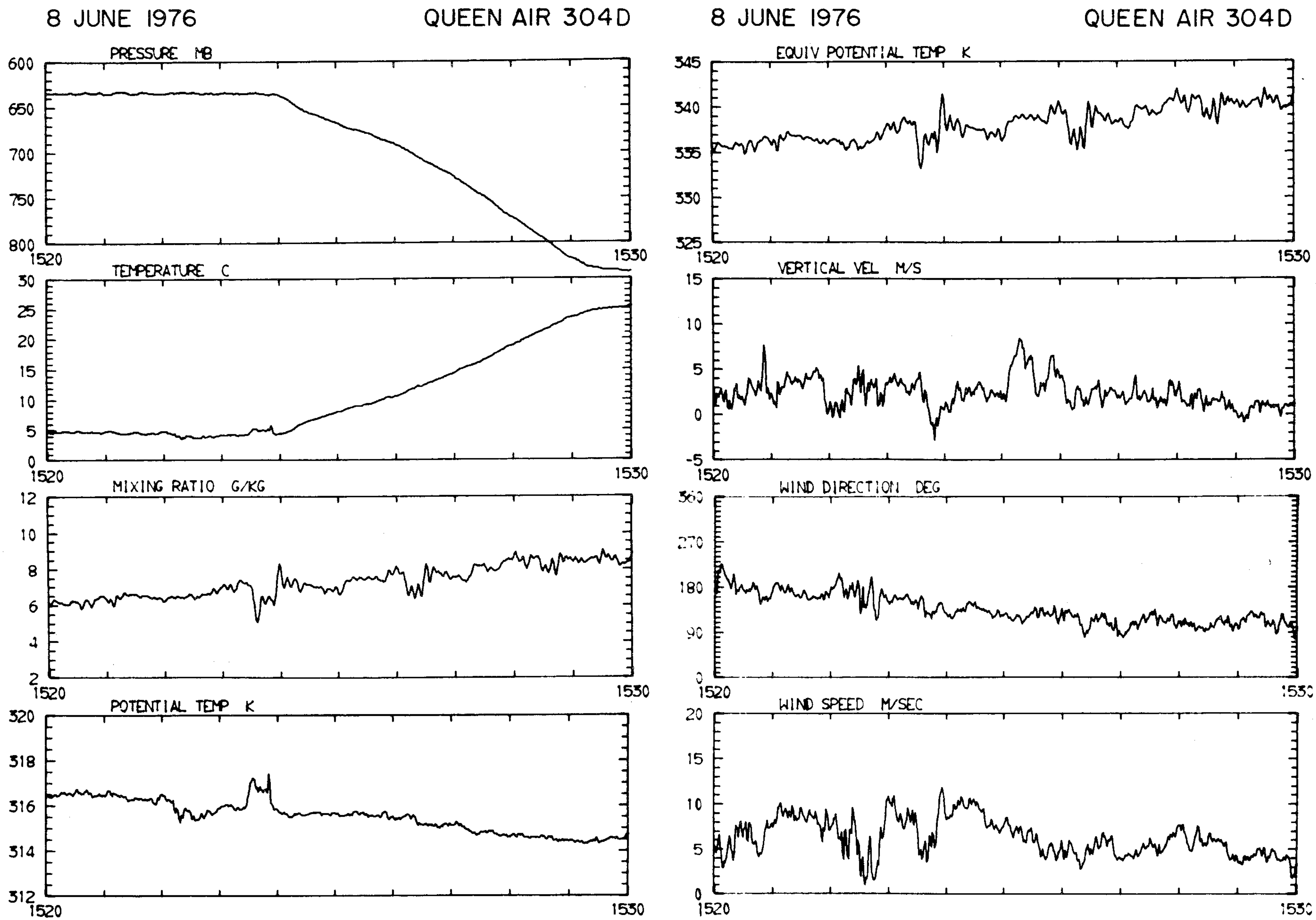

Fig. 22i. Same as Fig. 22a except from 1520 to 1530.

wind direction at these times. The θ_e trace is also generally correlated with the vertical velocity trace.

The broad updraft-inflow area mentioned above was near the reflectivity cell investigated by 10UW and the T-28 between ∿1425 and 1455, and described in Section III. During the few flight paths through this area, 10UW data show some cloud water and weak updrafts above 304D's position at about 1429 and 1435 (see Figs. 6b and 7b). The T-28 also measured cloud water as well as some ice particles east of the penetrated cell in Pass 3 at 1452 - 1454 (Fig. 14c). East of the reflectivity cell, the strongest updrafts sampled by the penetrating aircraft were slightly west of the broad updraft area encountered by 304D. Since the cell tilts slightly eastward with height, a connection appears to exist relating the cloud base updraft area and the cloud physics features detected by the penetrating aircraft in their investigation of this cell.

From 1524 to 1530, 304D made a descent sounding from the storm eastward to Grover through inflow conditions. These data have been plotted on the Grover sounding (Fig. 3) which was obtained from the rawinsonde released immediately after passage of 304D.

B. WYOMING QUEEN AIR 10UW

The Wyoming Queen Air 10UW made three east-west passes below cloud base between 1500 and 1520. The aircraft track during this period is presented in Figs. 23a and 23b, and has been corrected for a storm motion of 3 m s^{-1} to the south-southeast. The resultant track should be within 1.5 km of true position, but care should be exercised in correlating aircraft position with smaller scale echo features since these features can develop and move quite differently than the overall storm. Since the updraft velocities obtained from 10UW are filtered and smoothed, little accuracy or resolution is lost by plotting the relative strength and position on the track rather than presenting them with the other data. Pressure (P), temperature (T), mixing ratio (Q), potential temperature (θ), and equivalent potential temperature (θ_e) for the cloud base passes are presented in Fig. 24.

The 10UW data substantiate the subcloud conditions found by 304D. Values of θ_e are 337-339 K in the inflow areas, with a strong, broad updraft at about 1502 - 1504 and a weaker, less consistent updraft at 1505 - 1507 in the same area as that investigated by 304D. Strong, more cellular updrafts were also detected by 10UW under the areas penetrated in Passes 4, 5, and 9. The temporal continuity of updrafts in the south and southeast regions of the storm at different levels sampled by the aircraft support the radar observations of storm development into these areas.

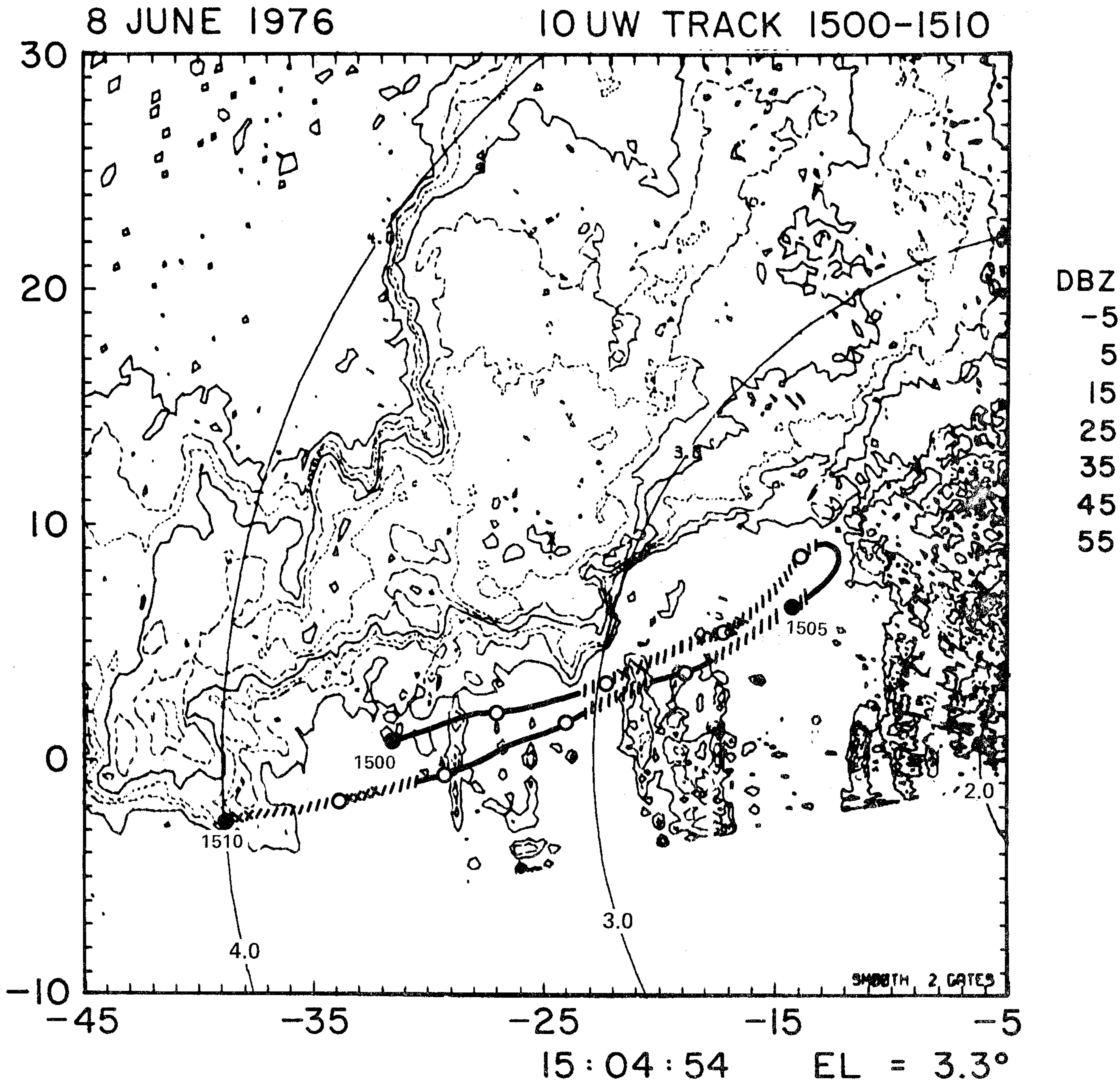

Fig. 23a. Radar reflectivity on 40 km x 40 km PPI map at 15:04:54 and 3.3° elevation angle showing corrected 10UW track (heavy line) from 1500 to 1510. Track is marked every minute and labeled every 5 min. Updrafts between 0 and 5 m s^{-1} are cross-hatched, and updrafts >5 m s^{-1} are X'ed. Reflectivity contours are every 10 dBZ beginning at -5 dBZ. Constant altitude arcs are at 2.0 km, 3.0 km, and 4.0 km.

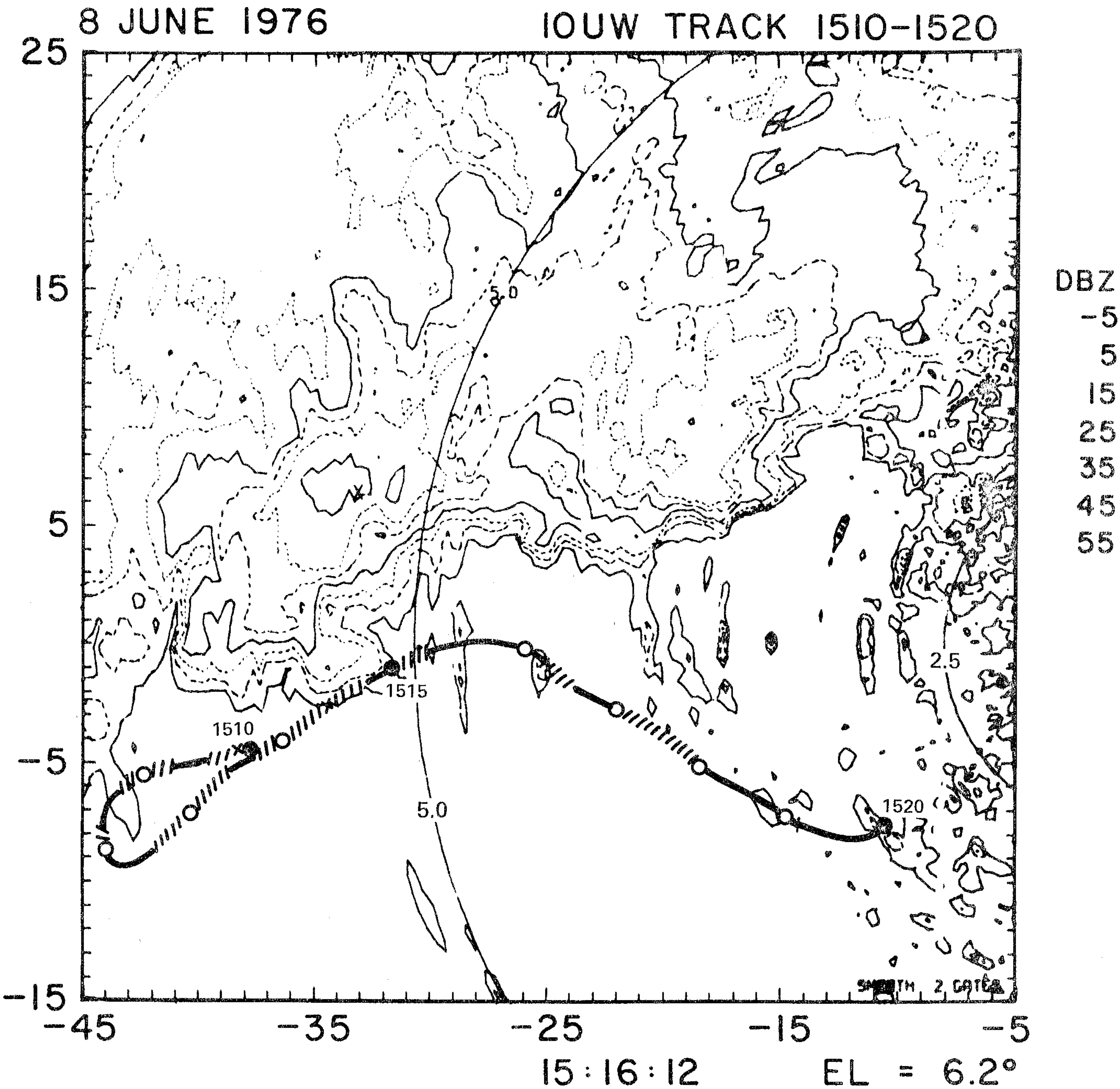

Fig. 23b. Same as Fig. 23a except PPI is at 15:16:12 and 6.2° elevation angle, and track is from 1510 to 1520. Constant altitude arcs are at 2.5 km and 5.0 km.

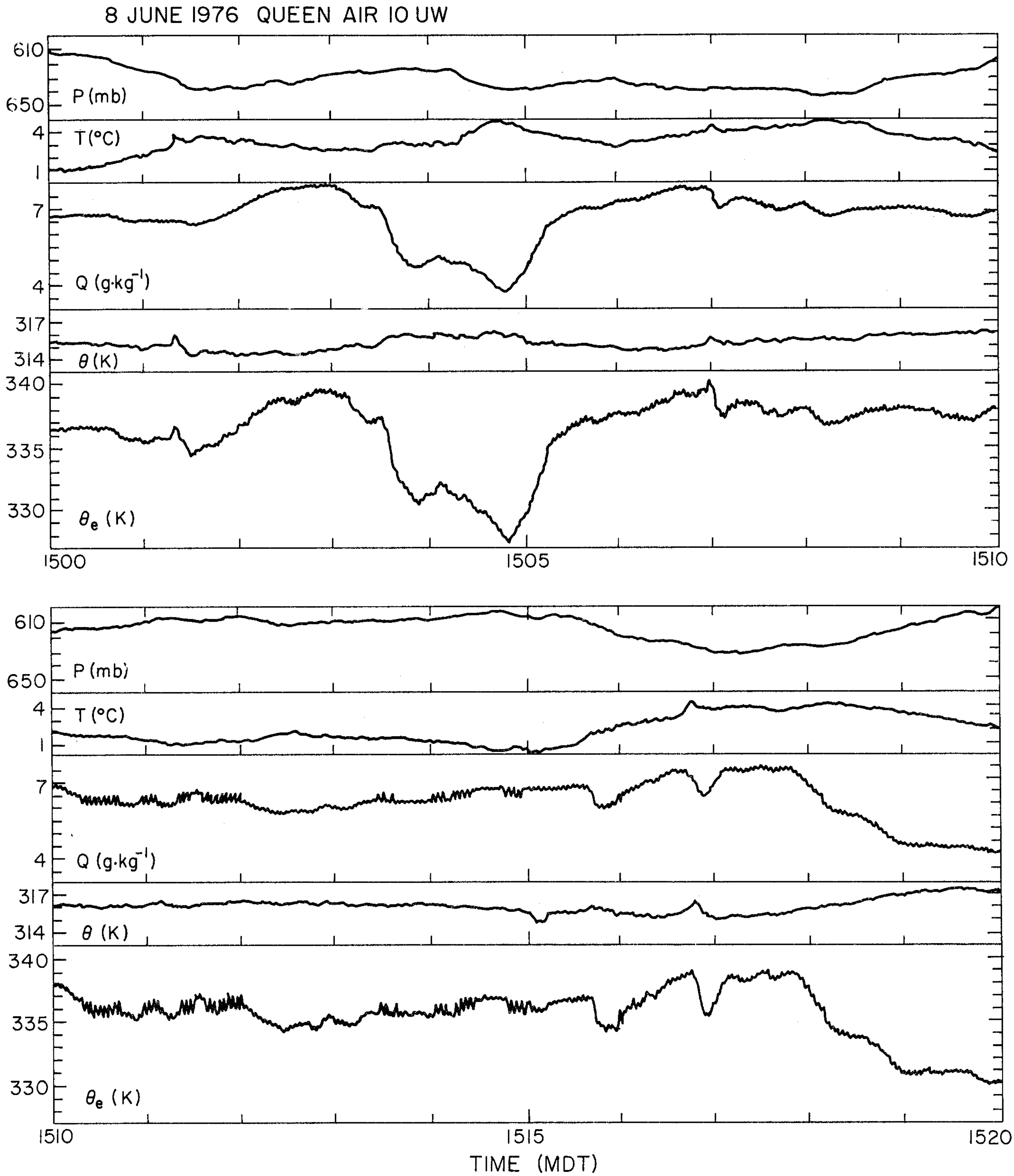

Fig. 24. Data from 10UW for time period 1500 to 1520 showing pressure, temperature, mixing ratio, potential temperature (θ), and equivalent potential temperature (θ_e). Time ticks are every minute.

V. OTHER DATA

A. MESONETWORK

The analog charts of the 31 conventional mesonetwork sites are available, and analog traces from 1600 to 2200 have been recorded on microfilm from the 15 Portable Automated Mesonetwork (PAM) stations. A gust front analysis from these data has been done on a later storm which affected the west and northwest area of the network. However, the storm of this study passed entirely outside the network.

B. DOPPLER

The two NOAA Doppler radars (NOAA-C, NOAA-D) gathered data during the early development of the storm from 1350 to 1511. The location of the storm area along the baseline of the two radars makes the dual-Doppler mode very marginal during this period. From 1511 to 1819, NOAA-C, NOAA-D, and the NCAR CP-3 Doppler radars made 15 volume scans of the storm which had moved to a more favorable position for Doppler coverage. The location is not optimal for tri-Doppler analysis, but the data should be usable. Processing of the data will commence in the near future.

C. TIME-LAPSE PHOTOGRAPHY

The film from the Grover camera, operated from 1330 to 1800, was slightly overexposed and hence the contrast was poor. Distinguishing cloud features is difficult, and frequent changes of camera direction provide little continuity of identifiable features. Any data analysis from this site is doubtful.

At Sterling, the pre-storm cumulus congestus could be seen at about 1315, and subsequent development could be followed to about 1545. The use of these data is marginal, however, because the cirrus outflow to the east began to obscure the view of the storm and the actively growing southern flank moved out of the field of view fairly early in its development. The distance of the storm from the camera site is also a limiting factor.

The film contrast from the Lindbergh data was fair after about 1430, which is when the storm moved into the camera's field of view. From 1430 to 1600 photographic coverage from the north side of the storm was fair to good, although the development on the south side was completely obscured. Scud cloud formation was visible on the east side, and the development and movement of the precipitation shaft is well covered during this time period. After 1600, the sky became more obscured by closer clouds and the storm had moved restrictively far from the camera site.

Data from the Greeley camera site are of good quality, although overall coverage of the storm was only fair. The active growth region to the south and southeast of the storm moved into the field of view at about 1600, while the cirrus outflow had moved into view at 1420. The coverage of growing turrets on the south side was good from 1600 to 1700, after which time nearer clouds and precipitation obscured the view.

D. SATELLITE PHOTOGRAPHS

Photographs from the SMS-GOES (east) satellite positioned at 75°W are available every half-hour for the time period 1600 Z on this day to

0030 Z on 9 June 1976. These photographs have one-mile resolution and show some detail of the southern flank of the isolated storm at 1530. More complete satellite data are available from any ground receiving station.

E. NCAR QUEEN AIR 306D

The NCAR Queen Air 306D investigated subcloud conditions from 1605 to 1745 as this mature storm moved southeastward. After determining the extent of inflow conditions to the northeast, 306D made approximately 20 east-west passes on the southeast side of the storm in general inflow conditions. Cloud base passes were made in the beginning, in the middle, and at the end of the investigative period. The southern "apex" of the storm intensified during this period, and achieved the highest reflectivity of the storm by 1620 (see Fig. 4e). The storm had a well-defined, bounded weak echo region and produced hail several inches deep over a short swath during this period. This organized phase of the storm will be the object of a later study.

VI. SUMMARY

Although low-level moisture was adequate (surface mixing ratio of $\sim 8\ g\ kg^{-1}$) and the atmospheric thermal structure was moderately unstable, no large-scale synoptic feature existed to organize the convection on this day, resulting in fairly isolated development and movement of convective cells. The merger of two of these cells northeast of Cheyenne created the nucleus of a major storm. Initially, the storm moved eastward with the mid-level winds, then shifted to a southeasterly direction at about 1420 as its development apparently began to respond to the low-level inflow. New cells that gained some southeasterly momentum tended to merge with and intensify the reflectivity core that had formed on the southeastern end of the storm mass.

Investigations by the three aircraft (304D, 10UW, T-28) from 1400 to 1545 show some areas of convergence and localized updrafts below cloud base, with similar updraft structures aloft along the southern and southeastern boundaries of the storm. Queen Air 10UW and the T-28 made coordinated penetrations in a cell that had developed southwest of the reflectivity core and moved around the southern end of the storm before merging with the higher reflectivity area. It existed as a definable entity for about an hour ($\sim$1420-1520) with consistently detectable updrafts of variable strength. The periphery of a larger cell was penetrated by 10UW and the T-28 at about 1540 as it was rapidly growing southwest of the main storm. Moderate updrafts, some strong downdrafts, and little development of ice particles were detected in the penetrations along the west side of the cell. The cell later merged with the storm, extending the high reflectivity area southward as the storm mass moved southeastward.

APPENDIX A

GROVER RADAR SPECIFICATIONS

The radar reflectivity data presented in the text were obtained by the Grover S-band radar (CP-2) during the 1976 field season. The specifications of the radar set are given in the table below.

Table 1. Grover S-band Radar Specifications

Antenna	
Horizontal beamwidth (deg.)	0.99
Vertical beamwidth (deg.)	0.94
Gain (dB)	44.2
Transmitter	
Frequency (MHz)	2801
Wavelength (cm)	10.7
Peak power (kw)	650
(dBm)	88.1
PRF (s^{-1})	937.5
Pulse duration (μs)	0.92
Receiver (logarithmic)	
Minimum detectable signal (dBm)	-107.4

In calculating Z_e (effective reflectivity) from the radar equation for meteorological targets, $|K|^2$ was set equal to 0.93, which is the value for water targets. ($|K|^2$ is related to the complex index of refraction of the target.) The CP-2 radar has an unambiguous range of 160 km.

Methods used for calibration of the radar and more detailed information about the radar are described in Foote *et al.* (1976) and Eccles (1975).

APPENDIX B

10UW INSTRUMENTATION

The following table is the complete set of instruments flown on 10UW during the 1976 field season, and has been provided by the Department of Atmospheric Science, University of Wyoming. The coincidence errors inherent in the FSSP, as discussed in the T-28 appendix and by Breed (1978), have not been corrected in the data presented. Also, the hot-wire LWC values are inaccurate for this time during the 1976 field season, and are presented only to show encounters of cloud water by 10UW and the relative fluctuations.

UNIVERSITY OF WYOMING RESEARCH AIRCRAFT INSTRUMENTATION

Part 1: Continuous Variables

			Combined Performance of Transducer, Signal Conditioning and Conversion			
Parameter Measured	Instrument Type	Manufacturer and Model Number	Range	Accuracy	Time Constant	Useable Resolution*
Time	Crystal osc	University of Wyoming, Dept. of Atmos. Science	12 mo	1 sec	NA	1 sec
Temperature	Platinum resistance	Rosemount Eng. Co. 510BF9 Bridge Model 102 Probe	±50°C	0.5°C	1 sec	0.1°C
Temperature	Platinum resistance, reverse flow	NCAR - probe Minco Inc. - element	±50°C	0.5°C	1 sec	0.1°C
Dew Point	Peltier cooled mirror	Cambridge System Inc. Model 137-C3	±50°C	1°C	5-10 sec	0.3°C
Liquid Water	Hot wire	Bacharach Inst. Co., Model LWH	0-3 gm/m^3	0.3 gm/m^3	1 sec	0.1 gm/m^3
Turbulence	Pressure	Meteorology Research Inc. Model 1120	0-10 IT	1 IT	3 sec	0.1 IT
Radiation (upper)	Pyranometer	Eppley	0-1.77 cal cm^{-2} min^{-1}		1 sec	
Radiation (lower)	Pyranometer	Eppley	0-1.654 cal cm^{-2} min^{-1}		1 sec	
Altitude	Total pressure	Rosemount Eng. Co. Model 1301 A 2A A4AX	0-15 psia	0.015 psia	1 sec	0.007 psia

*See footnote next page.

UNIVERSITY OF WYOMING RESEARCH AIRCRAFT INSTRUMENTATION

Part 1: Continuous Variables (contd.)

Parameter Measured	Instrument Type	Manufacturer and Model Number	Combined Performance of Transducer, Signal Conditioning and Conversion: Range	Accuracy	Time Constant	Useable Resolution*
Indicated Airspeed	Differential pressure	Rosemount Eng. Co. Model 1301 B 1A D1AX	0-3 psid	0.003 psid	1 sec	0.002 psid
Aircraft Manifold Pressure	Pressure	Rosemount Eng. Co. Model 1331	0-50 psia	0.1 psia	1 sec	0.1 psid
Rate of Climb	Calibrated leak pressure	Ball Eng. Co.	±3000 fpm	50 fpm	1 sec	50 fpm
Heading	Magnetic	King Radio Corp. Model KPI 550A	0-360°	±1°	1 sec	10
Position (azimuth)	VOR	King Radio Corp. Model KNR 660	0-360°	±1°	1 sec	10
Position (distance)	DME (VOR)	King Radio Corp. Model KDM 700	0-100 n mi	0.1 n mi	1 sec	0.1 n mi
Ground Speed	Doppler radar	Singer-Keorfott Model APN-153V	80-800 kt	1 kt	1 sec	1 kt
Drift Angle	Doppler radar	Singer-Keorfott Model APN-153V	±30°	0.35°	≈5 sec	0.35°
Yaw	Vane-driven synchro	University of Wyoming, Dept. of Atmos. Science	±180°	0.5°	1 sec	0.35°

*Values quoted are estimates of overall useable resolution which can be expected for actual flight conditions. Theoretical resolutions are one part in 4095 for all the above parameters except for heading, position, ground speed, drift angle and yaw, which are one part in 1023.

UNIVERSITY OF WYOMING RESEARCH AIRCRAFT INSTRUMENTATION

Part 2: Discrete Variables

Parameter Measured	Instrument Type	Manufacturer and Model Number	Range	Resolution	Sampling Rate	Useable Concentration
Cloud Droplets	Optical scattering	Particle Measuring Systems Model ASSP	0.5-7.5μm dia 1-15μm dia 2-30μm dia 3-45μ	(15 channels)	850 cm^3 km^{-1}	1-10^3 cm^{-3}
Cloud Droplets	Slide replicas	University of Wyoming, Dept. of Atmos. Science	4μm dia and up	15%	25 cm /slide ∿1 slide/min max	
Ice Crystals	Shadow imaging	Particle Measuring Systems Model 2-D	25μm dia and up	25μm	50 ℓ km^{-1}	10^{-2}-10^5 $ℓ^{-1}$
Ice Crystals	Direct sampling in decelerator; microscope examination	University of Wyoming, Dept. of Atmos. Science	10μm dia and up	2μm	50 ℓ km^{-1}	10^{-2}-10^5 $ℓ^{-1}$
Aerosols	Optical scattering	Particle Measuring Systems Model ASAS	0.08-0.21μm dia 0.18-0.43μm dia 0.30-0.69μm dia 0.45-3.90μm dia	(15 channels)	0.18 cm^3 sec^{-1}	1-10^3 cm^{-3}
Aitken Nuclei	Expansion chamber	Environment One, Inc., Model Rich 100	50Å and up	NA	50 cm^3 sec^{-1}	300-10^7 cm^{-3}

Aerosol Collector:	Filter sampler: sets of four filters, max 45 mm dia, total flow rate 60 ℓ min^{-1}
Air Sampler:	Bag samples: 120 ℓ filled over 1 min
Precip Collector:	Bottle sampler held outside aircraft
Precip Impactor:	Foil with gridded backing held outside aircraft
Events:	Ten selectable events marked from each of three stations

APPENDIX C

T-28 INSTRUMENTATION

The stated accuracies and determination of reliability of the following instruments are based upon publications by Sand (1975) and Heymsfield and Parrish (1979). Only those instruments related to the parameters presented in the Technical Note are included in this appendix. A more thorough discussion of the T-28 data system can be found in the references.

Static pressure. Pressure is measured by a Rosemount variable capacitance probe (Model 1301) with an accuracy no worse than ± 1.0 mb. Altitude is obtained from the hydrostatic equation with a representative sounding as input. Amplification of the pressure signal yields higher resolution, useful in calculating dz/dt for the vertical velocity computations.

Temperature. A sensing diode mounted in a reverse-flow housing measures temperature to ± 0.5°C. Wetting of the diode during encounters with liquid water does not appear to occur.

Vertical velocity. Rate of climb, manifold pressure (power setting), and indicated airspeed are combined in an equation derived from the T-28 flight characteristics which yields vertical airspeed. The rate of climb is measured by a Ball variometer (Model 101A), and the response time is estimated to be 2-3 seconds. Rate of climb is also computed from the pressure transducer, and comparison of the two independent measurements is generally very good. It is felt that the error in computing the vertical velocity is no worse than ~ 2 m s^{-1}.

Liquid water content. A Johnson-Williams hot-wire device is used for measuring liquid water content. Calibration and comparison discussions are presented in Heymsfield *et al.* (1978). Best estimates suggest an accuracy within ±20%. The probe mounted on the T-28 has operated with consistent reliability.

Cloud particle measurements. The T-28 is equipped with a PMS forward scattering spectrometer probe (FSSP) which measures cloud droplet spectra. It sizes particles 3-45 μm in diameter with a suggested error of ±10% or ± 3 μm, whichever is greater. The sizing accuracy has not been accurately established, however, and the concentration determination is questionable. The effective sampling area of the FSSP as it operated in 1976 has not been absolutely determined. Coupled with this is the problem of coincidence errors in the design of the probe that results in a greatly reduced measured droplet concentration in comparison to the true concentration. A more detailed explanation is provided in an appendix in Breed (1978). A correction equation for the concentrations has been incorporated in the FSSP data presented in this Technical Note, which is only the LWC from the integrated spectrum, but the accuracy of these measurements is still uncertain.

A PMS 2-D particle imaging probe is mounted on the T-28, and was the primary instrument used in determining ice particle concentrations and sizes. The size range of the 2-D probe is 25-800 μm diameter, with processing techniques enabling an extrapolation of particle sizes to 5 mm. A complete description of the probe and data reduction procedures are presented in Heymsfield and Parrish (1979).

APPENDIX D

NCAR QUEEN AIR INSTRUMENTATION

Only those instruments related to the data presented in this Note are listed below. A more complete list of the Queen Air instrumentation, specifications and characteristics is being prepared by C. Biter for publication in an NCAR Technical Note.

Temperature. A Rosemount temperature probe (Model 102E2AL) is used on both aircraft and has an accuracy of ±0.5°C.

Dew point. A Cambridge dew point (or frostpoint) hygrometer (Model 137) is used on both aircraft and has an accuracy of ±0.5°C. Occasionally the dew point data have oscillations due to various sources.

Static pressure. A Rosemount variable capacitance probe (Model 1301) measures pressure to an accuracy of ±1.0 mb on both aircraft.

Vertical velocity. On 304D a fixed vane gust probe and an INS are used to calculate vertical velocities. Accuracy is ± 1 m s^{-1}.

On 306D measured aircraft characteristics and an INS are used to calculate vertical velocities. Comparison of this computational technique with one using a fixed vane gust probe (as on 304D) showed differences less than 1 m s^{-1}. But, although accuracy of the 306D system is comparable to the 304D system, it applies only to those situations where large variations in vertical velocities occur at frequencies less than 0.3 Hz ($\gtrsim$260 m at a true airspeed of 80 m s^{-1}).

Descriptions and detailed discussions of vertical velocities calculated from these techniques are given in Kelly and Lenschow (1978) and Lenschow *et al.* (1978).

Horizontal winds. With a combination of information from the gust probe sensors (fixed vane on 304D and rotating vane on 306D), the differential pressure flow angle sensor, and the INS, horizontal wind velocities can be calculated within ±1 m s^{-1} with an additional error of 0.5 m s^{-1} hr^{-1} due to drift of the INS with time. A detailed discussion of air motion measurements is presented in Lenschow *et al.* (1978).

REFERENCES

Breed, D. W., 1978: 22 June 1976: First echo case. NCAR Technical Note No. TN-130+STR, 49 pp.

Eccles, P. J., 1975: Developments in radar meteorology in the National Hail Research Experiment to 1973. *Atmos. Tech. Winter 1974-75*, NCAR, 34-45.

Foote, G. B., R. C. Srivastava, J. C. Fankhauser, F. I. Harris, T. J. Kelly, R. E. Rinehart, C. G. Wade, P. J. Eccles, E. T. Garvey, M. E. Solak, R. L. Vaughan, B. E. Weiss and R. J. Wolski, 1976: Final Report - National Hail Research Experiment Randomized Seeding Experiment 1972-74. Volume IV: Radar Summary. NCAR, 326 pp.

Heymsfield, A. J., P. N. Johnson and J. E. Dye, 1978: Observations of moist adiabatic ascent in northeast Colorado cumulus congestus clouds. *J. Atmos. Sci. 35*, 1689-1703.

_____, and J. L. Parrish, 1979: Techniques employed in the processing of particle size spectra and state parameter data obtained with the T-28 aircraft platform. To be published as an NCAR Technical Note.

Kelly, T. J., and D. H. Lenschow, 1978: Thunderstorm updraft velocity measurements from aircraft. *Preprints Fourth Symposium on Meteor. Observ. and Instrum.*, Denver, Amer. Meteor. Soc., 474-478.

Lenschow, D. H., C. A. Cullian, R. B. Friesen and E. N. Brown, 1978: The status of air motion measurements on NCAR aircraft. *Preprints Fourth Symposium on Meteor. Observ. and Instrum.*, Denver, Amer. Meteor. Soc., 433-438.

Sand, W. R., 1974: Use of the armored T-28 aircraft to obtain observations in hailstorms with emphasis on the characteristics of the high radar reflectivity zones. Institute of Atmos. Sci., SDSM&T, Report 74-14, 76 pp.